05

V.7- 10216 Part No. I

CR - 154799

III

I.D. No 29690

THE FRENCH ATLANTIC LITTORAL

AND THE MASSIF ARMORICAIN

Prof. Fernand VERGER

Dr. Jean-Marie MONGET

Dr. Jean-Yves SCANVIC

ECOLE PRATIQUE DES HAUTES ETUDES

61, rue Buffon

75005 PARIS-FRANCE

July 1977

Type III final report for period

January 1975 - March 1977

Part I

by F. VERGER and J.-M. MONGET

CENTRE NATIONAL D'ETUDES SPATIALES

129, rue de l'Université

75007 PARIS-FRANCE

29690

. D. Number 29.690	2. Final report - Part 1	3. Recipient's catalog No.
. Title· THE FRENCH ATLANTIC LITTORAL AND THE MASSIF ARMORICAIN	5. Report Date : March 1977	
	6. Period Covered : January 1976 January 1977	
'. Principal investigator Prof.. Fernand VERGER	.8. No of pages :	
l. Name and Adress of Principal investigator's Organization ECOLE PRATIQUE DES HAUTES ETUDES 31, rue Buffon 75005 - PARIS. France	10. Principal Investigat.-Rept No 3	
	11. GSFC Technical Monitor Harold OSEROFF	
2. Sponsoring Agency Name and Adress ENTRE NATIONAL D'ETUDES SPATIALES 29, rue de l'Université 5007 - PARIS. France	13. Key Words (Selected by Principal Investigator) part 1 : Tidal marsh ; littoral transport, estuary ; beaches ; wetlands ; computer analysis part 2 : Faulting ; ore deposits	

ORIGINAL PAGE IS
OF POOR QUALITY

4. Supplementary Notes

Prepared in cooperation with Dr J. M. MONGET and O. GUERIN,
R.M. POISSON and Y. THOMAS

Original photography may be purchased from
EROS Data Center
Sioux Falls, SD 57198

5. Abstract :

   This final report gives results on Landsat - 2 data received and evaluated 5
scenes have been received in CCT Format and 65 scenes in film Format. These have been
chosen to complete or extend time-series covering significant test areas.

   Data processing was mostly digital and different classification techniques were
developped and comparatively evaluated with other available techniques.

   Output was in the form of colour or B/W maps using one or more scenes concur-
rently.

   Significant results were obtained in the following areas of investigation :

   - coastal geomorphology, with possible applications in shullfish aquaculture or
     recreation devlopment ;

   - sedimentary transport, with identification of numerous sedimentary plumes
     (Loire estuary, Gironde estuary, Gulf of St-Malo, etc...)
   - methodological aspects of classification techniques.

LIST OF CONTENTS

1 - INTRODUCTION

This report covers the whole of the FRALIT-B investigation period.
A number of data processing techniques were developed and applied
to LANDSAT-2 CCTS.

On arrival, magnetic tapes were reformatted to our data bank standards
(4 strips reassembled as a single scene file) and stored on direct access
units.

Classification of pixels in various spectral categories was followed by
mapping and interpretation using ground truth. Spectal signatures were
gathered on site using an EXOTECH radiometer and used in the training phase
of the classification process. Emphasis was put on the mapping of coastal
areas, extending seaward out to the limit of coastal sediment transports,
and landward into salt marshes, dunes and polder environments.

Comparisons were conducted in various test areas between LANDSAT data and
other remotely sensed information (airplanes or other satellites). Ground
resolution as well as spectral band variations were assessed.

Applications of remote sensing in coastal geomorphology were identified
with particular reference to shell fish aquaculture and recreation
development.

2 - TECHNIQUES

2. 1 - COMPARATIVE ASSESSMENT OF DIGITAL TECHNIQUES

The different classification methods used in the FRALIT program were applied to data from a test site on the French Atlantic coast. For critical evaluation of performance, this data was also processed by non-FRALIT methods (LARSYS, LARS JSC, IMAGE-100). Before describing some of the results from this comparison, and the test site itself, we will define some terms we shall use to characterize different techniques.

2. 1.1 - Definitions

Many different data processing techniques have been used in order to classify the spectral signature of remotely sensed data, into a given number of categories showing different terrain units or taxons (categories).

In a classification process, operator participation (in the broadest sense) can occur at different phases and in various fields of competence. Therefore, we propose to use the following terminology :

- assistance : participation of the operator in data processing. This can take place at different phases.

- pre-assistance : assistance occuring before the actual classification process.

- post-assistance : assistance occuring after classification.

- co-assistance : assistance carried out during the classification process. Pratice shows that the level of co-assistance is likely to increase with the speed and efficiency of man-machine interaction.

The experience required for operator assistance can be drawn from different fields of competence. Therefore operator assistance can be termed spectral, taxonomic or geographical.

- spectral assistance is based on the knowledge of the statistical characteristics of spectral signatures. The decision to subdivide a class having a bimodal spectral signature histogram is a case of spectral assistance.

- taxonomic assistance requires prior knowledge of the physiographic units or taxons in a scene. An example is the decision to subdivide a forest class into coniferous and deciduous.

- geographical assistance uses prior knowledge of the area covered by a given type of landscape or of the limit between two terrain units. Geographical assistance, for example, is the decision to group into one class all the pixels belonging to a given ground area.

Taxonomic and geographical assistance are linked when they are based on the unambiguous association of a taxon and a clearly defined geographical area.

Assistance is internal when it is based on the knowledge of the intrinsic characteristics of the data. The operator then participates by assessing these characteristics in order to make decision.

Conversely, assistance is external when data from other sources are used. This is the case when ground truth data is available and taken into account.

The following table identifies the different processing techniques tried by FRALIT using the types of assistance as a classification criterion.

2. 1.2 - Test zone description

All the processing techniques used were tried out on the Fromentine test zone for the following reasons (Fig 2.1.A) :

1/ This area was imaged a number of times both by LANDSAT 1 and LANDSAT 2. Indeed, it had the lowest cloud cover of all the area studied in the FRALIT program.

2/ It has a variety of coastal terrain units whose study is the subject the FRALIT program. Each of these units is large enough to be compatible with the spatial resolution of the remote sensors used.

3/ It had been extensively studied by the FRALIT team.

The Fromentine test site lies in the Vendée area and is defined by the following quadrangle :

      Lat   46° 47' N to 46° 57' N
and Long 2° 0' W to 2° 20' W

It includes the following terrain-types : (Fig. 2.1.B)

- Landward : Southern part of the island of Noirmoutier
           : Breton Marsh

- Seaward : Southern part of the bay of Bourgneuf
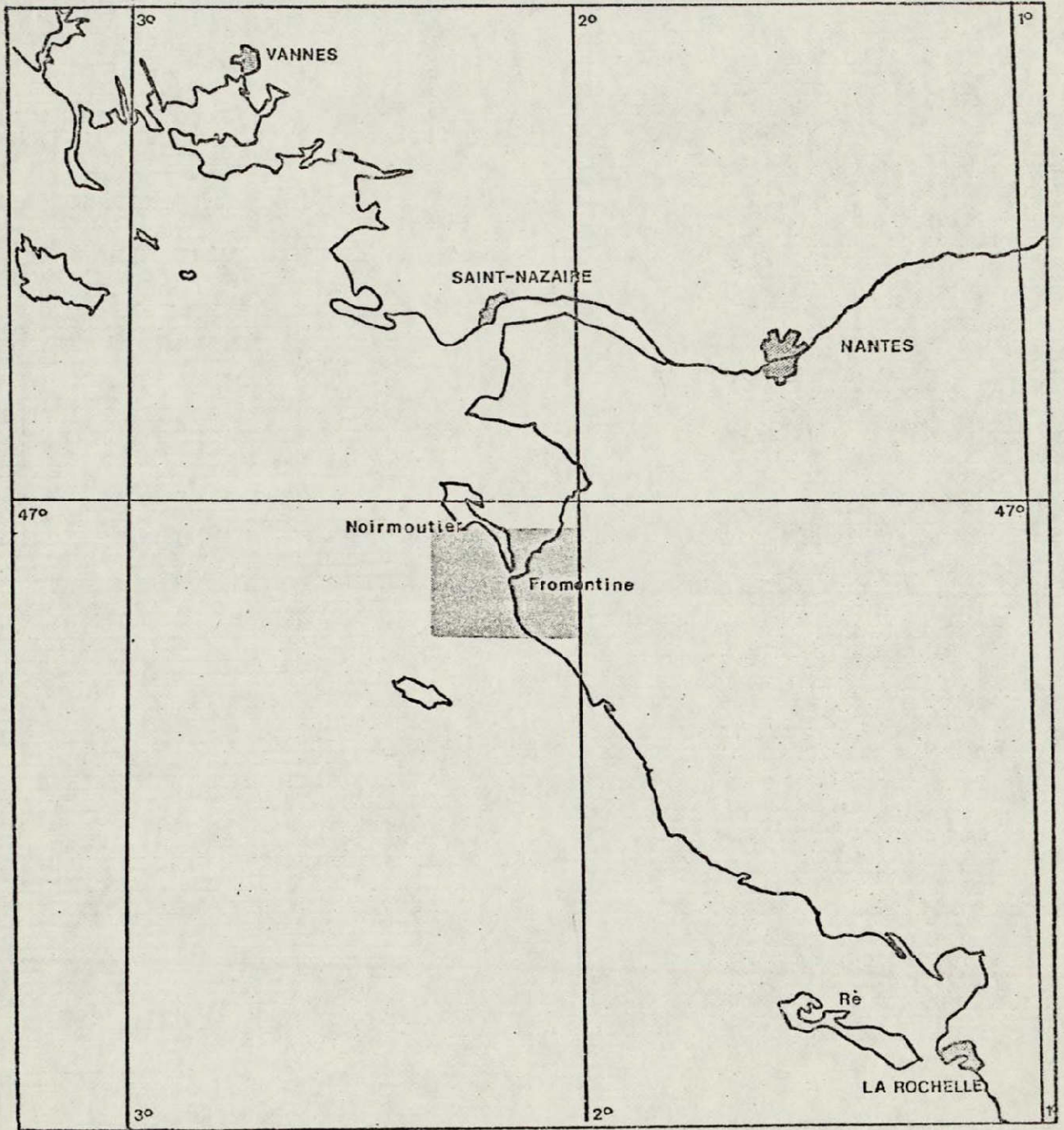   : Atlantic Ocean (Bay of Biscay)

Fig. 2.1.A - Geographical location of the Fromentine test site
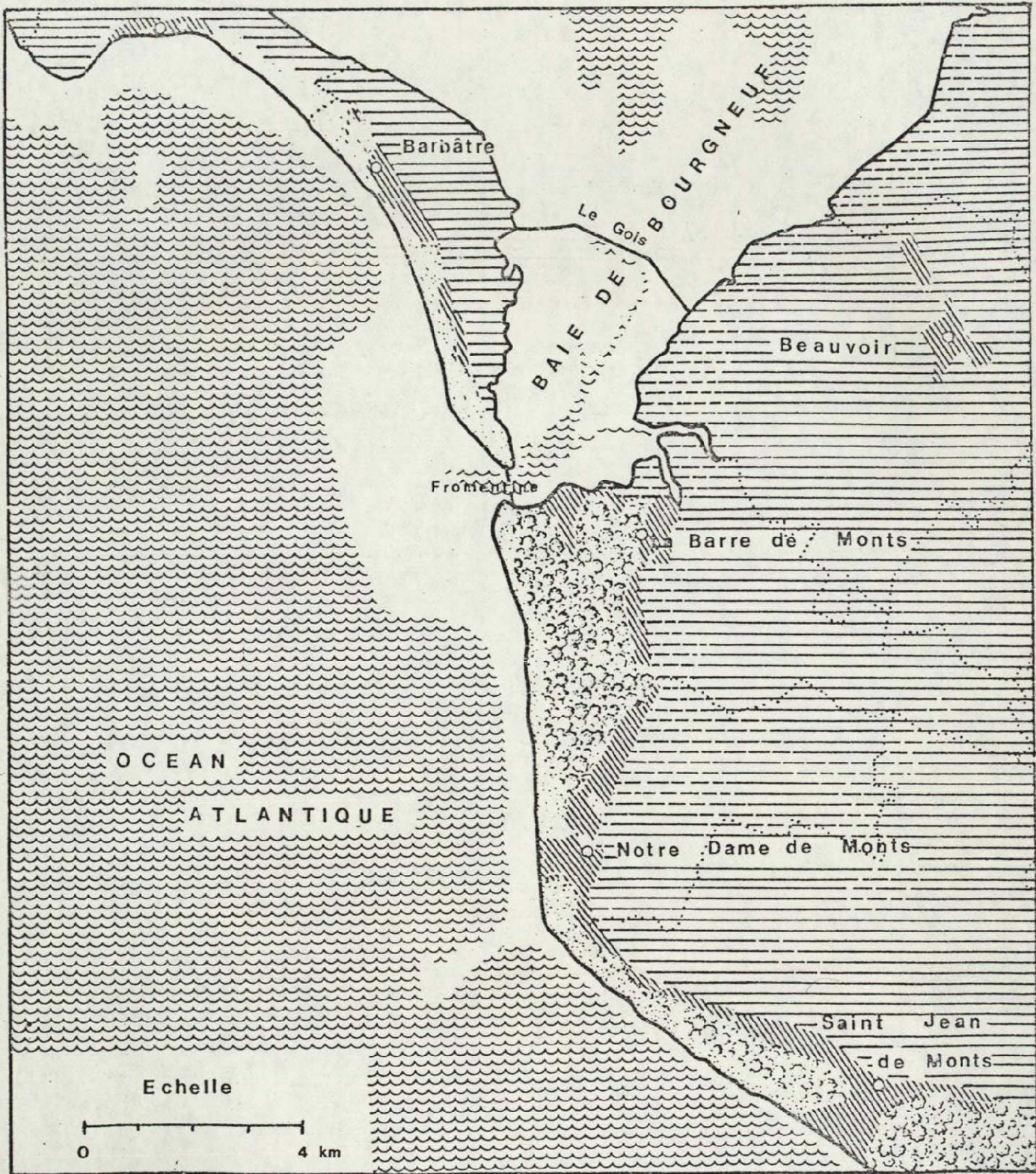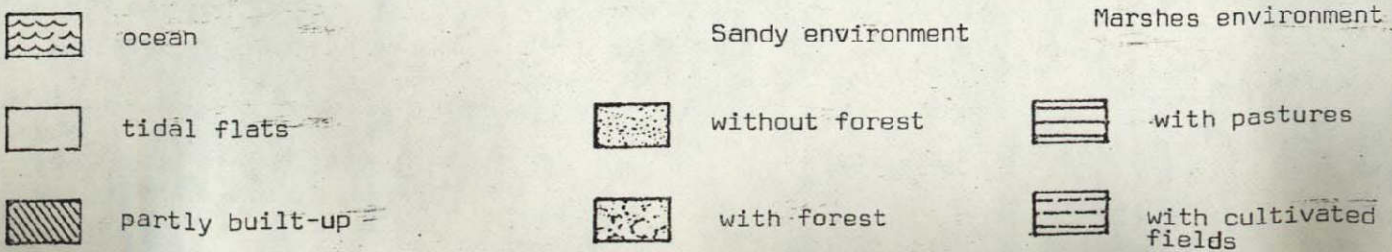
Fig. 2.1.B - Ground truth map of the Fromentine test zone

	ocean	Sandy environment	Marshes environment
	tidal flats	without forest	with pastures
	partly built-up	with forest	with cultivated fields

a - Land environments

a-1- Southern part of the Island of Noirmoutier

This is basically a sand spit built against tertiary
limestone out-crops. This spit includes coastal dunes with
psammophyte cover locally mixed with maritime pine or
Lambert's cypress.

East of dunes, a sandy marsh is divided up into small,
variously cultivated stips. This marsh zone was extenred
by reclamation from the middle ages to the 19th century.
The latest dyke lies north of the Gois ford : the Barbâtre
polder holds nearly 300 acres and was hollowed out by the
flood. The dyke was patched round the outside of this dip
so that a stagnant pond remains : the "Trou de Sebastopol".

a-2- Breton Marsh

The Breton Marsh is a marine alluvial accumulation
(mostly clay), protected by the dune covered bar of
La Côte de Monts. The dunes are mostly built up along the
sand bar to the West. Eastward, they lie across the bar
and locally reach 20 metres height. They were planted
with trees, mostly maritime pine, in the nineteenth
century.

Housing is mostly developed where the dunes meet the marsh.
Villages such as Fromentine and Notre Dame de Monts have
fanned inland from the coast, with well-spaced houses and
numerous gardens.

Land use in the marsh itself is very diversified : pastures
in the east, with salt marshes (active or abandoned), sand
or clay cultivated areas (Barre de Monts and La Crosniere)
and occasional oyster beds (Bouin). Ancient polders have
been invaded by the sea and partly reclaimed on the bay
of Bourgneuf coast.

The area is abundantly drained by narrow and winding
canals, often linked to drainage ditches.

Winding roads also run through the marsh. A four-lane
highway crosses the south of the island of Noirmoutier,
in line with the bridge linking the island to the continent
near the narrowest point of the straits.

b - Marine environment

The marine parts of the test site are under the influence of a
semi-diurnal tide.The tide drives a complex system of coastal
currents which can reach 5 knots in the Goulet de Fromentine.
Tidal variations lead to the drying out of parts of the
foreshore both in the southern bay of Bourgneuf and on the
Atlantic coast. The Noirmoutier bridge marks the limit between
these two environments.

b-1- <u>Southern Bay of Bourgneuf</u>

From high to low tide marks, the foreshore can be subdivided into :

. A polder, flooded by the sea in 1940 and never reclaim since : the Grande Prise de Fromentine. It has been largely silted up and the highest parts are covered by halophiles, mostly Suaeda Fruticosa. It is partly used as submersible oyster-beds.

The Pointe aux Herbes de la Crosniere tidal marsh includes the following species from top to bottom : Suaeda Fruticosa on and near the dyke ; Puccinella maritima and Salicornia radicans, Obione portulacoïdes Suadea maritima and Aster Tripolium ; Salicornia herbacea and Spartina Stricta.

, Flooded polders with little or no halophile vegetation Beauvoir polder reclaimed in 1862 then enlarged in 186 and abandoned in the twentieth century.

. Sandy mudflats behind the nineteenth century dykes. Geomorphologically active sand bars such as the Piau t

. Mixed sand and mud areas on either side of the Gois sedimentary ridge and its causeway. North of the Gois these areas include oyster beds.

. Tidal channels of varying depths above L.A.T. levels, running towards the straits in the southern part of the bay. To the North, the test-zone reaches the deep Fain French.

b-2- <u>Atlantic Ocean</u>

On the shores of the Atlantic Ocean, the following tidal areas can be distinguished :

. Sand beaches on the Island of Noirmoutier, on the Mon coast and the shores of the strait.

. Calcareo-siliceous limestone outcrops : the la Fosse rocks.

. Sand banks (submarine delta at Fromentine) for up to two miles seaward. These banks often include low frequency crosswise ridges with a changing morphology

The water itself changes considerably with the tide and also with the weather. Three main types can be observed muddy waters in rough weather on a lowering tide in the Goulet de Fromentine ; sand-laden waters over the sub marine delta on a rising tide ; clear water off-shore o near the Côte de Monts beaches.

Sea state is variable : waves and swell are frequent in the Atlantic ocean, whereas the formation of foam takes place in the south part of the Bay of Bourgneuf where waves are weak.

2. 2 - CLASSIFICATION BY TAXONOMIC PRE-ASSISTANCE (FRACARTE)

2. 2.1 - Introduction

The results presented here were obtained at the Ecole Normale Superieure (Montrouge) using the batch system FRACARTE tailored to the needs of the FRALIT team.

Computation is done in batch processing on an IBM 370/168. The test area is the Fromentine area as surveyed by LANDSAT2 on July 1975.

. Computing time can be separated into two parts :

- 12 seconds of CPU for legend construction during the pre-assistance phase which was conducted by selection of training samples drawn from the entire population of 40 800 pixels.

- 9.6 seconds of CPU for the actual plotting file generation of a category map covering the 16 800 pixels test area. Off-line plotting was done in 45 minutes on a BENSON 122 ink-plotter.

2. 2.2 - Software organization

The system includes in two programs : .FRALISIM and FRACARTE.

FRALISIM is used to identify the spectral signatures of the know taxons located in the area of interest. This category determination is drawn from the selection of sufficiently homogeneous training areas in the image to be processed. When the geographical area to be catagorized is too small, it is necessary to select training samples outside it in order to draw conclusions from homogeneous taxons covering a statistically significant number of pixels. The spectral signature determination is done on gray scale prints or plain listing outputs. These listings help in the determination in each spectral band of the radiance intervals which bound the multispectral signatures of each taxon.

Once this determination is complete the spectral characteristics of each category are input on punched cards to the FRACARTE program. This module generates a magnetic tape plotting file which is used to drive the off-line BENSON plotter. Any projection and scales can be selected. In the example presented the operator selected a Lambert2 projection and 1:50 000 scale.

2. 2.3 - Theoretical backgroung

All the philosophy of this system relies on a high level of pre-assistance used for the determination of radiance intervals bounding the spectral characteristics of each recognized category (taxon).

This determination can be guided using two types of approaches :

a - Assuming the taxons belong to spectrally well defined and
homogeneous categories. Their geographical boundaries as
well as their spectral limits are clearly defined because
the spectral gradients at their boundaries are strong. In
LANDSAT data this type of signature is more frequent on
land than at sea and is very often associated with man-made
environments rather than natural ones. However it is possibl
to find moderate gradients at sea (Fig. 2.2.A) especially
in estuarine or coastal areas.

In this case, the taxonomic pre-assistance will produce
unambiguous spectral bounds for each category. It is seldom
necessary with LANDSAT to use the entire set of spectral
bands, 2 spectral bands are sufficient in most cases.

b - The taxons cover continuously varying environments which
are really obtained by mixing in various proportions a
limited number of categories. The limits are in this case
rather fuzzy and variations of signatures do not generate
significant gradients.

We propose to call them spectral continuums. They can be fou

- in coastal waters, especially in the inside of bays

- in the intertidal environments

In this case, the taxonomic pre-assistance can usefully be
followed by a spectral pre-assistance working on the statis-
tics of data. For example, types of waters defined by
spectral intervals can be mapped by increasing turbidity as
this parameter is correlated with spectral bands MSS4 and
MSS5.

The weak points of this approach are :

- its dependance on careful choice of training areas
in which categories are known for their homogeneity
by collecting appropriate ground truth.

- its reliance on the "a priori" knowledge and skills
of the operator.

But, it is also very useful because of :

- its simplicity of use

- its small computing times

- and its results in the case of spectral continuums
classification because the produced maps are equivalen
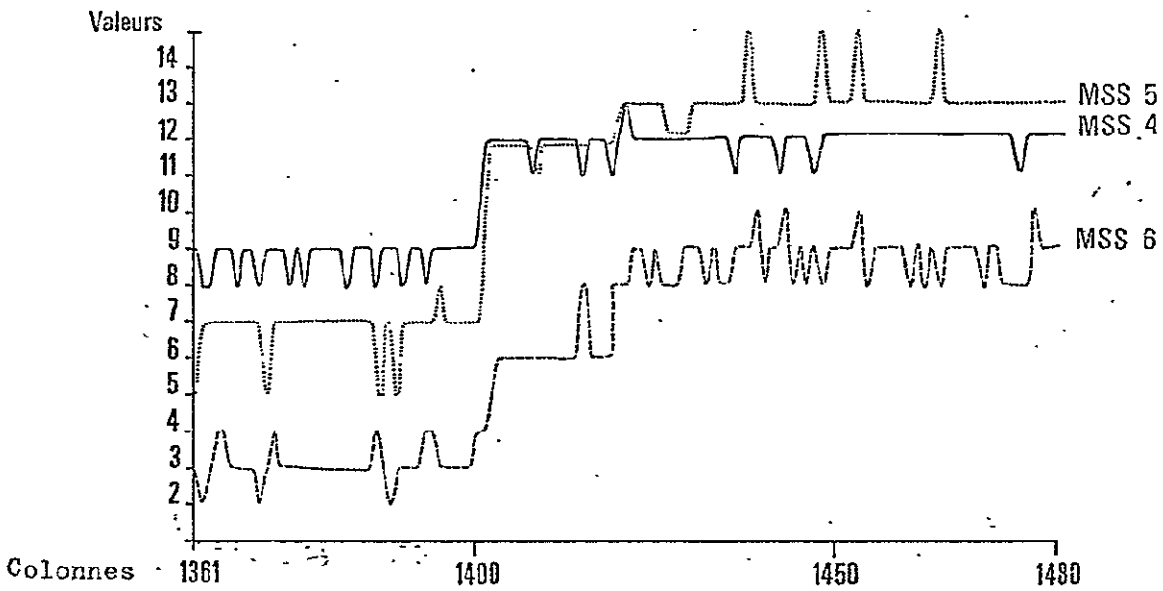to photographic isodensity slicing.

Fig. 2.2.A - Example of coastal water color gradient
At ebb tide, the plume of turbid waters
coming out the Maumusson strait expands
over clear ocean waters (E.2331 - 10110,
19 Dec 75, line 1566)
Values in MSS7 were not drawn because always
equal to zero or one.

2. 2.4 - An example of processing

The first step of the processing of the Fromentine area leads to
the determination of class spectral intervals drawn from
homogeneous training samples. The listing output of FRASILIM
gives a list of values for the four MSS spectral
bands. Each individual symbol is assigned to a specific radiance
value (Fig. 2.2.B).

From this listing the spectral signatures of 6 categories were
identified :

- water

- tidal flats

- sand and built-up areas

- dense forest

- cultures, meadows, vegetated sand dunes and open forest

- dispersed cultures and settlements with gardens

These definitions are assigned to each signature by taxonomic
assistance. Two categories from this set can be interpreted as
spectral continuums : the water and tidal flat environments.
Theoretical considerations on spectral signatures or ground-
truth radiometric measurements done with an EXOTECH radiometer
lead to the subdivision of the first environment into 5 sub-
categories of water ranked by their radiance values in spectral
band MSS5 :

- MSS5 :   23 - class 1
- MSS5 : 24-27 - class 2
- MSS5 : 28-31 - class 3
- MSS5 : 32-35 - class 4
- MSS5 :   36 - class 5

These waters are ranked by increasing turbidity level. The tidal
flat category extends its signature in MSS7 from radiance value
6 to 12. It is divided into two sub-classes using the intervals
[6,9] and [10,12] . This gives us a separation between humid
slikkes and tidal flats with lower water content.

The previous taxonomic pre-assistance has been refined by
spectral interpretation of the spectral continua. The subsequent
intervals are input to FRACARTE which outputs a 1:50 000 scale
map. (Fig. 2.2.B). The legend of this document can be described
as follows.

1 = Clear marine waters. They extend off the Monts coast
    (lower left part of map).

2 = Slighly turbid marine waters in Bourgneuf bay and North
    of the Gois ford (upper left part of map) as well as on
    the outer edge of the Fromentine submarine delta.

3 = Average turbid marine waters.

4 = Highly turbid marine waters.

5 = Marine waters with very high sediment content in suspension often mixed with slightly covered tidal flats.

6 = Very humid slikkes.

7 = Tidal flats with low water content.

8 = Maritime pine forest and salt marshes (Monts forest and salt marshes on the rim of the Bourgneuf·bay coast).

9 = Cultures, open forest, meadow and vegetated sand dunes.

10 = Dispersed cultures and garden settlements.

11 = Sand and built-up areas.

Objects of different natures such as the maritime pine forest of Monts and the salt marshes of the abandoned Grande Prise polders may have the same spectral signature. In fact, three pixels belonging to these areas display identical quadruplet signatures : 23, 24, 37 and 16 respectively in spectral bands MSS4, 5, 6 and 7 (cf. quadruplets NM=G in Fig. 2.2.C). Resolving such ambiguities may involve the use of time varying signatures (diachronic) or spatial signatures (texture).

Results can be further refined on land but misclassification may increase due the complexity of the agricultural pattern of the Marais de Monts and Noirmoutier island. We decided to keep this level of category division because it is well correlated with physiographic units and broad categories of land use.
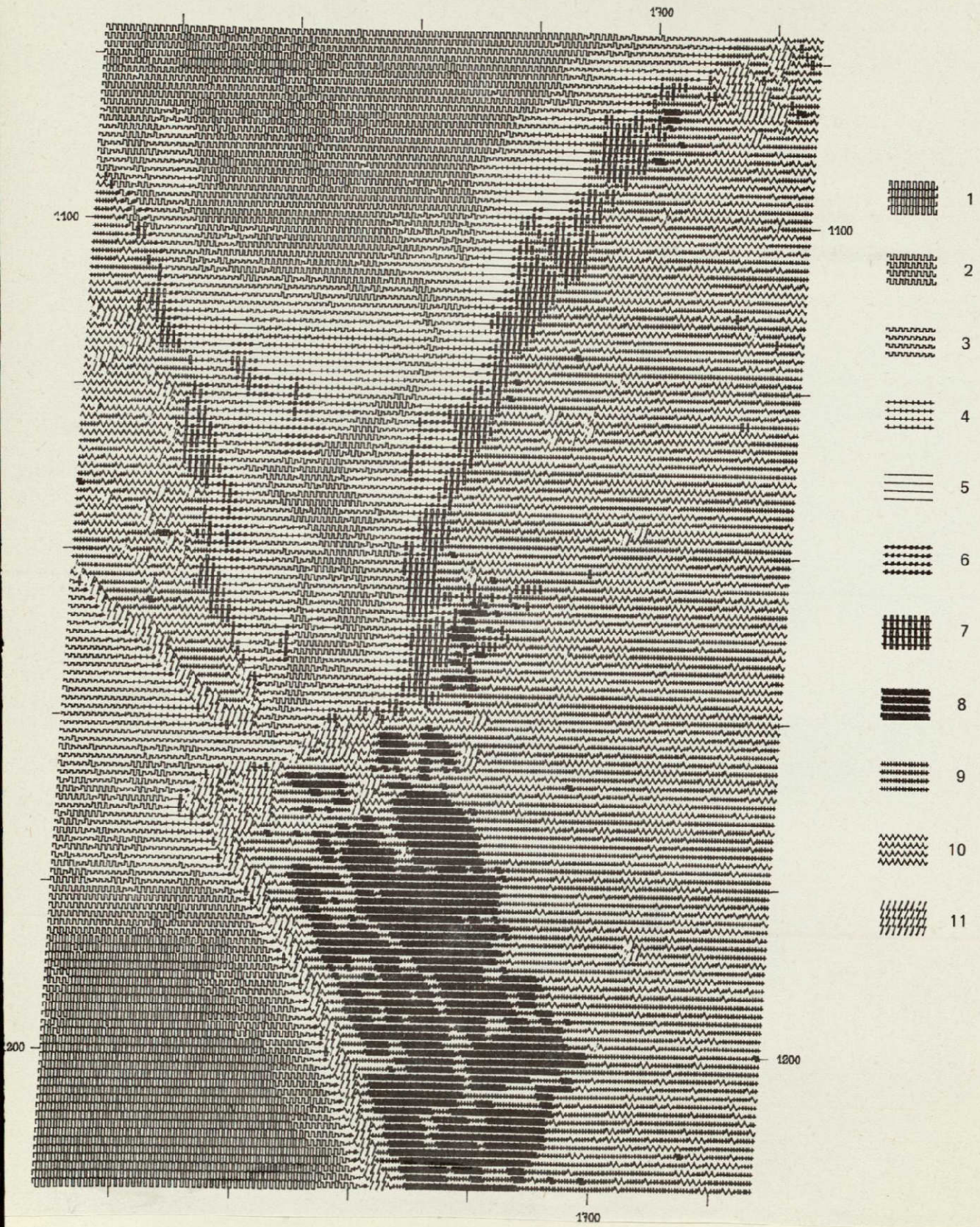
Fig. 2.2.B - An example of classification by taxonomic pre-assistance
Map of the Fromentine area at 1/50 000 scale generated
from LANDSAT2 data (E2188-10181 - 29 July 1975)

```
UTL4 UTN6 SUP6 UXR7 UXUA SXSA SQS7 PPUC NP=F NM=G
VXK7 VXVA SXTA SVVA SVXA VXVA STR9 OOTD RU-F MM-F
UYVA UYVA UYVA UVUB UYYB UVVB OPSA NMYE OO.F OU=G
VYXA TYVA TWXB TYXC VYZC RSTA PPVB OPZL PP-G OM.G
UUW9 UWWB UWWB SWYB SWYB UWWB UW-C QR-E NN-G PRYC
TYVA SVVB TYYB TVYC SYYC SVYB ST-C PO+G OM.H PSVC
RTU9 RUUA SUZB JUZC SX=D PQ=E PU=E PQ=F PP=G NP.H
SXVA STTA RTRA SVVA SV-E RS-F MO-G OO+H OO+H OU-E
SVVA SYUB UVUA UVVB UYZF RS=F OO2G OO2J OPZH UP.G
TWT9 TTV9 TWTA VYZC VYZC RSXB PP.I OPZL OSZI PQZK
UWT8 SWT9 SWT9 UZ-C SA.E SSW9 SS-D SS.G SW.F PR.G
N++D N+ZF W.9J Y7MO W.9K W2ZK W2EO N+ZU SVZM PT7G
S+7J UZGN U+EO XZGN XZEO X4GN S+9O UZEO SXGN S+9N
V.8L W4DM SZBL OSGJ MOZK RVBK V.BM V.BM S+8M S-8M
OTSN S-8N S-8L NM.I LL=H LMYG NO=H OSZJ RYBM RYBM
MLZK USBM RYAM UQZJ JK-I NL-I ML-I MK.I OUZL RYAM
NLZK NR7L PS7K ML.J KJ-G ML-H MK.H ML.H MLoH SZ9M
S-GM T+ZP S-9M ML.H MO.H SY9L PS4J MJ.H OM.H PS7K
RTBL S.GO RX7M LK=I LM=I UZBL RT.I NL+I PQ.I NMZL
MOZH NPIJ MPBL LLIJ MO+I SX4J S+3K SX5J SVBK SX8M
LK=H LL=H OPZH OSZH OSZI RTZI NPZH NO=H NP.H OSZJ
RWZJ OM-G JK.G JJ-I JJZG JLZG JKZG JLZG OQZK RWBN
ML-G KJ-G MK-G MLYF MK-G MK-G MK-F MK-G MK.H NR7M
JJ+G MLYG ML-H JL+H ML-G JL-G JJ+H ML+G ML-H ML.H
JK=G JK=G LL=G LL=G LM=H LL=H JK=H LK=H LL=G LLZG
LLII JK+H JK-H JK-H LL-G LM+H LL+I LI-I LK-I LL+H
NMZK LI.I LLYH LL=F LL=G LL=H NL=G JK=G LK.H LKYG
PWGO RTBN OMBK MKZF JLZG NL-I UL.I JMZF MK-G JG-J
GZ9O XGKU SWGQ MK-G KLYF NL-G MK.H KJ-G KJ-G KJ.H
UP4J PV8P OP4L JJ+H JLYG MN-H JM+G MQ-H MO+H MM+H
NP.H LL+I NL=H LKZH LM=H NP=I NP=H JMZG LLZG LL+H
LM+I LU+J LLZI LL+H LL-H JL-H LM+I LL+I LM-F LL-H
LK.H LL.H LM=H LL=G LK=H LK=G LL.I NQZL LOZI LL=G
JK.I JK-J MM.I MM.I JMZG MM-I ML.J MMZK JLIJ JL-J
MJ.H MK-G NN.G NN-H KL.H MK.J NK.J NL.K NN.G ML.F
ML-G JL+H OO+H OO+H MJ+H MJ+I ML.I ML+H ML-G JJZI
LL=H LM=G LL=G NM=H LL=H LK=H JM=H LLZG LL=G JK=I
LM-G LL-G LL-H LL+I LL+I MM+I LM+H JM-G LKXH JK-H
NM=G NM=G LL.G LK=G LM.H LM.H LM=G JIYG JI.G NI.H
```

Fig. 2.2.C – Part of a FRALISIM output listing for the
Fromentine area (29 Juillet 1975). Each quadruplet
gives the value taken by one pixel in the four
spectral bands MSS4 to MSS7.
The coding of individual values is hexadecimal.
The determination of category (taxon) signature
is taken from such a document during taxonomic
pre-assistance. The quadruplets NM=G (values 23, 24,
37, 16) have been circled out. They are associated
to the Monts forest (last line of display) or the
Grande prise salt marshes (first line of display)

2. 3 - CLASSIFICATION BY SPECTRAL PRE-ASSISTANCE (AGREG)

2.3.1 - Introduction

Data processing results discussed here, were obtained using the AGREG program which is part of the CLAMS classification system. This system was developped by Ecole des Mines under contract with the Centre National d'Etudes Spatiales (CNES). It is implemented in batch processing at the CNES computing center in Toulouse, using a CDC 7600. Overall CPU computing time for treatement of the Fromentine area was about 1 minute and 20 seconds.

Graphic output related to the classification results is generated as printed lists and graphs drawn on black and White microfilm using a CALCOMP 1670 COM system.

2. 3.2 - Software organization

The use of the AGREG algorithm causes the execution of several modules integrated in the CLAMS system. They perform the following actions : -

- supervised clustering per se (AGREG)

- image display of classification results

- spectral statistics

"A priori" knowledge by the operator of the number of classes and of their spectral statistics (average and RMS) is needed in order to run AGREG. These characteristics can be acquired using various means of information :

- a spectral data bank built by collecting typical spectral signatures. In this case the statistics are estimated by the variability expected from natural environments.

- a previous classification applied to a sample of the original image using a limited number of pixels. The reduction in the number of objects to be classified would in this case be linked to the use of more sophisticated methods than AGREG thus more costly in computing time.

- a previous classification carried out on a different area or even on data acquired for the area of interest but at a different date. The philosophy is in this last case to extend in time and in space the results obtained on an intensive test site where ground thruth was thoroughly collected.

Once clustering has been performed around cluster centers initialized by spectral pre-assistance, category display and spectral statistics help in assessing the quality of the subsequent mapping.

2. 3.3 - Theoretical background

The supervised clustering performed by AGREG belongs to the general family of algorithms in which spectral radiances are assigned to classes which are "a priori" defined by their statistical characteristics.

Several practical approaches are found in order to solve this type of problem. They are generally of three types :

- assignment by computation of the conditional probability that a spectral signature belongs to a specific class

- assignment by reference to a decision table

- assignment by computation of the distance seperating a spectral signature and a specific class.

a - Assignment by conditional probability

The first type of approach relies on the theory of probability. The basic information used in this case is the joint radiance histogram computed for the entire set of spectral bands.

This basic set of data can be information compressed at various degrees depending on the available computing time and core memory space. This compression usually involves the use of probability distribution modelling of the spectral radiance values repartition of pixels known to belong to specific classes. This training is done by "a priori" gathering of ground truth.

The model may use a limited number of parameters. This is for example the case of Gaussian hypothesis used in the LARSYS system. Illustration of this type of parametric approach can be found in Fig 2.3.A in the case where two spectral bands are used. A more precise but more complex solution can be found by the use of general types of distributions as in the general class of non parametric methods.

b - Assignment using a decision table

The basic information used is the same as in the preceeding method, namely the joint radiance : histogram.

But in this case no effort is done to model this distribution. Data compression is only performed in the storing phase in order to built a multidimensional decision table (Fig 2.3.A).

The assignment is in this case very quick but core memory used is often in the order of several tens of thousands of bytes. Memory reduction is in this case enterily dependent on computing skills developed by trained personel.
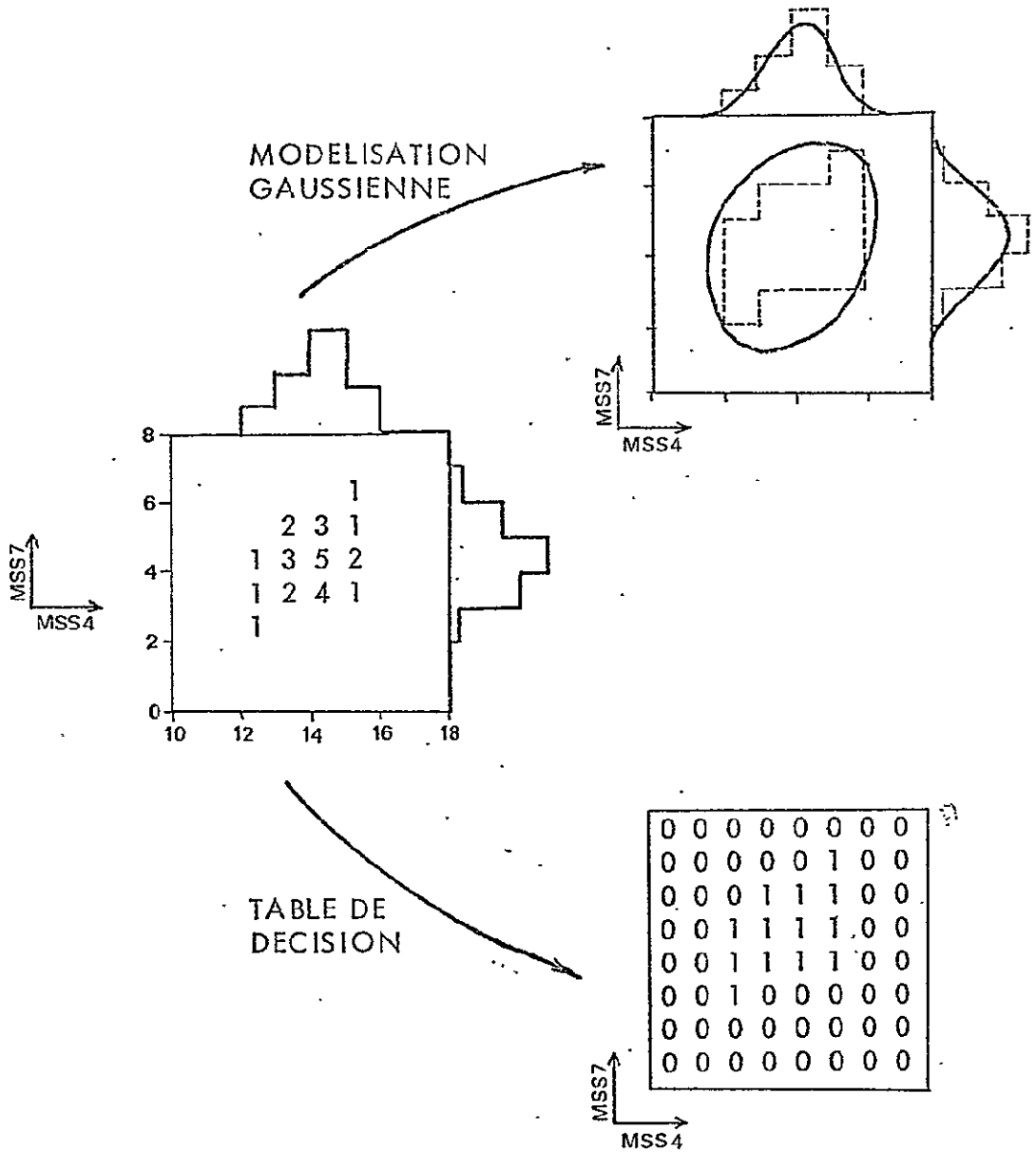
Fig. 2.3.A - Two types of assignment methods using
the joint radiance histogram of spectral
signatures

c - Assignement using a distance criterion

The degree of similarity between a spectrum and a class is computed in this case in place of the conditional probability of a spectrum to belong to a class. The solution used in general is to compute the Mahalanobis distance which uses for each class C_i, its average signature m_i and the associated variance-covariance matrix Σ_i.

$$D_M(z, C_i) = (z-m_i)'\Sigma_i^{-1} (z-m_i)$$

where : Σ_i^{-1} = inverse of matrix Σ_i

This formula defines a quadratic form associated to the Mahalanobis metric.

The AGREG program designers prefer a distance which uses the average signature m_i and the vector σ_i which set of components σ_{ik} are the spectral variances class C_i for the spectral band k. It is defined as follows :

$$D(z, C_i) = \sum_{k=1}^{n} |x_k - m_{ik}| / \sigma_{ik}$$

The use of this distance gives classification results which are equivalent in quality to the use of D_M. However it is more simple to compute than the last distance, leading to a saving in computer time.

A reject class (unclassified points) is built using a criterion equivalent to the mean divergence.

Methods of assignement using similarity indexes do save the computing time used in fitting specific models to the radiance joint distribution histogram but this saving is often lost when the assignment phase involves a large number of pixels.

2. 3.4 - Data processing example

a - "Apriori" class statistics

Decision was made to categorize the Fromentine area into six "a priori" classes (Fig 2.3.B) whose statistical characteristics were drawn from a detailed classification computed on a regular sampling of the studied area.

The six classes are related to land use themes and do not cover sea water or tidal flats.

b - Classification performance evaluation

A solution to the "a posteriori" evaluation of the supervised clustering performance may be found in the comparaison of the position of means and variances of "a priori" classes in relation to the "a posteriori" spectral signature histograms computed in each spectral band.
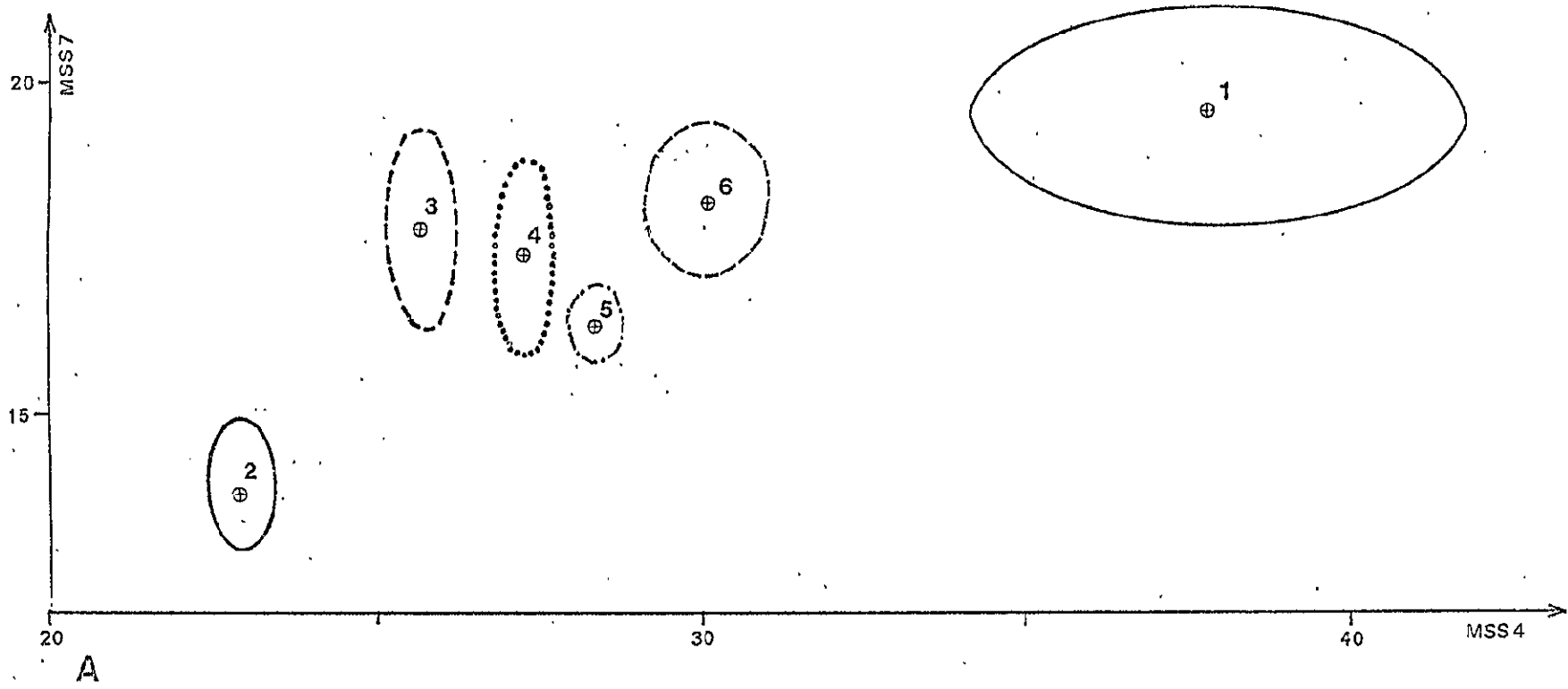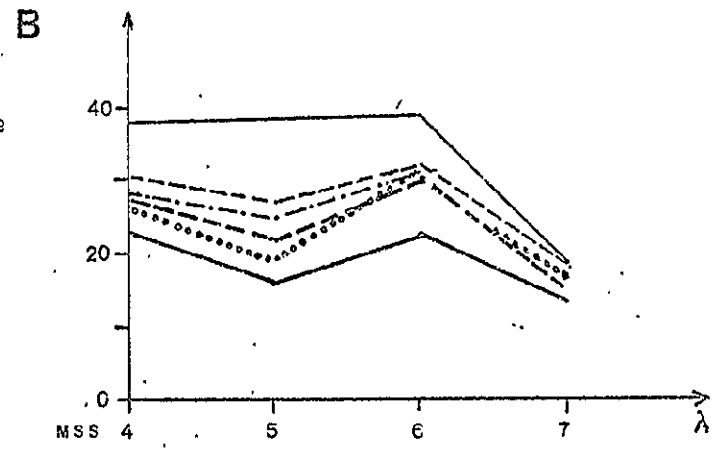
Fig. 2.3.B – Spectral characteristics of the classes
involved in the supervised clustering phase

A – Spectral means and variances for each
group for spectral bands MSS4 and MSS7

B – Average spectral signatures

This test was performed on Fig 2.3.C comparing the MSS4
histograms of groups 1 and 2. The hatched part in each
histogram is related to the radiance interval $[m-\sigma, m+\sigma]$
computed from the "a priori" spectral characteristics
of the associated class.

A good fit is noticeable for group 2 between "a posteriori"
histogram and "a priori" spectral characteristics.

This is not the case for group 1 for which the histogram has
a trend toward bimodality. This property was not taken into
account in the similarity distance formula used in AGREG
because it is only computed from spectral mean and variance.
A probability assignment method, using a non-parametric
approach, might have given a better result to the expense
of more computing time.

c - Results display

The cartography presented on Fig 2.3.D is an enlargement
of a display generated on microfilm.

The reject class is represented in white. It contains the
pixels which spectral radiances were found to be too diffe-
rent from those of the "a priori" classes.

The taxonomic significance of the classes was found to be
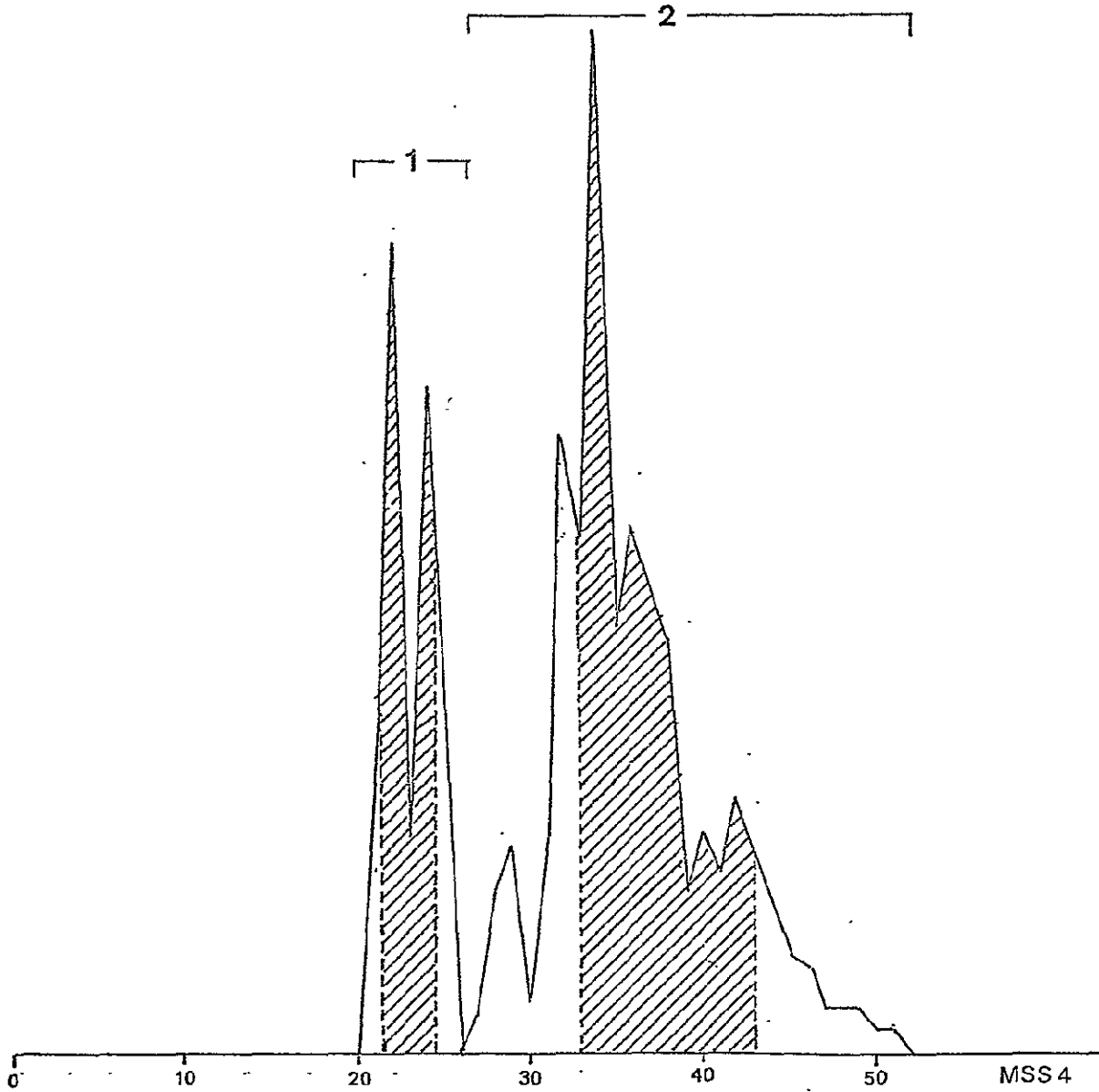in good relationship with existing land use patterns.

Fig. 2.3.C - Comparison of "a posteriori" spectral
characteristics of groups 1 and 2 with
the "a priori" parameters used in the
clustering phase
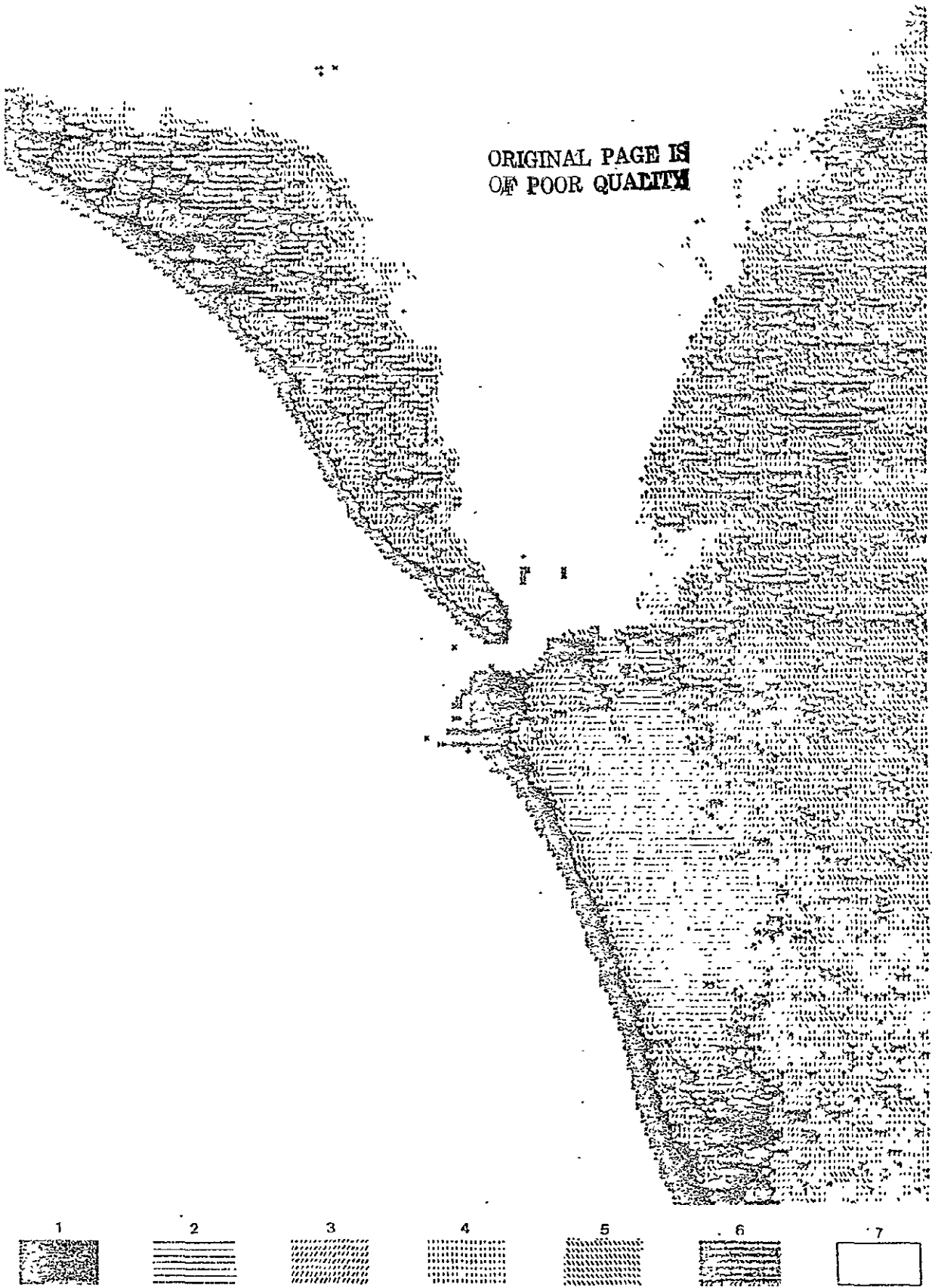
ORIGINAL PAGE IS
OF POOR QUALITY

Fig. 2.3.D - Enlargement of AGREG classification display
generated on a COM microfilm device

2. 4 - CLASSIFICATION BY SPECTRAL COASSISTANCE AND TAXONOMIC POSTASSISTANCE (FRACAM)

2. 4.1 - Introduction

The data analysis results presented here are taken from the Fromentine area, overpassed by LANDSAT1 on July 11, 1973 (Ref. number: 1353-10244). The equiment used is a CII IRIS-80 computer linked in the time-sharing mode to a Tektronix graphic display terminal. The graphs and maps produced on this interactive console can be hard-copied on paper using a Versatec printer-plotter.

The overall computing time for a classification involving 40 000 pixels is about 20 minutes.

2. 4.2 - Software organization

The FRACAM system has been developped at the Ecole des Mines (Paris). It is organized in four separate modules, whose functions are :

- data display and spectral statistics (FRAC1),

- correspondence analysis (FRAC2),

- ascending hierarchical classification (FRAC3),

- adaptative clustering (FRAC4).

The FRAC1 program has various display capabilities whereby images can be presented as :

- black and white binary maps related to a specific interval of radiance values in a given spectral band or to a spectral class produced by a previous analysis.

- gray-scale images, with a limited number of gray scales (4 levels at maximum), by modulating the intensity of the electron beam impinging on the storage tube.

- as an infographic map using the same logic as the FRACART program.

This program produces graphs related to the following statistical results :

- radiance values histogram, in a specific spectral band, computed on the entire image or restricted to a spectral class produced by a previous analysis.

- average and RMS signatures of pixels associated to a spectral class or to an interval of radiance values in a given spectral band.

- bidimensional histograms obtained by the comparison of two spectral bands (MSS4 and MSS7, for example). These ca be computed for a complete image or can be restricted to spectral class.

- a display of spectral class signatures in the plane of
  two spectral bands.

The maps produced by FRAC1 are geometrically corrected using
LANDSAT orbit parameters and scanning geometry specifications.
The hard-copies generated on the printer-plotter match the
Lambert 2 projection system at any scale between 1:1000 000
and 1:10 000.

Another function of the FRAC1 program is to prepare the coding
of data, either by slicing the histograms in isopopulation
intervals, or by adapting these intervals to the spectral
contrasts the operator is able to assess in the image before
any classification (opposition between water and soil, for
example). The first step in any pattern recognition problem
is to select an appropriate feature space by data coding and
also, in most cases data compression. This is done in the FRAC2
program. Feature space selection uses a two step procedure where
data coding is followed by data compression. A binary coding of
the radiance values using the previously determined histogram
intervals is followed by correspondence analysis. This multidi-
mensional statistical method similar to factor analysis enables
the operator to select a sub-space of limited dimensions (5 typi-
cally) in which hierarchical classification and clustering will
be performed. This analysis can be carried out for the entire
image or can be restricted to a spectral class produced by a
previous analysis.

The FRAC3 program helps in initiating the clustering of radiance
spectra in groups of similar shapes. The number of groups that
one would expect to find in the data set is objectively determined
as a result of an ascending hierarchical classification of the
spectral intervals used in the data coding performed in FRAC2.

Dialogue between the computer and the operator is required in this
phase, because the determination of the expected number of groups
involves the interactive "pruning" of a dendogram resulting from
the hierarchical classification. Along with the number of groups
the position of their centers of mass in the feature space is
estimated as well.

FRAC3 output is used in order to initialize the adaptative
clustering performed by FRAC4. It uses an iterative procedure
of the same principle as the ISODATA clustering algorithm.
Within each iteration every radiance spectrum is assigned to
a specific group whose center of mass is updated at the end of
the assignment phase. Various convergence criteria are used
such as an upper bound on overall center displacements or total
number of class assignments changes between each iteration.
Operator action is limited to the choice of the maximum number
of iterations in the case where convergence does not occur
using built in criteria.

The FRACAM system is organized so as to enable the operator to
perform a layered classification by sequentially refining the
spectral groups (spectral co-assistance) in relation to their
taxonomic significance (taxonomic post-assistance).

2. 4.3 - Theoretical background

a - Methodology

The relationship existing between an object located on the surface of the earth and the shape of its radiance spectrum as mesured by LANDSAT is the basic principle of remote sensing. It lends itself to automatic cartography through the use of numerical procedures which by mathematical nature belong to pattern recognition techniques.

The recognition of spectral shapes is solved by two types of methods. Segmentation of the set of spectral radiances is based, in the supervised approach, on the "a priori" knowledge of the nature and location of typical objects existing in a given test area. In the unsupervised approach, clustering using objective criteria.

The classification method used in FRACAM belongs to the latter type. It is built around an adaptative clustering algorithm : similar to the ISODATA method.

As the number of objects to be recognized can be rather large (8×10^6 for a complete LANDSAT image), special care has been taken to reduce computing time. For an ISODATA type algorithm this mainly requires the minimization of the number of iteratio necessary to reach convergence. This problem is equivalent in some respects to the search for initial centers of mass as clos as possible to their final positions after convergence.

Correspondence analysis of J.P. BENZECRI as a multidimensional method for data structure analysis provides an answer to the search for reliable centers of mass. It results in the selectio of a sub-space of limited dimensionality (feature space) in which it is possible to undertake a detailed study of the similarities existing between the spectral bands or their coded equivalents. The groupings thus determined are used in the initialization phase of the clustering algorithm. Initial centers of mass are computed using the simultaneous representati formula of correspondence analysis which builds a straightforwa link between the factor space of the spectral bands and the fac space of the spectral signatures.

Using this general framework, the FRACAM system is logically organized in three steps :

- use of correspondence analysis in an objective study of the data set structure followed by the selection of a factor sub-space which is retained as feature space. This data compression very often filters instrument noise

- determination on the filtered data of an ascending hierar chical classification of the spectral bands or their code equivalents. This similarity study leads to the recogniti of associations between spectral bands and spectral shape

- construction of spectrally homogeneous groups by adaptati clustering where the initial positions of the centers of mass in the feature space are calculated from the results of the previous phase.

b - Data coding

In order to have more flexibility in the determination of spectral band groups, it is preferable to transform the originally measured spectral radiances. This transformation is called complete disjunctive coding or isopopulation coding.

Such a code is generated by the following steps : computation of the radiance histogram of each spectral band j for the area of study, determination of n_j isopopulation radiance intervals for each spectral band j and replacement in the original data set of each measured radiance spectrum by its complete disjunctive code.

Each n dimensional spectrum (n = 4 for LANDSAT) is thus replaced by a K-dimensional vector, with :

$$K = \Sigma \left\{ n_j \mid j = 1, n \right\}$$

Each component of this vector associated to a given radiance interval takes a binary value 1 or 0 depending wether the corresponding spectrum radiance value in the spectral band j belongs to the given radiance interval or not.

The principle of this coding is illustrated in Fig 2.4.A when the four spectral bands of LANDSAT are split into four isopopulation intervals.

The use of this procedure was justified by an increase in overall classification performance, specifically regarding the number and spectral definition of classes.

c - Correspondence analysis

After transforming the data set, it is interesting to study its structure with particular reference to the similarity existing between the K coded equivalents to the n initial spectral bands.

We will call transformed band $c_{j\alpha}$, the binary instrument whose output is 1 or 0, wether the observed object radiance in band j falls or not in the isopopulation radiance interval of rank α.

In the example of Fig. 2.4.B the transformed band C_{42}, is a very simple incremental instrument whith an output of 1 when the measured radiance in band 4 (MSS7) falls between intensities 4 and 16 or 0 for any radiance value outside this interval

The total number of transformed bands is K (K=16 in Fig. 2.4.) they will be indexed by k in our formulas as long as the explicit identification of the relationship between spectral bands and transformed bands is not required.

Resolution element i
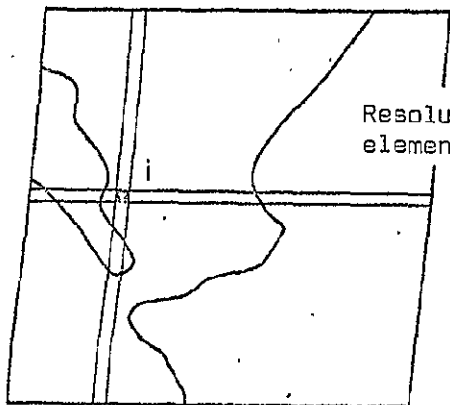
Measured radiances in i

| 37 | 27 | 15 | 7 |

| 0010 | 0010 | 0100 | 0100 |

Coded spectrum

Number of pixels

Radiance

MSS 4

28   3436   39   53

MSS 5

15   22   27   35   52

MSS 6

1   13   34   41   60
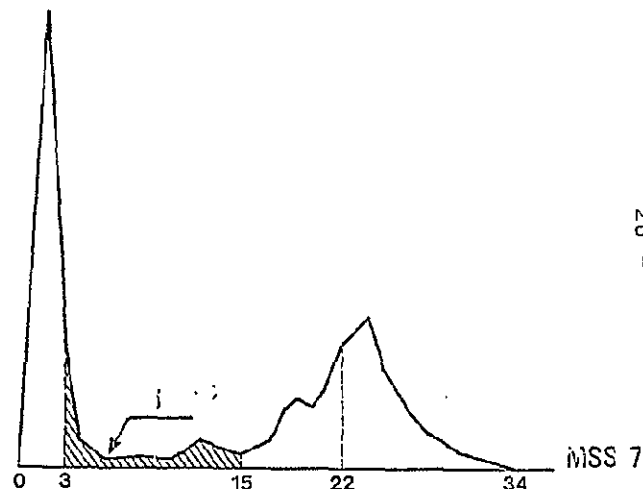
MSS 7

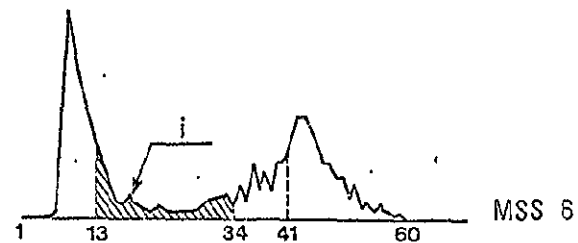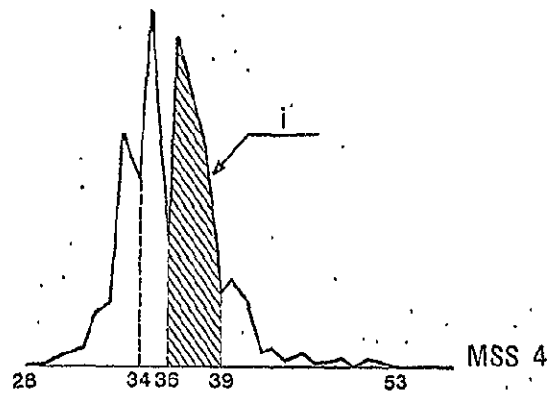0   3   15   22   34

Fig. 2.4.A - Principles of complete disjunctive coding in isopopulation intervals

- 26 -
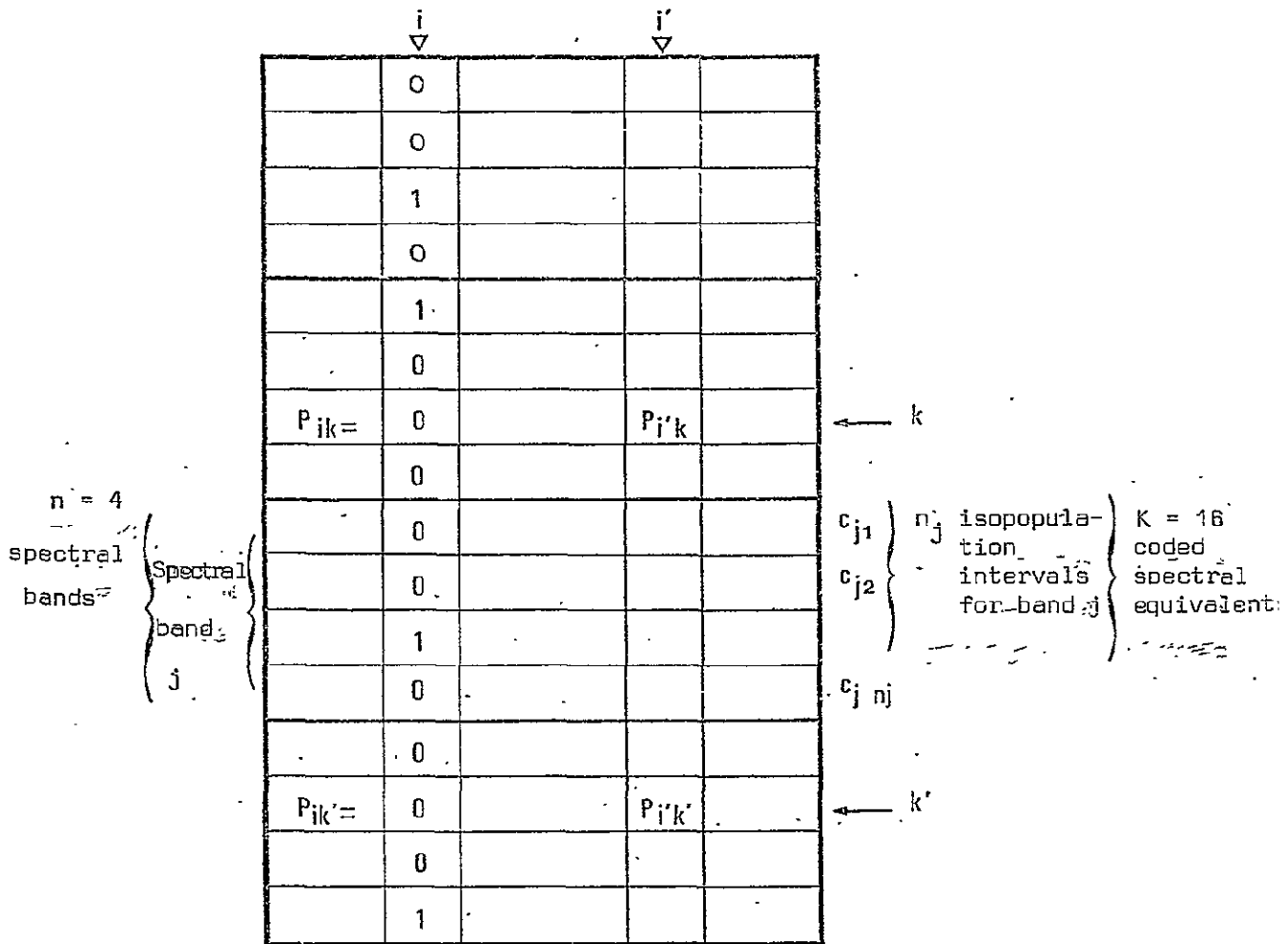
Coded spectral radiance $S_i = \{ p_{ik} \,/\, k = 1, K \}$

Global energy
equivalent sensed
in coded spectral $\quad = p_k = \Sigma \{ p_{ik} \,/\, i = 1, I \}$
band k

Equivalent image C_k
sensed in coded spectral $\quad = \{ p_{ik} \,/\, i = 1, I \}$
band k

Fig. 2.4.B – Matrice structure of complete
disjunctive coded LANDSAT data

The study of the similarity between two transformed bands k
and k' in done by using the following algebraic structure.
The transformed bands are considered as points of an I
dimensional vector space E_I, in which I is the number of
pixels to be classified. The origin of this vector space
is the average radiance computed in each spectral band
for the entire set of pixels.

Fig. 2.4.B gives an example of the data table associated
to the situation shown in Fig. 2.4.A. If one seeks a
mechanical equivalent to this data set, it can be thought
of as a "cloud" of K transformed bands scattered in the
vector space E_I.

Each point k belonging to this "cloud" in E_I is given a
weight p_k which is the global energy received by the
incremental band k. The metric of E_I is defined by a
similarity distance called χ^2 distance (Chi square distance)
defined as follows :

$$d^2_{kk'} = 1/m \ \Sigma \ \left\{ (p^i_k - p^i_{k'})^2 \Big| \ i = 1, I \right\}$$

with :

$$- \ p^i_k = p_{ik}/p_k$$

$$- \ n = \text{number of actual spectral bands (n=4 for LANDSAT)}$$

This distance is equal to zero when the binary images
associated with k and k' are identical. Theoratically the
computation of the distance existing between each couple
(k,k') is sufficient for the study of their similarity.

Unfortunately the computation of $d^2_{kk'}$, in E_I is long and
tedious because of the very large number of dimensions
of this vector space. Typically several billions for a
LANDSAT image.

Fortunately, correspondence analysis enables us to select
a feature space F_m of limited dimensionality (m=5 for exampl
F_m is a sub-space of E_I which is choosen so that in F_m the
distance between the projections of the transformed bands k
and k' is a good approximation of the true distance $d_{kk'}$,
between the two points E_I. The base vectors of F_m are the
eigenvectors of the "cloud" N_K built with the K transformed
bands weighted by the p_k . The associated eigenvalues λ_α
are ranked by decreasing order :

$$\lambda_1 > \lambda_2 > \ldots > \lambda_m$$

Each of them can be interpreted as representing the percen-
tage of information (or inertia) born by the associated
eigenvector Φ_α. These eigenvectors are the coordinate axes
of F_m which is often called factor space. It is in F_m that
the other steps of FRACAM take place.

d - <u>Typology of transformed bands</u>

In order to find reliable initial conditions for the adaptative clustering of spectra in F_m, it is necessary to have an estimation both of the number of groups they form and of the positions of the corresponding centers of mass.

Our philosophy is to consider that groups of similar transformed bands are most likely to characterize specific types of spectral shapes (or signatures). This is why groupings of transformed bands are sought for in F_m.

Using the simultaneous representation formula of correspondence analysis we will then be able to associate to the center of mass of each group of transformed bands a point in the spectral space which is a good approximation of the "true" center of mass of the corresponding group of similar spectra.

Before performing this spectral band to spectral signature transition, a detailed study of the geometric structure of the "cloud" built by the projections of the transformed bands is undertaken. This is done by using an ascending hierarchical classification algorithm in F_m.

The construction of a hierarchy on the set on K projections is done by gradually building a series of mutually inclusive classes fitted one into another. A dendogram representation is given to this series (Fig. 2.4.C) in which each node is indexed by a number proportional to the diameter in F_m of the corresponding class. The ascending character of the selected algorithm comes from upward construction of the dendogram (tree), the classes being formed by sequencially grouping points or groups of points which are close to one another.

The determination of the characteristic groupings between similar bands is done by "cutting" the dendogram at a given diameter by the operator thus defining an upper bound to the diameter of the classes being constructed.

In the case of Fig. 2.4.C three groups of similar transformed bands are selected as :

     - group 1 : C_{44}, C_{42}, C_{14}, C_{24},

     - group 2 : C_{11}, C_{33}.

     - group 3 : C_{13}, C_{22}, C_{32}, C_{21}, C_{31}, C_{41},

                 C_{12}, C_{34}, C_{43}, C_{23}.

A center of mass (center of gravity) is associated to each of those groups as a points in F_m. The spatial distribution of the groups of transformed band "points" corresponding to the previous determination is presented in Fig. 2.4.D. We have limited ourvelves to a plane representation restricted to the first and second factors (m=2).
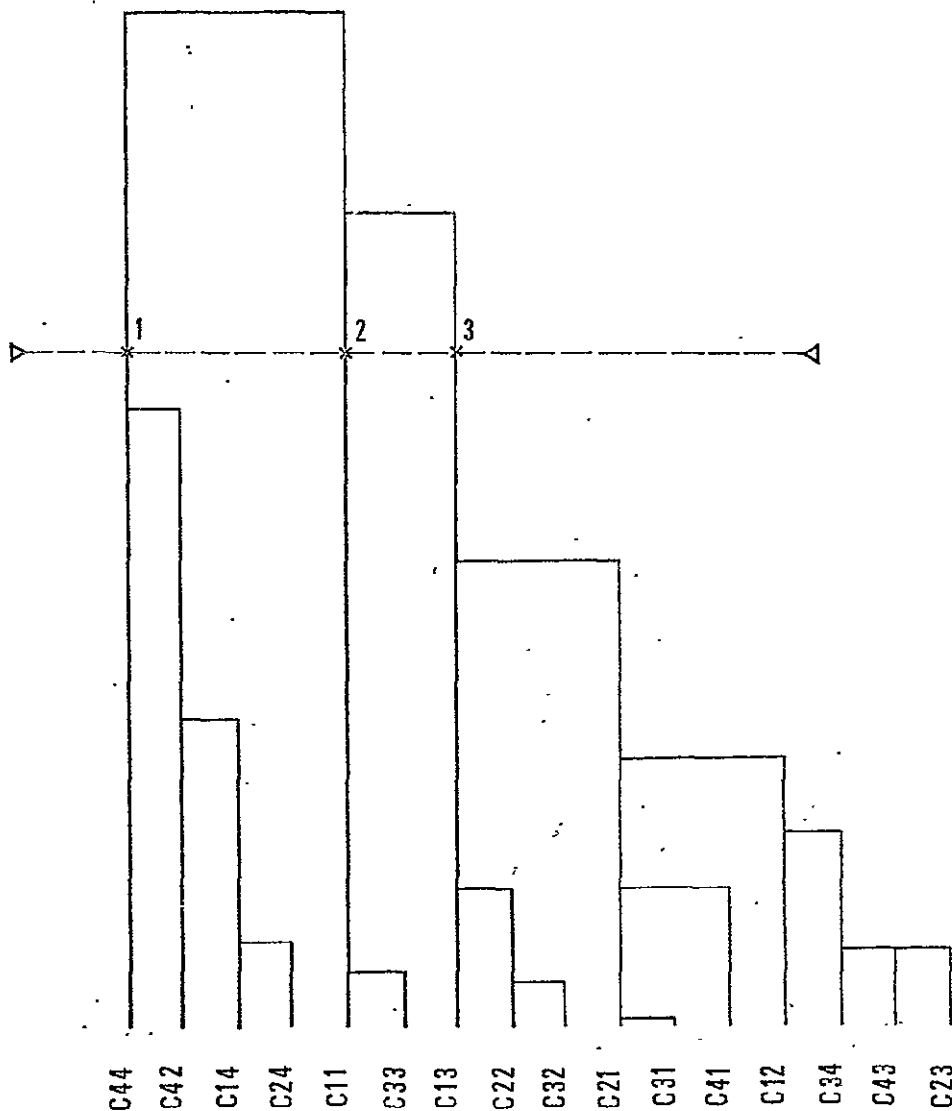
Fig. 2.4.C - Tree representation of similarities
existing between coded equivalent spectral
bands in the sub-space of the five first
factor axes.
"Cutting" of the tree at constant diameter along the
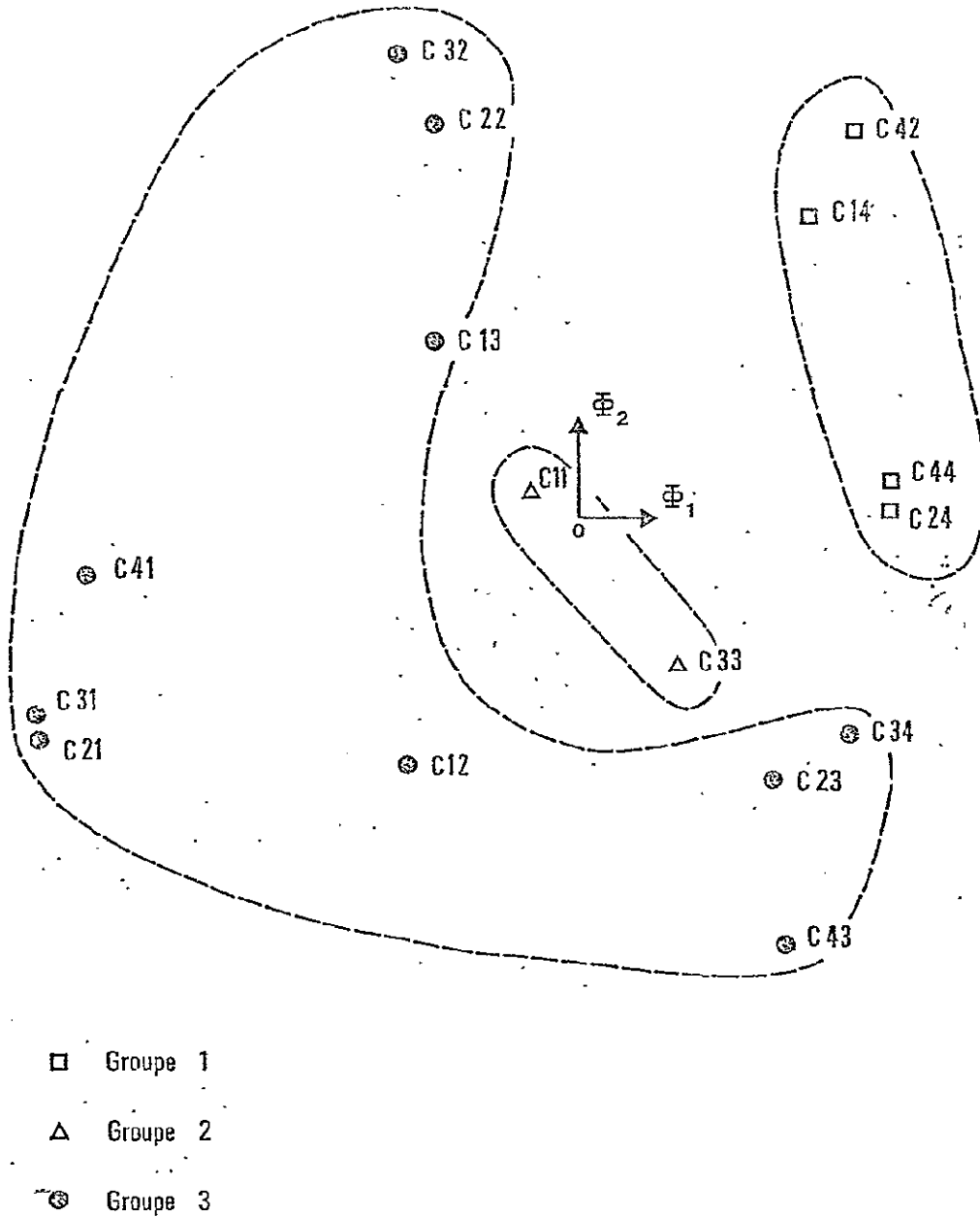dotted line defines three groups of coded bands

Fig. 2.4.D - Display of a hierarchy of coded spectral
bands generated from the results of
Fig. 2.4.C.
The representation is done in the plane
of factors 1 and 2.

e - Clustering of spectra

One of the more important properties of correspondence
analysis is to solve at the same time the twin problem
of structure analysis of similarities both between spectral
bands and between spectral signatures. In fact, the set of
eigenvalues $\{\lambda_\alpha \mid \alpha = 1,m\}$ which is used in order to built
F_m can also be used to built a feature space G_m of the
measured spectra with the same number of dimension as F_m.
This sub-space G_m is constructed from F_m by simple multipli-
cation of the base vectors components by the square roots
of the associated eigenvalues λ_α.

Clustering takes place in G_m using an adaptative centers
of mass algorithm which borrows some of its properties from
the K-means and the ISODATA algorithms. Initialization takes
place by specification of the number of groups and initial
positions of the cluster centers.

In the present case the number of spectral groups is equal
to the number of groups of similar bands as determined by
the previous phase. The initial cluster centers are the
projections in G_m of the centers of mass of the groups of
similar bands determined in F_m. Projection is easily done
by multiplying each of the m components of the centers of
mass by the corresponding eigenvalue λ_α.

The clustering algorithm is stoped and radiance spectra
are assigned to a class by using a minimal distance criterio
in G_m. Namely each spectra is assigned to the closest cluste
center. After each iteration, the cluster centers are update
with regard to the effective population of each class.

The philosophy of this approach is that after a certain
number of iterations, cluster centers and cluster cardinals
are sufficiently stable to give a reliable classification.
Various stability criteria are computed at the end of each
iteration in order to assess the quality of the classificati
The criteria are : the ratio between intra-class variance an
inter-class variance, the overall displacement of cluster
centers between their previous and updated positions and the
number of class assignment changes from one iteration to
the next.

At the end of previous algorithm, various results are availa
First, a cartography in which each pixel is given a symbol
uniquely associated to the class to which the associated
radiance spectrum belongs. Statistical results are also
produced for each class in the form of average and R.M.S.
radiance values for each spectral band.

Experience has shown that the initial cluster centers, as
determinated from the transformed bands typology are very
reliable. This has enabled us to reduce the number of itera-
tions to 2 our 3 thus obtaining a considerable saving in
overall computing time.

f - <u>An adaptative descending classification</u>

In the pratical use of unsupervised clustering algorithms, two approaches are possible.

In the first case, a·large number of clusters is determined, with the risk of having to follow·up the· clustering phase by a similarity study of the groups in order to reduce their number. In the second case, the clustering algorithm proceeds by successive dichotomy until the desired number of classes is reached.

The first type of heuristics is used in the LARSYS system, in which the first step leads to the determination of a large number of·potential classes taken from the training area. The study of the similarities existing between those groups of limited cardinals, enables to regroup them following a typical phase of taxonomic pre-assistance. This method uses an <u>ascending</u> approach whereby the complexity of a weak data <u>compression</u> (large number of groups) is reduced by the relative simplicity of a taxonomy often guided by typical application themes (oceanography, agriculture, geology ...)'.

The algorithm used in ISOCLS belongs to the second type of approach, it proceeds by successive dichotomy between each iteration. This is a <u>descending</u> approach going from the general to the particular.

The structure of the FRACAM system looks well suited to the second type of heuristics. The "cutting" phase of the hierarchical dendogram enables the operator to control the number of groups while performing a polytomy which is more complex than ISOCLS. This descending classification process is also made <u>adaptative</u> because at each downward move, correspondence analysis and hierarchical classification are computed again in order to adapt their results to the statistical properties of the group which the operator wants to refine.

Several criteria for assessing the need to pursue the subdivision of a group can be used. We propose to rely on the shape of the radiance histogram in MSS7. The subdivision is pursued if the group histogram is multimodal or does not fit a simple probability distribution model (Gauss, uniform or lognormal distributions): For example, we have reproduced in Fig. 2.4.E the spectral distributions of the class of pixels obtained after a first classification of the Fromentine area on July 11, 1973. Six groups were determined, the use of above criterion leads us to the following conclusions :

- groups 4, 5 and 6 do not need to be subdivided
- groups 1, 2 and 3 are on the contrary eligible for futher processing

Going from divisions to subdivisions, the FRACAM system is able to perform an adaptative descending classification guided by a spectral coassistance taylored to the group spectral statistics.
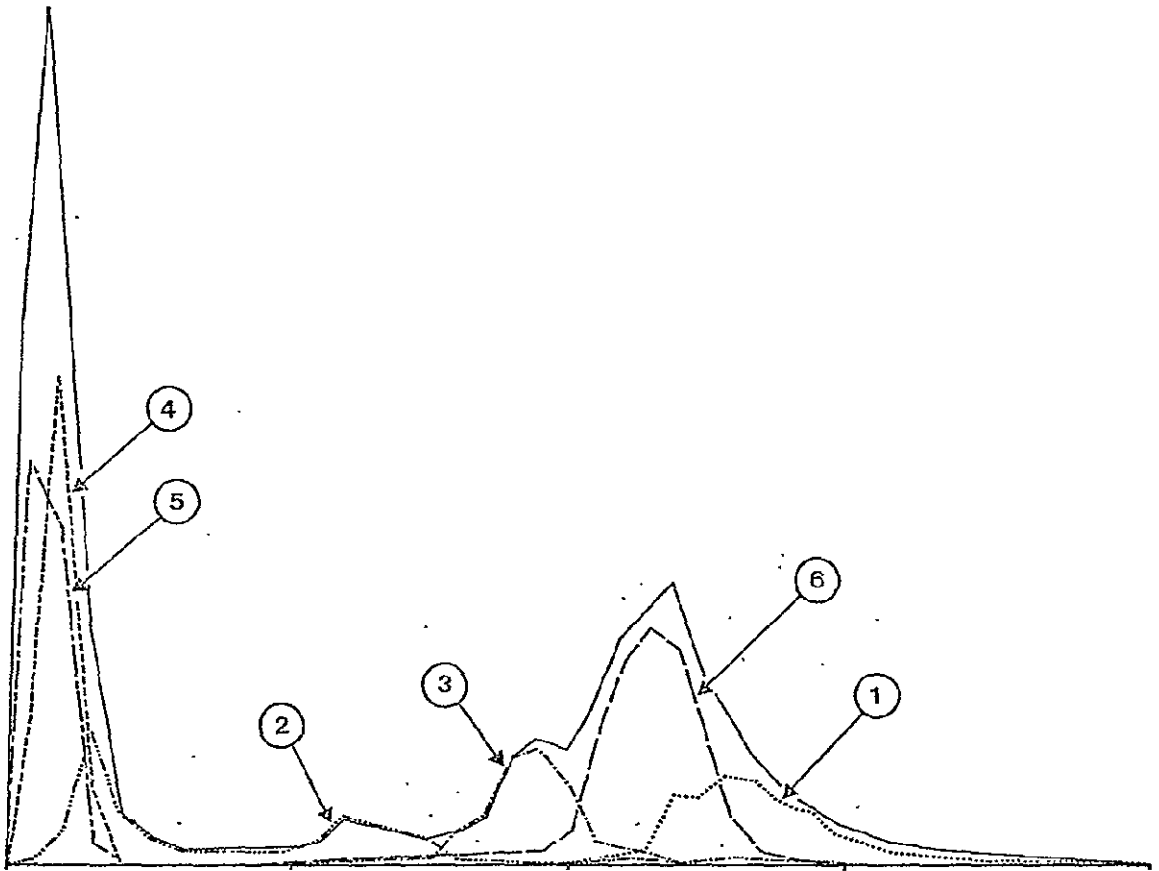
Fig. 2.4.E - MSS7 spectral band histograms for the
six groups obtained after the first phase
of treatment preceeding spectral co-assistance
The unnumbered plain line is the MSS7 histogram
for the entire image.

2. 4.4 - An example of processing

The processing of the Fromentine area surveyed on July 11, 1973
was done in two steps. In the first step, complete disjunctive
coding of MSS4 to MSS6 in eight intervals and MSS7 in seven
intervals led to the determination of six groups. Spectral
coassistance was performed on the band MSS7- histograms (Fig.2.4.E)
thus resulting in the further subdivision of groups 1, 2 and 3.
The adaptative descending classification was pursed for these
groups, by first generating a new complete disjunctive code
with four intervals in each spectral band. This code was adaptated
to each group's statistics seperately. Finally, eleven groups
were determined by the classification and submitted to interpre-
tation in the taxonomic post-assistance phase.

a - The results of the first phase

Regarding correspondence analysis we present on Fig. 2.4.F
the projections of the transformed bands in the plane of the
first and second factors. In this representation, each spec-
tral band (MSS4 to MSS7) was assigned a letter (A to D) and
a number corresponding to a complete disjunctive interval.
For example B7 is the the transformed band related.to the
seventh spectral interval determinated from the MSS5, histogram.

. Each factor can be interpreted as follows :

- on the first axis, the general structure corresponds
  to a transition from low radiance values to high radiance
  values in spectral bands MSS5, MSS6 and MSS7.

- on the second axis, spectral.band MSS4 is organised
  from low to high values except for the near center
  position of A1 (radiances from 26 to 32 in MSS4).

The two dimensional plane representation enables us to
refine this interpretation. A strong correlation is observed
between MSS6 and MSS7. The parallel structures drawn by these
spectral bands are organised in two arcs of opposite curvature:

- a first arc spreads over factor 1 going from C_1, D_1 to
  C_4, D_3

- a second arc spreads over factor 2 going from C_5, D_4
  to C_8, D_7

This general organization is due to a broad dichotomy in the
data set between two types of spectral signatures correspon-
ding, in the surveyed area, to the opposition between water
themes (sea, channels, tidal flats) and land themes (cultures,
forest, marshes).

The ascending hierarchical classification has led to the
determination of six groups of transformed bands which are
oultined in Fig. 2.4.F. The resulting.spectral clusters were
displayed one groupe at a time as binary maps. One can find
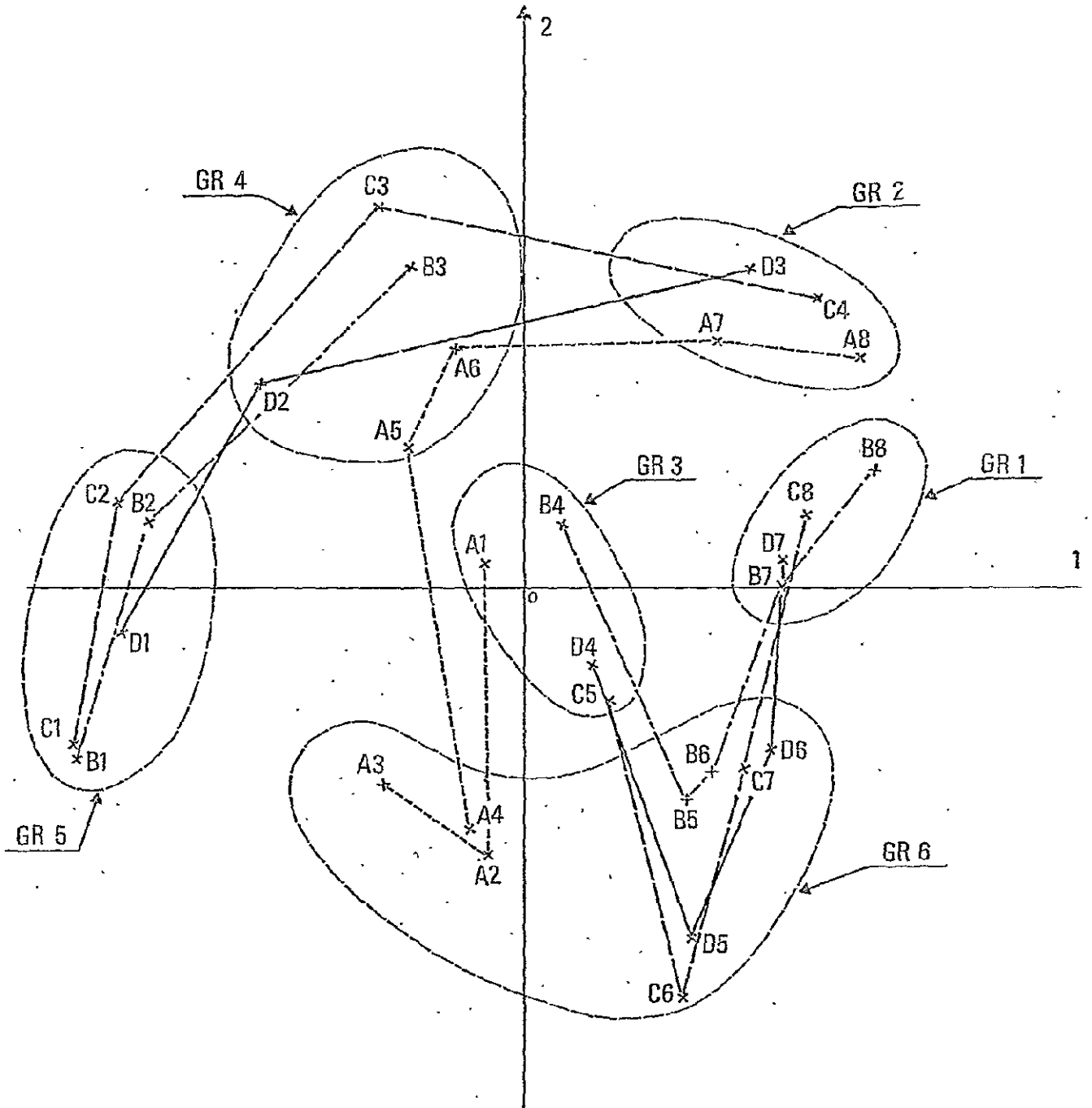an example of a such a map in Fig. 2.4.G.

Fig. 2.4.F - Display of first phase results in factor
plane 1-2.
Groups of coded equivalent spectral bands
were determined by hierarchical ascending
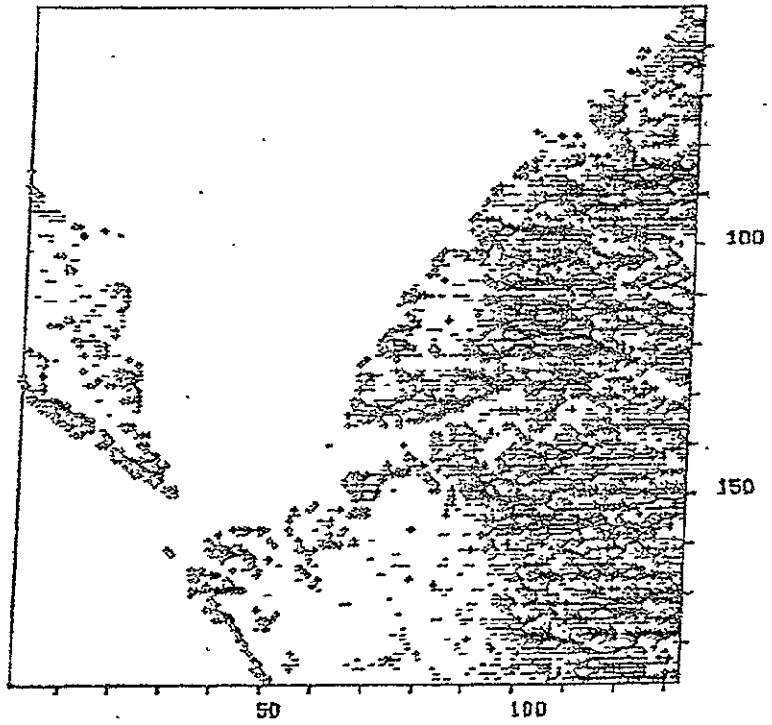classification.

Fig. 2.4.G - Display of pixels belonging to group 6
as determined in the first treatment phase.

This display of group 6 was obtained as a Versatec printer-
plotter hardcopy of a Tektronix graphic display.

The spectral coassistance phase involves the active partici
pation of the operator in assessing the spectral individual
of each group. This is done using spectral signature statis
for each group : radiance values histogram, average spectre
signature or even bidimensional histogram crossing two spec
bands. An MSS4/MSS7 bidimensional histogram is shown on
Fig. 2.4.H in which each pair of radiance values is assigne
to a group when a one to one relationship exists. A bispect
representation being unable to take into account the divers
of spectral signatures (in four spectral bands) there are
some pairs of radiance values which are assigned to several
groups at the same time. Such ambiguities are pin-pointed o
the display by a vertical bar symbol.

Taking account of these results, it was decided to pursue t
subdivision of groups 1, 2 and 3.

b - Results of the subdivision phase

The histograms of class 1, 2 and 3 were divided into 5
equipopulation intervals. The entire process was started ag
seperately for each group. Hereafter, we restrict our repre
sentation to the subdivision of group 3.

Correspondence analysis of the spectral signature of the pix
of group 3 was followed by an ascending hierarchical classi
cation whose dendogram is presented in Fig. 2.4.I. The simi
larities between transformed bands lead to the determination
of three spectral sub-groups.

After clustering, the individuality of each sub-group can be
assessed by the unimodality of its spectral histogram in MSS
(Fig 2.4.J). Separability between sub-groups is however bet
understood using the whole set of spectral bands. The averag
spectral signatures (Fig. 2.4.K) can be used for this purpos
One could note that for these objets, separability is maximu
in MSS4 and MSS5 but very low in MSS7. This can be noticed t
the overlapping of MSS7 histograms (Fig 2.4.J).

In the display generation (FRAC1) composite maps can be
produced in which pixels assigned to each sub-group are
represented by different symbols. Those maps were interacti
vely generated on the display console of the FRACAM system.
Fig.2.4.L to Fig.2.4.N are illustration to the subdivision
of groups 1, 2 and 3.

c - Interpretation phase

Each class now remains to be interpreted by taxonomic post-
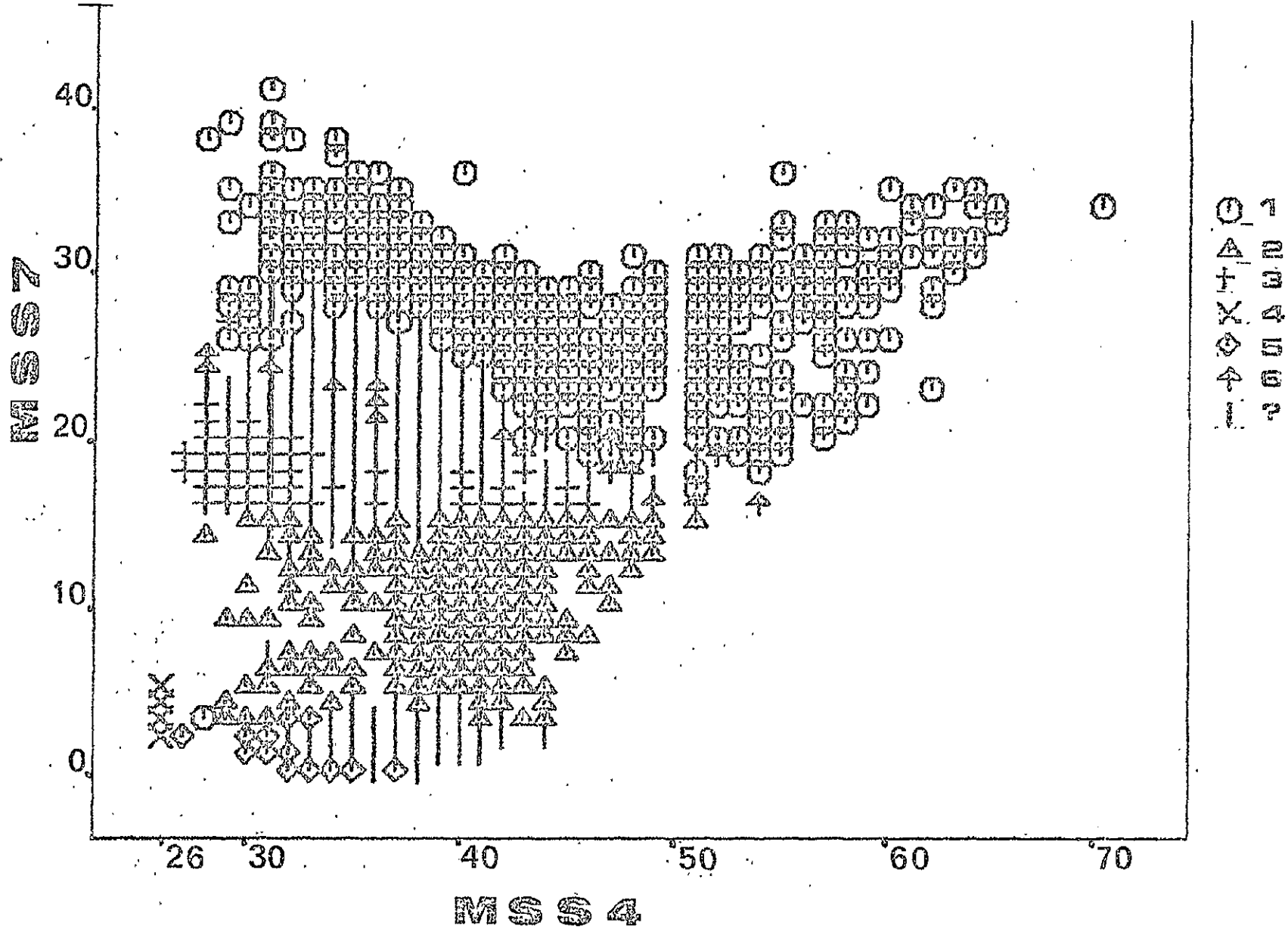assistance and the objects it represents must be identified.

Fig. 2.4.H - Joint MSS4/MSS7 histogram. Symbols are assigned to pair of radiance values which were associated to specific groups in the first phase of treatment
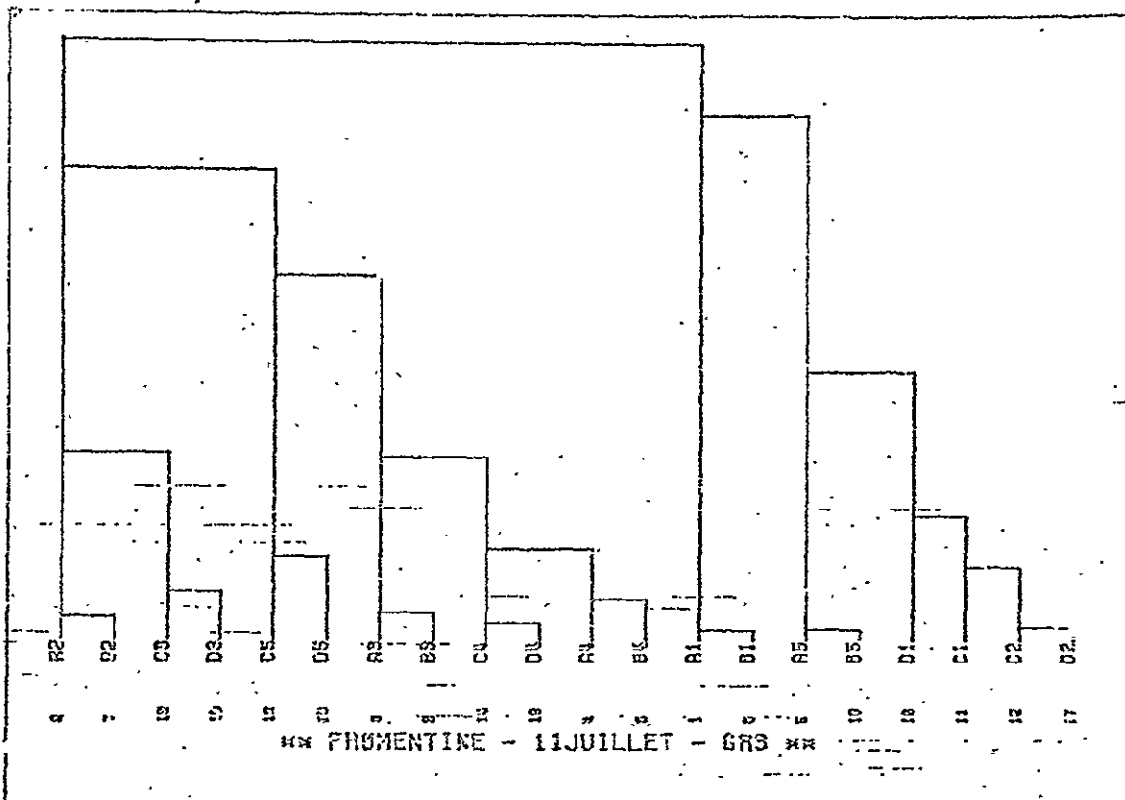
Fig. 2.4.I - Ascending hierarchical tree representation
of coded equivalent spectral bands determined
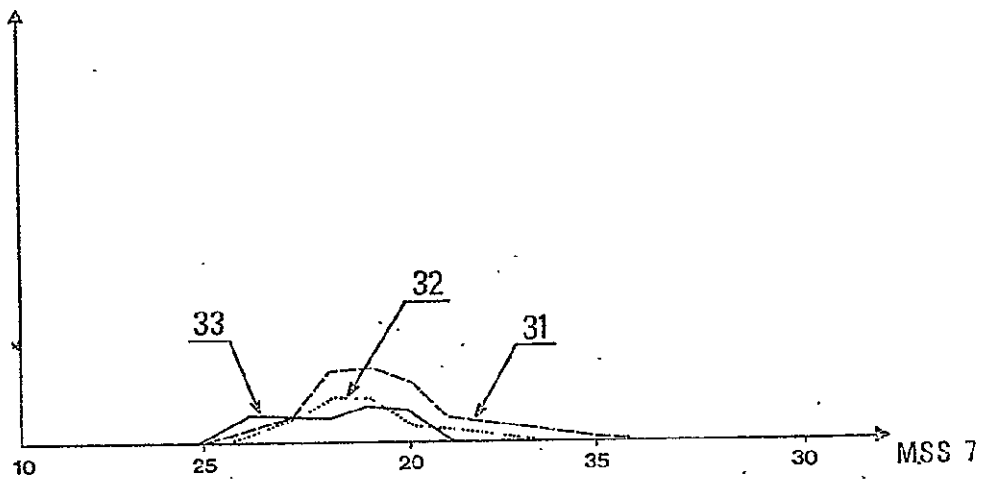by the subdivision of class 3 histograms

Number of
pixels

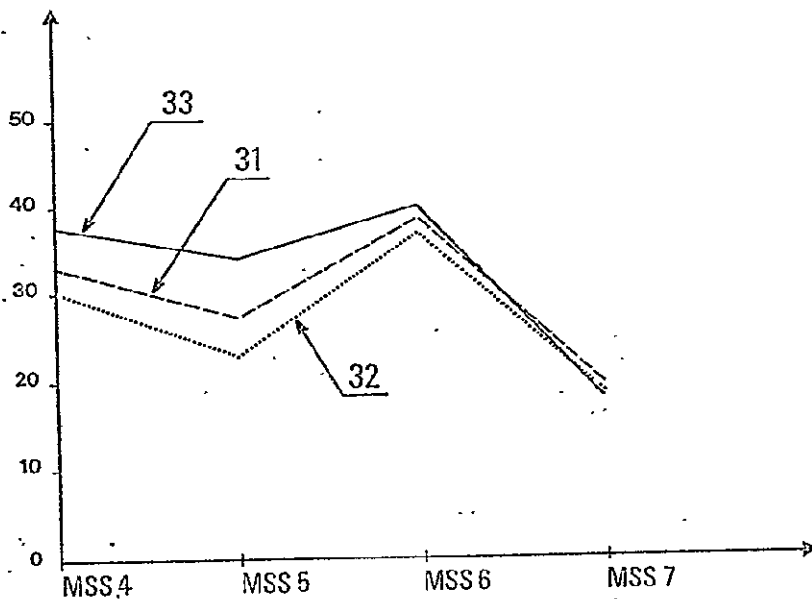Fig. 2.4.J - MSS7 histograms of groups 31, 32 and 33,
subdivided from group 3

Fig. 2.4.K - Average spectral signatures of subdivided
groups from group 3

Class 5 shows areas of clear water a indicated both by its
spectral signature and its location. These waters
are found to the North of the studied area :
satellite overpass took place at mid-flow. The sou-
thward tidal current through the Fosse du Fain carr
relatively clear water acrosa the Gois ford. Clear
water also occurs :

- extensively :

. in the South part of Bourgneuf Bay where pools
  between emerged banks hold relatively calm water
  which is low in sediment content.

. in the open sea off the Fromentine channel where
  waters are clear at mid-flow.

- locally : (as isolated pixels)

. in the Trou de Sebastopol (line 94, column 19),
  a pool in a dip formed by marine erosion during
  a storn which breached the main dyke. The breach
  was repaired by rebuilding the dyke round this
  dip, outside the polder.

. on the continent, in the pond of the new polder
  at Bouin (line 57, column 133). This pond formed
  in the lower part of this polder between the old
  seadyke which was destroyed by a storm in 1940
  and the new dyke rebuilt in 1965.

In these last two cases, the pools are so small tha
only one pixel was correctly identified as clear,
stagnant water. Surroundings pixels were only partl
covered in water and the classification process
misplaced them in another class.

Class 4 is sediment laden sea-water

Class 22 is associated to very turbid or shallow water.
In this case, the refletance spectrum is influenced
by the sea-bottom : this occurs, along Notre-Dame
de Monts point, in the outer tidal delta at
Fromentine. This class also outlines the border
between two environments. Thus, the bridge linking
the island of Noirmoutier to the continent at
Fromentine shows up as a row of class 22 and is
mixed with pixels of intermediate spectral signatur
overlaying two different environments.

Class 21 maps the emerged tidal flats at the time of overpas
These tidal flats line the western coast of the
island of Noirmoutier as well as the continent. The
also cover the top of sandbanks in the South of
Bourgneuf Bay. Class 21 is also found in ploughed
land or salt marsh areas physiographically similar
to tidal flats although they fall into a different
land use category. Finally, this class marks the
border between classes 22 and 11 with pixels of
intermediate spectral signature overlaying two
different environments.

Class 11 shows dry area of a dominantly mineral nature :
dry sandy beaches of Noirmoutier and the Monts
coast ; sand or shell banks in resses parts of the
Bourgneuf Bay coast ; sandy soils in the marsh and
the island of Noirmoutier ; sand and stone embankment
of the Bec de l'Epoids pit ; and several slighty
urban areas : Fromentine, parts of La Barre de Monts,
l'Epoids, la Fosse etc ...

Class 31 identifies vegetated areas such as the western part
of Monts forest (maritime pines), marsh channel
flats etc ...

Class 32 is similar in content and located nearby class 31 :
Monts forest (maritime pines, holm oaks) etc ...

Classes 12 and 13

show cultivated fields, but the crops in class 13
are partly bare (sandy plots on Noirmoutier Island)
whereas the crops in class 12 have more coverage :
on the Monts coast (near La Barre de Monts) or at
Crosniere.

Class 6 Shows grassy areas : pastures in marshes, coastal
dunes with psammophyte cover.

Class 33 shows marshes and damp border areas.

Its by combining a specific ground truth experience with
a general knowledge of spectral signatures that the operator
can give a meaning to the classes previously defined. For this
final step, which takes place after classification, we shall
use the term of taxonomic post-assistance.

Fig. 2.4.L - Cartography of subgroups 11, 12 and 13
obtained by subdivision of group 1.
Taxonomic interpretation follows :

11 - Built up areas, beach, dry sand

12 - Farming on calcareous, sandy soil
(Noirmoutier island, Crosnière)

13 - Farming along the Barre de Monts

Fig. 2.4.M – Cartography of subgroups 21, 22 obtained by
subdivision of group 2. Taxonomic interpretation is :
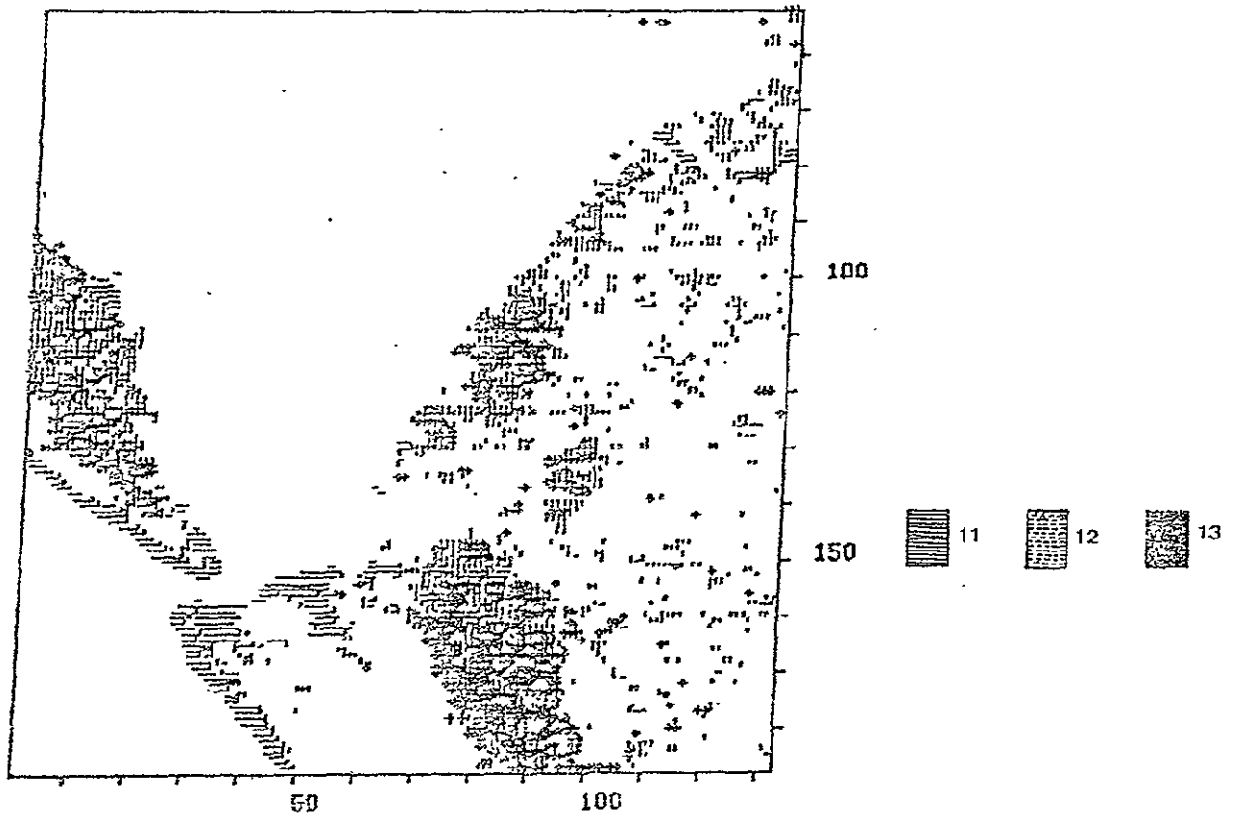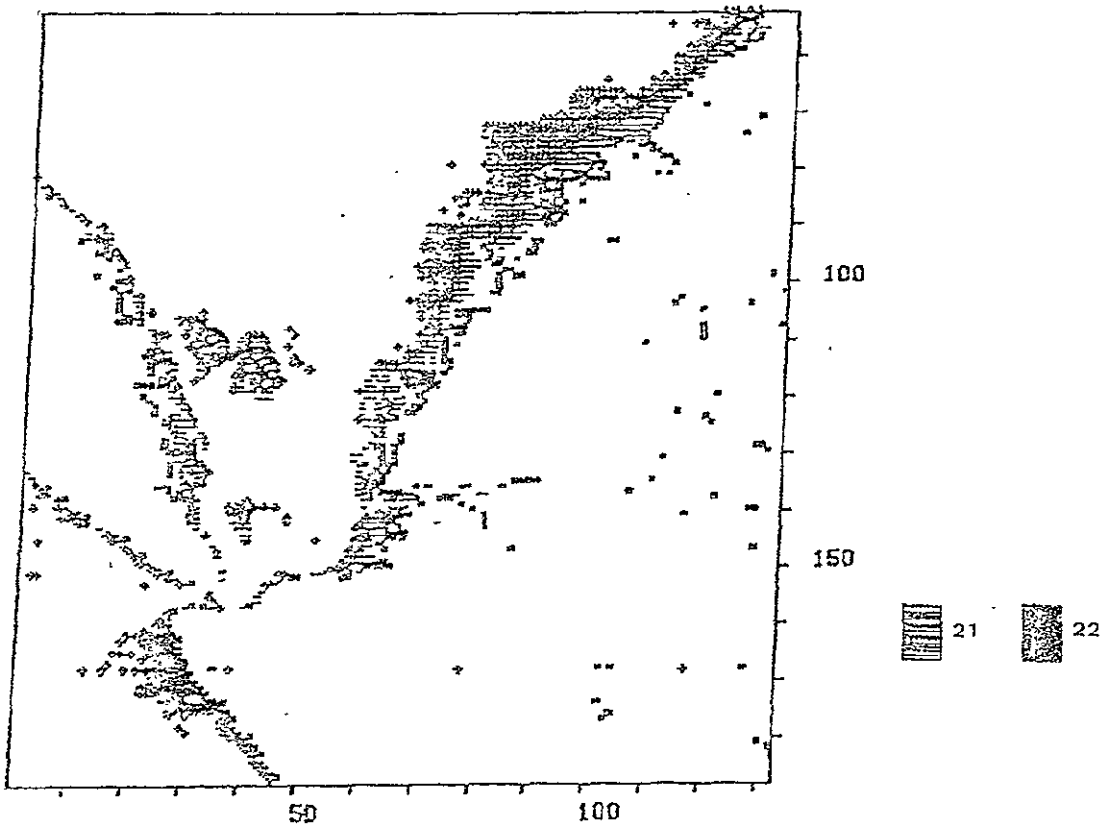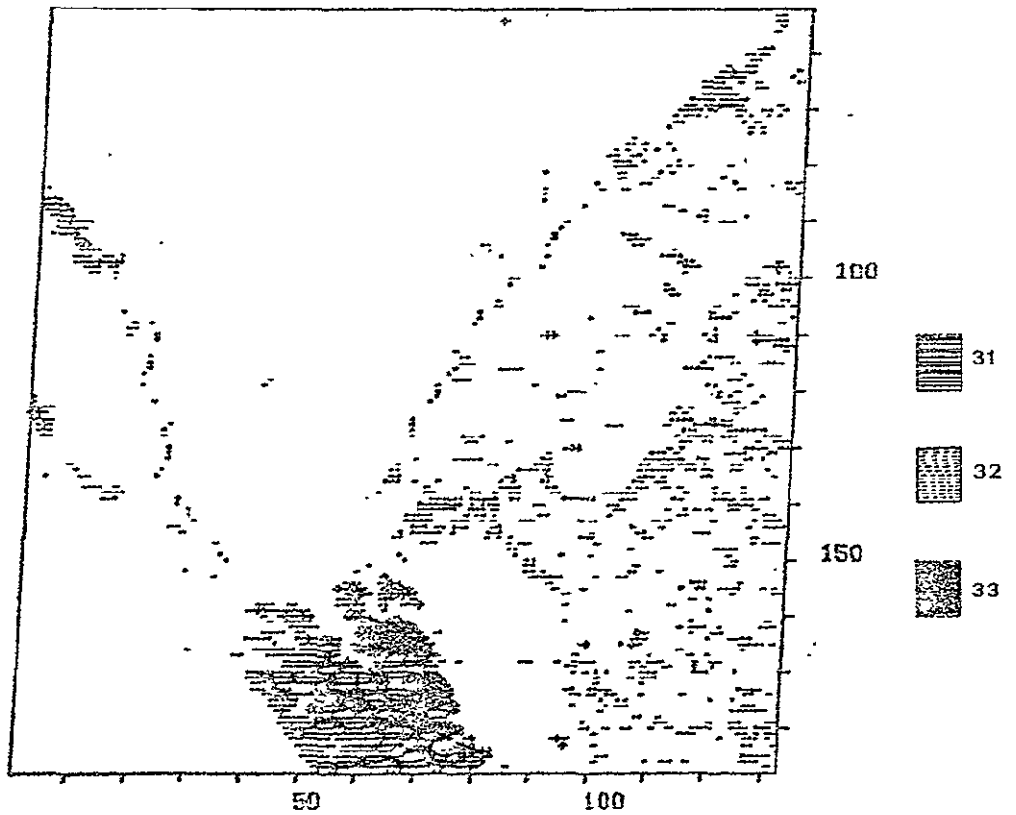
21 – Tidal flats

22 – Very turbid water

Fig. 2.4.N - Cartography of subgroups 31, 32 and 33
obtained by subdivision of group 3.
Taxonomic interpretation is :

31 - Fallow marshes, west of the Barre de Monts forest

32 - Damp border areas

33 - East of Barre de Monts forest

2. 5 - AUTOMATIC CARTOGRAPHY

The results from all the classification techniques developped in the
FRALIT experience can be output as colour maps on an ink plotter, by using
the programs described here.

2. 5.1 - The FRACARTO program (Fig. 2.5.A)

This program basically maps a pre-assisted classification
of multispectral data using spectral parameters selected and
input by the user. It replaces the FRACARTE program with
increased possibilities. It can also be used to map classifica-
tions resulting from other programs such a FRACAM (c.f. 2.4).

The main possibilities offered are :

- Simultaneous processing of data from two (or more) different
  images using all 8 (or more) spectral bands for LANDSAT.

- Raw or smoothed data output, using a majority vote type
  decision in the matrix surrounding each pixel ; this process
  can be iterated, and/or used conditionally.

- Mapping of each pixel by a given colour and symbol or
  contouring of areas with identical taxonomic content.

- Attainement of the best possible drafting speed according
  to the type of output, with automatic and permanent control
  of ink levels in each pen.

The user first selects the digital image, or images, to be
processed, and defines the scale and boundaries of his area
of interest.

If the proposed map exceeds the dimensions of the plotter, a
sampling procedure is provided, enabling one in n lines (and
one in n columns) to be mapped.

This possibility can also be used to avoid the sixth-line
banding often found in LANDSAT data. The map border is
annotated with line and column tick-marks. In order to save
time and lower costs, it is possible to leave blank an area
of little interest within the map boundaries by specifying
the appropriate lines and columns.

This program is currently implemented on the CNRS IBM 370/178,
computer using a three-pen BENSON plotter in the offline mode.
Pen selection is programmable and maps use up to 6 colours.

For offset printing purposes, an option in the program enables
a separation to be made of each colour overlay. These are drawn
in black on a stable base (Mylar) to conserve maximum accuracy
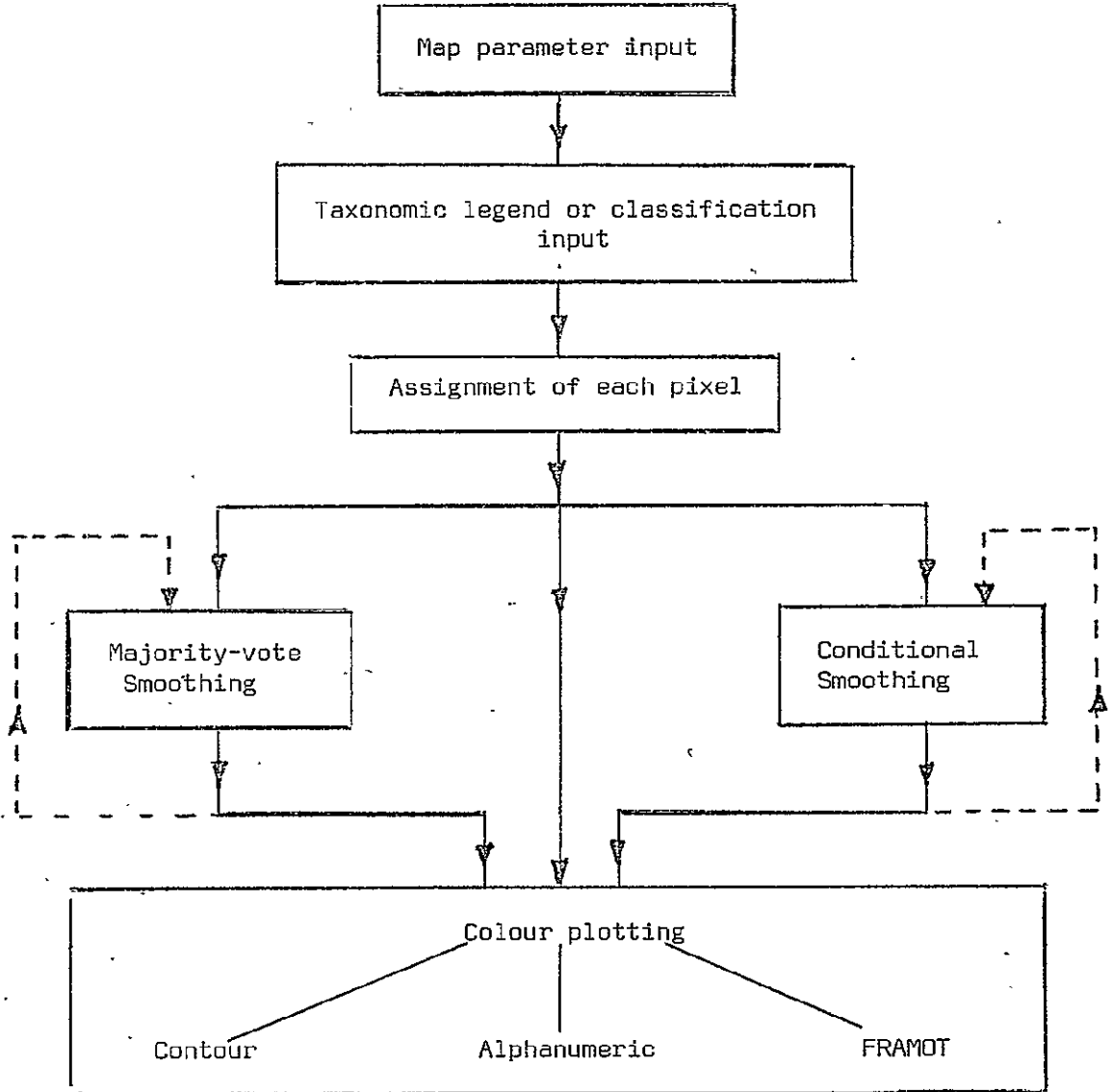in the preparation of the offset plate.

Fig. 2.5.A - Main functions of the FRACARTO
program.

Dotted paths indicate possible iterations
of the smoothing process.

When used for a pre-assisted classification, FRACARTO annotates
the map with a key giving spectral characteristics of each class
and the corresponding symbol. In every case, each symbol is
followed by the number of pixels, the area covered in km^2, and
two parallel caption lines (which can be bilingual).

Raw data mapping often shows up striping, wrong data values or
immediate pixels with spectral signatures mixing the values of
contrasted terrain units. The latter is a major cause of mis-
classification, but all three effects can be avoided to some
extent by smoothing the data before map edition.

As the bad pixels can be differentiated from the surrounding ones,
smoothing requires a form of neighbourhood analysis. Optionnally,
two types of smoothing are available :

> - majority-vote : here a pixel is replaced by the most
>   frequent one in the surrounding neigbourhood matrix. The
>   user selects the size of the neighbourhood matrix (3x3 or
>   5x5) and, if required, the number of iterations. This
>   techniques is fairly efficient, but eliminates much of
>   the fine detail in an image (Fig. 2.5.B and 2.5.C).

> - conditional : this was developed to eliminate intermediate
>   values. MSS7 spectral signatures are compared for the eight
>   pixels surounding the one being smoothed. Striping is
>   detected by comparing the current line with the ones
>   immediately before and after it. If these are identical
>   and the current pixel slightly different, its value is
>   replaced by majority vote. The resulting map is more
>   accurate than simple majority vote (Fig. 2.5.D)

The results of classification smoothing can be compared to the
corresponding unprocessed classification (Fig. 2.5.E).

After the optimal smoothing phase, mapping is carried out colour
by colour, in one of three modes :

Alphanumeric : each pixel is individually identified by an
alphanumeric symbol. This is costly in plotting
time as each symbol requires one or more pen
up-down calls.

FRAMOT : a set of symbols has been selected to give varied
tonal values and speed of execution (Fig. 2.5.F).
This has been found most useful both for variety
and efficiency of use.

Contour : identically classified pixels are oulined in groups.
This gives the quickest results but the maps are
only satisfactory if the classification is
previously smoothed to eliminate isolated pixels.

Fig. 2.5.B - Example of majority vote smoothing with one iteration.
Map of Fromentine area at a 1/50 000 scale generated from
LANDSAT2 data acquired on 29 July 1975 (E2188-10181)

Fig. 2.5.C - Example of majority vote smoothing with two iterations
Map of Fromentine area at a 1/50 000 scale generated from
LANDSAT2 data acquired on 29 July 1975 (E2188-10181)

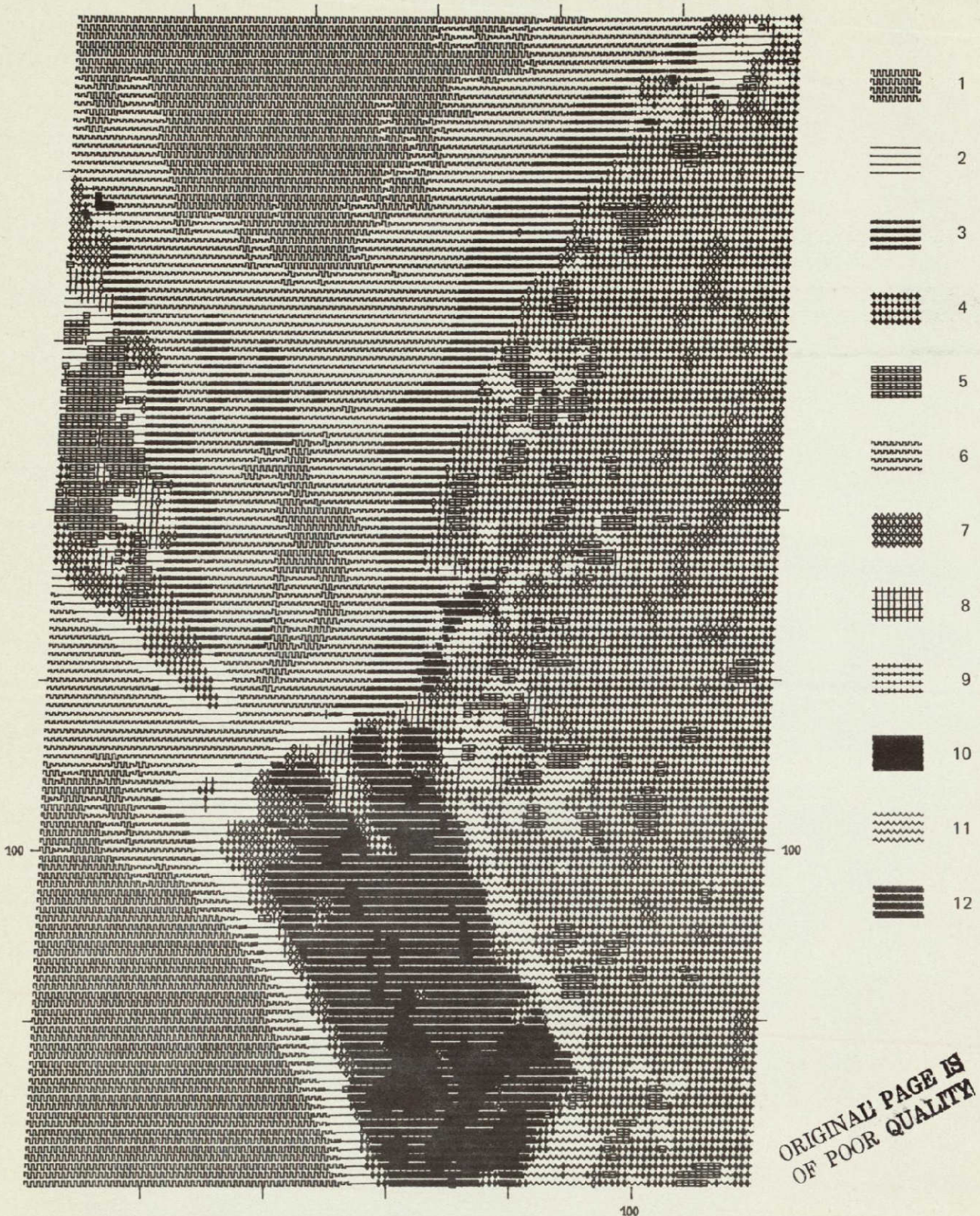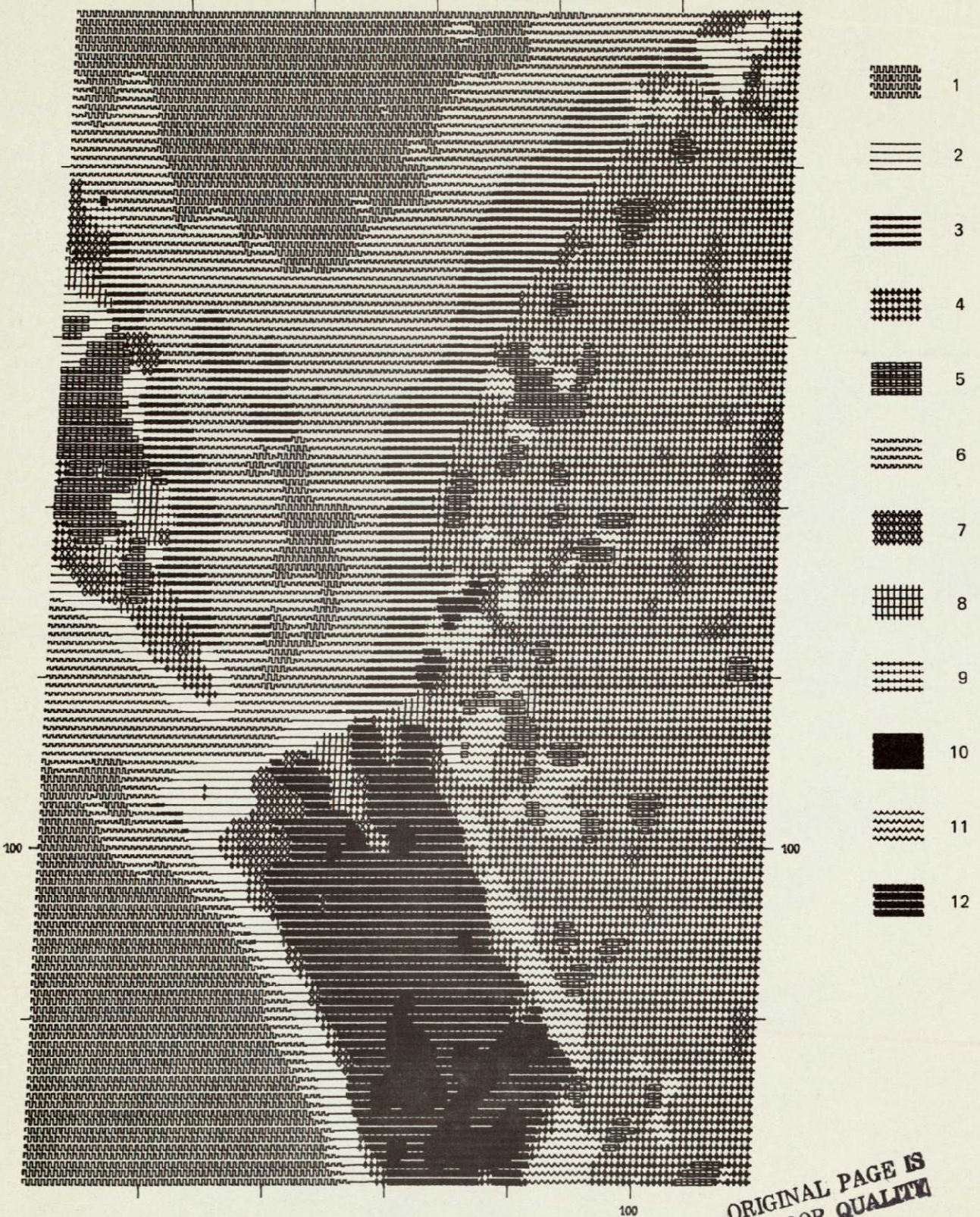Fig. 2.5.D - Example of conditional smoothing with two iterations
map of Fromentine area at a 1/50 000 scale generated
From LANDSAT2 data required on July 1975 (E2188-10181)

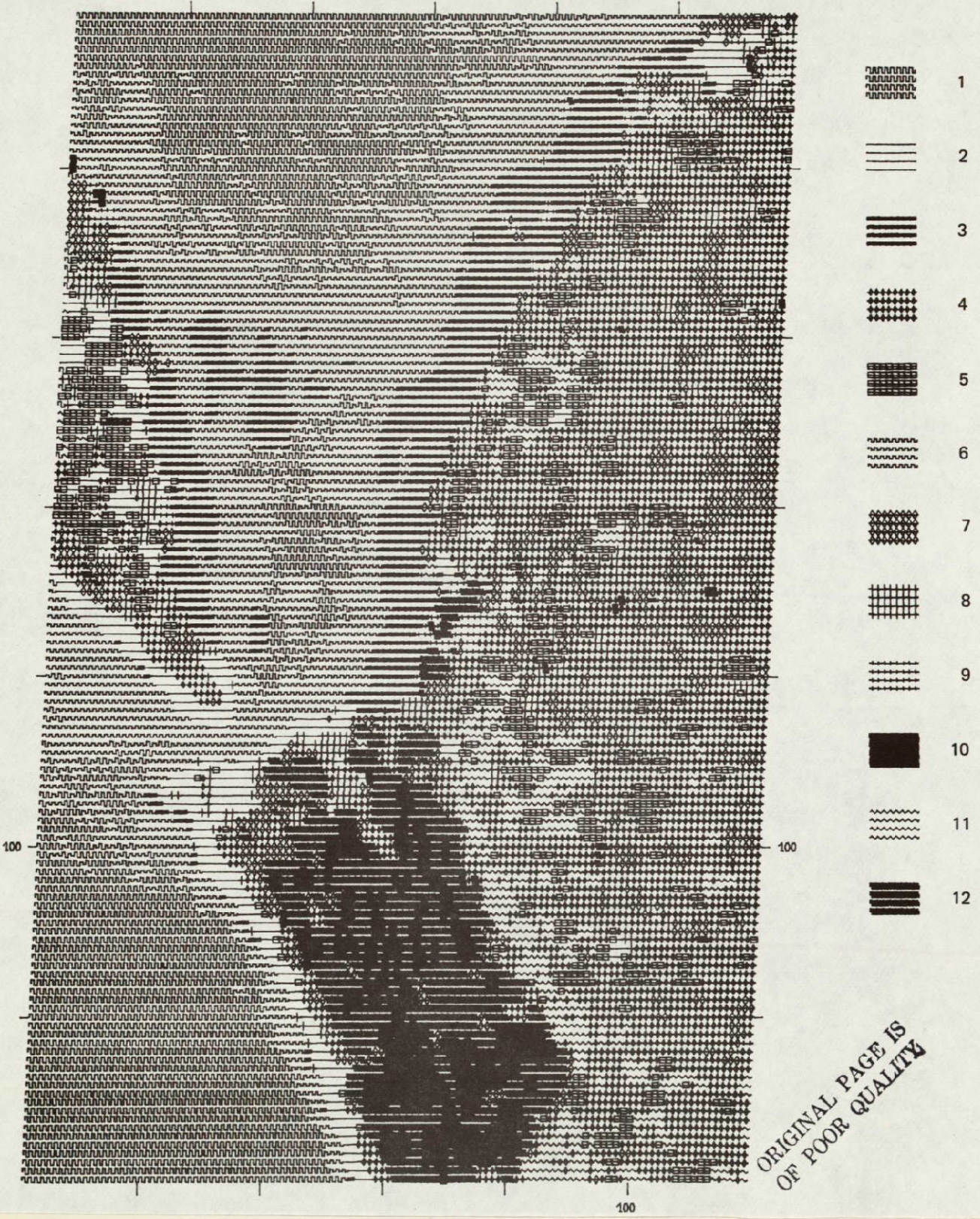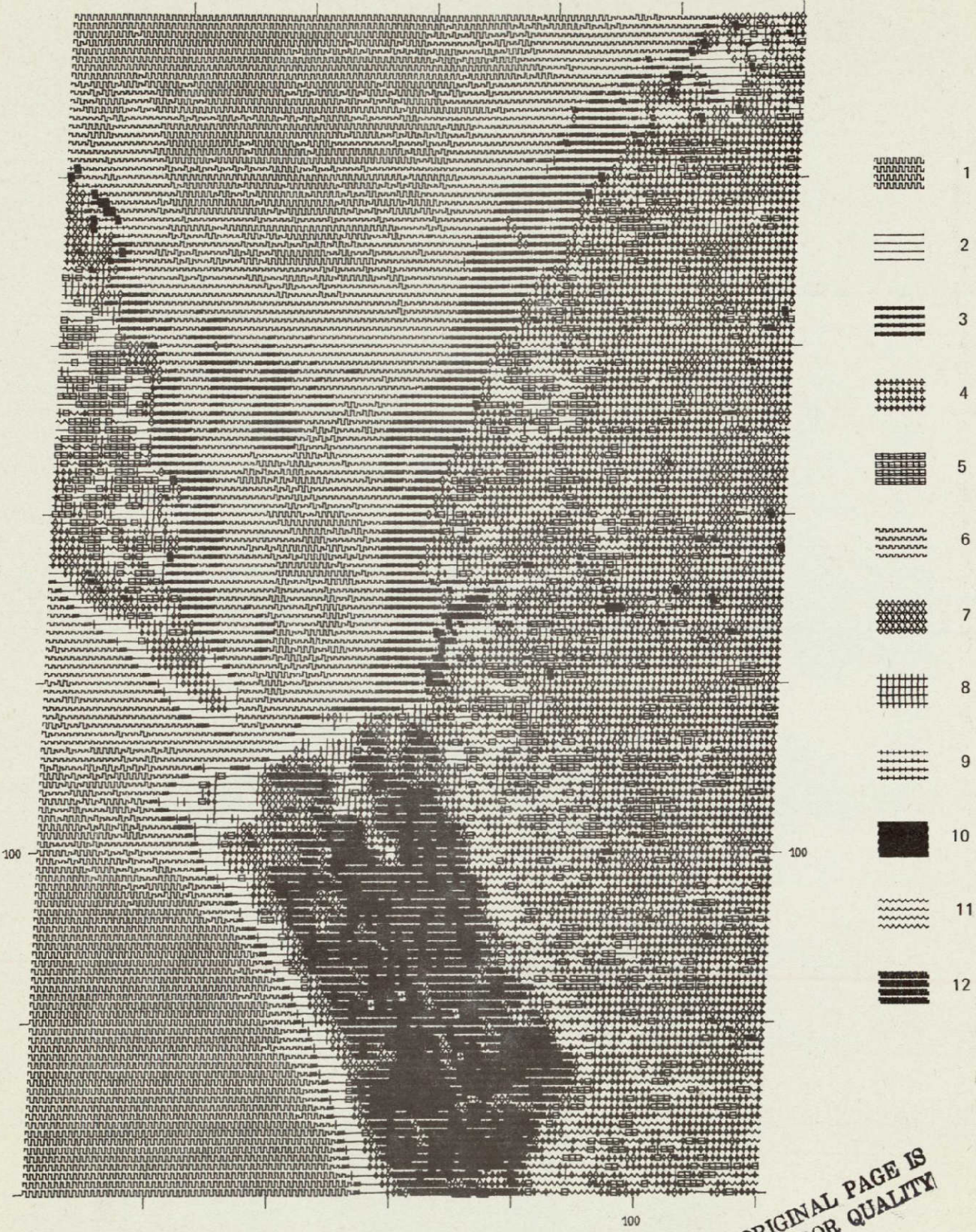Fig. 2.5.E - Example of classification résults before smoothing
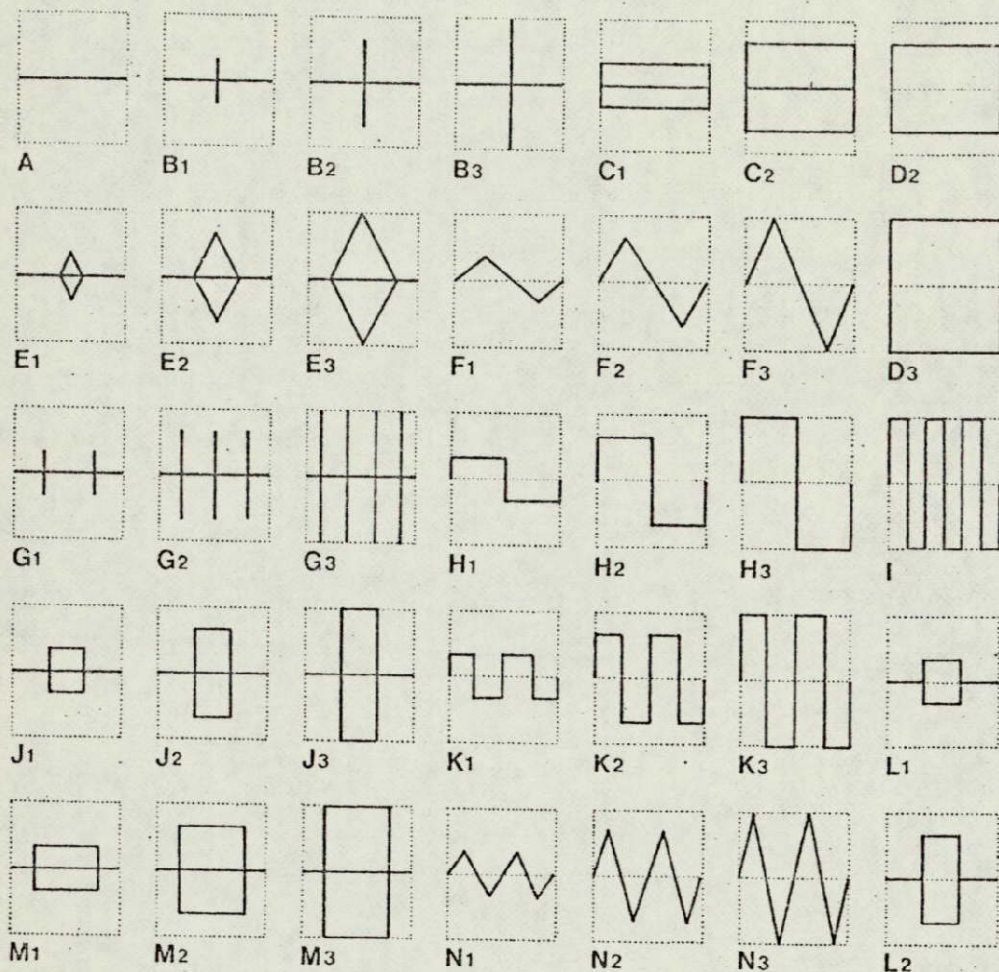
Fig. 2.5.F - FRAMOT symbol set
Some symbols are height parameterized
with simple (1), double (2) and triple (3)
height. All symbols are bounded by the same
rectangular grid.

2. 5.2 - The FRATHERM program

FRATHERM is a version of FRACARTO adapted for mapping visible
and infra red data from the NOAA VHRR. Two versions are presently
in use :

The first one is a FRACARTO adapted to the output from the TSS
(Sea Surface Temperature) programme. The two channels available
can be combined and the graphic options available with FRACARTO
are available.

The second one has been perfected to make the best possible choic
of colour or B/W scales for single-channel mapping. I/O transfers
and computer time are reduced to a minimum (Fig. 2.5.G).

Well designed, legible map output is the standard format for FRALIT
results. Experience shows that other types of output (line printer
cartography, tabular data, etc ...) are basically unattractive to potentia
users. On the contrary, a properly designed map, scaled for compatibility
with standard topographic map overlays has high user value both for resear
(geography, biology, sedimentology, oceanography) and applications (urban
or country planning). For these reasons a great deal of effort has been
put into the development of sophisticated automatic mapping procedures.
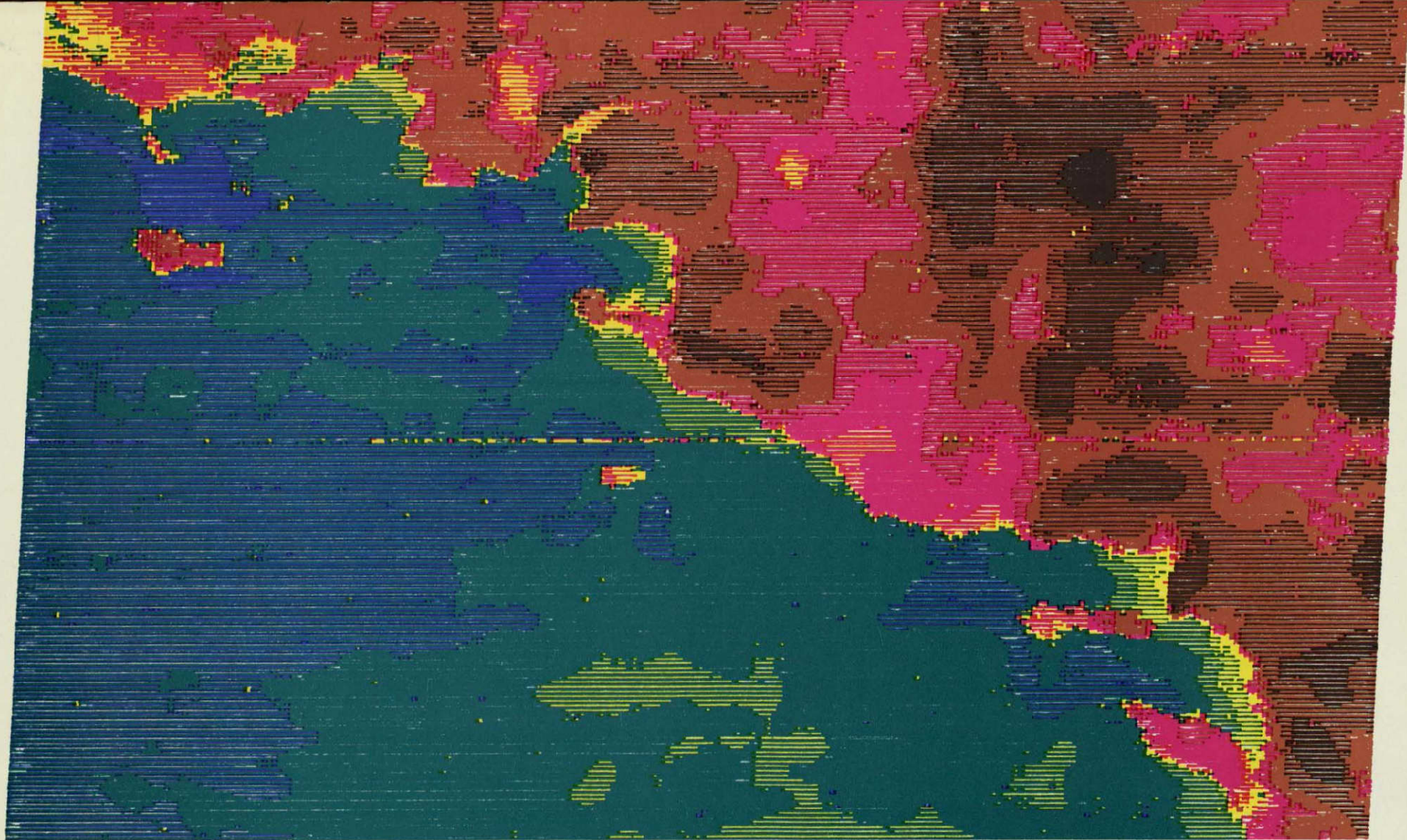
ORIGINAL PAGE IS
OF POOR QUALITY
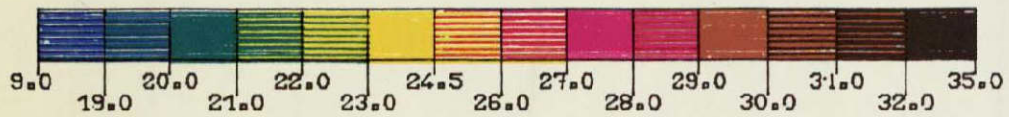
TEMPERATURE EN DEG. CELSIUS

9.0   19.0   20.0   21.0   22.0   23.0   24.5   26.0   27.0   28.0   29.0   30.0   31.0   32.0   35.0

FRATHERM - VERSION 2.2
LIGNES   21   A 200   /1
COLONNES 51   A 320   /1
ECHELLE: 1.1000000
JANVIER 1977

Fig. 2.5.G - NOAA thermography generated by the fratherm program
Satellite overpass was on 06/08/75 at 9H 30 MN TU.

2. 6 - GROUND TRUTH RADIOMETRIC MEASUREMENTS

Object réflectances measured by each of the four spectral bands of the MSS system build the LANDSAT spectral signature of this object.

The use of an EXOTECH radiometer (model 100-A) helps in undertaking ground truth operations as well as the necessary measurement of atmospheric parameters. It can be used for :

- the prediction of object LANDSAT signatures by "in situ" measurements

- the transformation of measured radiance by the MSS system of the LANDSAT satellite into a ground albedo which is independent of sun angle as well as atmosphere parameters.

2. 6.1 - The EXOTECH radiometer and its control equipment

The EXOTECH radiometer, model 100-A, acquired by Ecole Normale Superieure (contrat CNES 222/75) is a multichannel ground truth radiometer suitable for point by point measurement. It its present configuration the EXOTECH radiometer is made of a measurement optical head made by EXOTECH and a power source as well as a monitoring console built by Ecole Normale Superieure.

a - The EXOTECH radiometer

It is a four channel radiometer with seperate sensor optics, filter, detector and analog amplifier for each channel. It is capable of giving four simultaneous measurements is a non-sequential fashion. Simultaneous measurement in the four channels is a compulsory feature when sensing is to be done from a plane or from a ship.

The spectral characteristics of each of the four channels match the MSS spectral bands of the LANDSAT satellites :

channel 1 = band NDPF4 = 0.5 to 0.6 μm,

channel 2 = band NDPF5 = 0.6 to 0.7 μm,

channel 3 = band NDPF6 = 0.7 to 0.8 μm,

channel 4 = band NDPF7 = 0.8 to 1.1 μm.

The equipment is sold with 3 switchable types of sensor optics with the following fields of view :

Field of view	Aperture shape	Sensor optics
1°	square	lens
15°	circular	diaphragm
2π steradian	hemispheric	diffuse surface

The hemispheric sensor with a 2π steradian aperture enables the measurement of half-space illumination (in watts/cm^2) and is suitable for the measurement of down-welling solar illumination. The 15° circular aperture sensor enables the measurement of object radiance (in watts/cm^2.sr) and is suitable for ground truth collection. The 1° square aperture sensor measures the radiance of a target 260 feet wide (260 ft = 79.2 m) when mounted in a plane flying at an altitude of 2300 meters. This target is identical in geometry to a LANDSAT pixel.

The output signal of each of the four channels is a continuous voltage bounded by 0 and 5 volts. For each channel, four different gain factors can be selected. They are respectively of : 1, 5, 25 and 125.

The transformation of output volts into radiometric units is done by the use of a calibration factor which can take one of twelve values corresponding to a specific association between a channel and a type of sensor. Let us point out that the calibration of this type of radiometer sensing in the visible part of the electromagnetic spectrum is a difficult task. It is highly dependent on the precision of the reference source used during the calibration phase.

Consequently the precision uncertainty of the radiometer is no better than ± 5 %. The long term variations in detector characteristics must also be taken care of by frequent recalibration.

b - Power source and monitoring console

This console is made of a separate equipment box which helds : four micro-voltmeters allowing the simultaneous display of the four channels output, a Cadmium. Nickel accumulator power source and a built-in charger. A fifth commutator on the monitoring panel can be used in order to check on the accumulator charge.

2. 6.2 - Atmospheric parameters measurement

The EXOTECH radiometer (model 100 A) is suitable for the measurement of atmospheric parameters such as : atmospheric turbidity, water concentration as well as other absorbant materials. These measurements are necessary in order to transform the satellite measured radiances into ground albedo independent of solar angle and atmospheric parameters. This method has been introduced by R.H.Rogers and K. Peacock : A Machine Processing of ERTS and Ground Truth Data ; Conference proceedings of Machine Processing of Remotely Sensed data (LARS). October 16-18th 1973 at Purdue University - IEEE Catalog n° 73 CHO 834-2GE, pp 4A14-4A27.

Mesure de luminance L_c du ciel tel que $H_{sr} = H_{ss}$
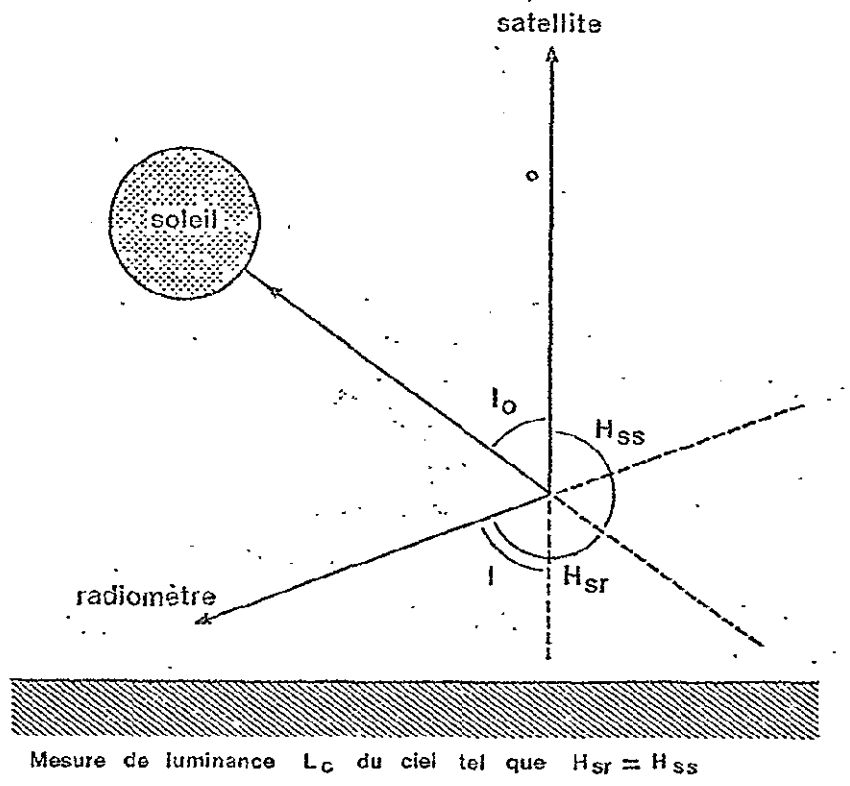
Measurement of sky radiance L_c such that $H_{sr} = H_{ss}$

Fig. 2.6.A - Diffusion toward radiometer and satellite

If ground reflection is perfectly diffuse, satellite measured radiance at nadir angle can be expressed as :

$$L = \frac{R_T}{\pi} \ E \ T_A + L_A \qquad (1)$$

where :

L = measured satellite radiance

R_T = ground albedo

E = irradiance of a perfectly horizontal ground target

T_A = atmospheric transmittance from the target to the sensor per unit of air mass

L_A = atmospheric path radiance

The radiance can be decomposed into two terms :

$$E = E_o \ T_A^m \ \cos I_o + E_D \qquad (2)$$

where :

E_o = solar irradiance outside atmosphere

E_D = diffuse sky irradiance

I_o = sun zenith angle

$m = \dfrac{1}{\cos I_o}$ is the air mass along I_o direction

Thus, the relationship between L and R_T is expressed by the following formula :

$$R_T = \frac{(L - L_A) \ \pi}{T_A \ (E_o \ T_A^m \ \cos I_o + E_D)} \qquad (3)$$

The different terms of relation (3) can be estimated by radiometric measurements at the time of satellite overpass. Solar angle I_o and air mass m are easy to determine. Diffuse irradiance E_D from the sky is measured by solar occultation. As E and E_D are measured and F_o is known from standard models, T_A can be de determined by equation (2).

The diffuse air radiance L_A is estimated from the measurement of sky radiance L_C so that the angle between viewing direction and solar path H_{SR} is equal to the angle between the viewing of sun and satellite H_{SS}.

Diffusions towards radiometer and satellite are proportional in such a system geometry, the corresponding ratio being a function of the difference in optical path for the two directions (Fig. 2.6.A) :

$$L_P = L_C \ \frac{1 - T_A}{1 - T_A^m}$$

This method is only applicable for zenith angles I_o smaller than 45°. When the sun zenithal angle is larger than 45°, viewing of the sun has to be done for I_o smaller than 45° and subsequently corrected.

The main interest in such an approach is to reduce all satellite measurements to physical albedo values. But it is also a fact that in such radiometric schemes, good calibration is a critical factor.

2. 6.3 - Ground truth measurements

The EXOTECH radiometer is also suitable to ground-truth measurements which aim at comparing satellite measured radiances and ground measured albedo.

This method has been introduced by H.W. Smedes, R.L. Hulstrom and K.J. Ranson : The mixture problem in computer mapping of terrain : improved technique for establishing spectral signatures, atmospheric path radiance and transmittance. Houston, NASA Earth Resources Survey Syposium, June 1975.First comprehensive symposium on pratical application of earth resources survey data, volume 1-B, pp 1099-1159.

If ground reflection is perfectly diffuse, a satellite viewing at nadir angle would measure the following radiance (equation 2) :

$$L = \frac{R_T}{\pi} \cdot E \cdot T_A + L_A$$

and the target reflectance is expressed as :

$$K_T = (L - L_A') \times \frac{\pi}{H * T_A} \qquad (5)$$

If reflectance of a set of targets is measured at ground level or at a small altitude, the comparison of the values of R_T and L shows a linear relationship :

$$L = a \times R_T + b \qquad (6)$$

The intercept is equal to the atmospheric diffusion : $b = L_A$ and the slope of this line is related to the downwelling irradiance and the atmospheric transmittance $a = \frac{E \cdot T_A}{\pi}$ are presented on Fig. 2.6.B.

Consequently the spectral signature of an object in albedo related to the four spectral bands of the LANDSAT MSS system can be determined as follows :

$$\left\{ R_i = (L_i - L_{Ai}) \times \frac{\pi}{H_i \cdot T_{Ai}} \mid i \in I \right\}$$

where I is the set of the four MSS sensors
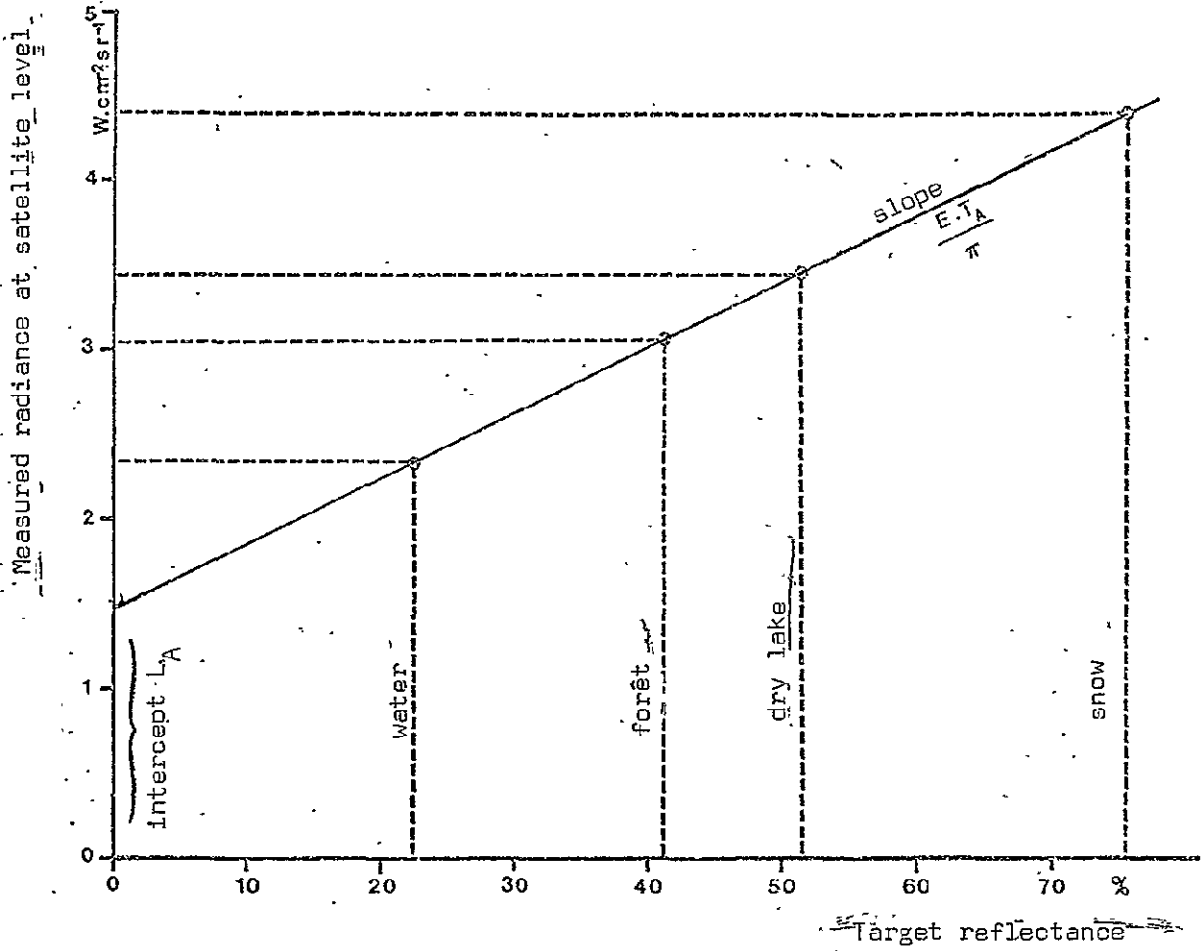
Fig. 2.6.B - Relationship between measured reflectance
             at ground level and nadir radiance measured by
             satellite

This method has several positive aspects :

- the value of the measured atmospheric radiance is a
  direct contribution to the signal sensed by the
  satellite radiometer,

- measurement of atmospheric effects is done in a global
  way(downwelling solar irradiance and atmospheric transmiss
  effects are integrated in the same term),

- no specific ground equipment set-up is necessary.

However two type of constraints are present :

- position of ground targets has to be known with a
  high degree of geometric precision,

- measurements usefulness is related to the quality of
  ground measured reflectances which implies a good
  knowledge of temporal variations of object signatures.

2. 6.4 - Typical ground measurements

Several "in situ" radiometric measurements were conducted in
various-environments :

- on the tidal flats and marine marshes of the Mont St-
  Michel bay,

- in harbour waters, on beaches and coastal ponds along
  the coast   of Golfe du Lion,

- in the Fromentine test area,

- on the lawn of the Scientific campus of University of
  Villeneuve d'Ascq , near Lille,

- on snow cover at the Ecole Normale Superieure in Montrouge,

- on several samples taken from the beaches and littoral
  sand dunes of the coasts of France (measurements were
  made in natural sun light).

These measurements were performed in spectral bands matching
these of the LANDSAT MSS system, using two types of radiometers

- 820 - 10 A ERTS radiometer head manufactured by Gamma
  Scientific,

- EXOTECH 100 - A ERTS radiometer manufactured by EXOTECH

Each measurement sequence is made of :

- reflectance R_i

$$\left\{ R_i = (L_{ci} \cdot G_{ci}) \times 100 \ / \ (L_{vi} \cdot G_{vi}) \ \middle| \ i \in I \right\}$$

- normalized reflectance R_{Ni}

$$\left\{ R_{Ni} = R_i \ / \ R_1 \ \middle| \ i \in I \right\}$$

with :

L_c = voltmeter output when measuring the target radiance

G_c = gain set when viewing the target

L_V = voltmeter output when measuring the downwelling irradiance

G_V = gain set when viewing the sky

i = channel index

Measurements are presented on the following tables (Tab. 2.6.C)

Tab. 2. 6.C - Examples of spectral signatures

e = Laboratory sample studied in daylight

d = depth of Secchi disk (in meters)

E = EXOTECH radiometer, model 100-A

G = Gamma Scientific radiometer, model 820-10 A

Sample		Material	Site	reflectance (in %)			
				MSS4	MSS5	MSS6	MSS7
01	E	beach sand	Mont St-Michel Bay	31 1	34 1.10	42 1.35	41 1.32
02	E	beach sand with shells	Mont St-Michel Bay	52 1	55 1.06	65 1.25	68 1.31
03	E	shell bar	Mont St-Michel Bay	67 1	69 1.03	84 1.25	82 1.22
04	E	very dry tidal clay	Mont St-Michel Bay	32 1	30 0.94	37 1.16	36 1.13
05	E	dry tidal clay	Mont St-Michel Bay	28 1	29 1.4	34 1.21	30 1.07
06	E	humid tidal clay	Mont St-Michel Bay	24 1	22 0.92	27 1.13	26 1.08
07	E	Salicorne field	Mont St-Michel Bay	11 1	10 0.91	53 4.82	69 6.27
08	E	Obione field	Mont St-Michel Bay	12 1	10 0.83	63 5.25	86 7.17

Tab. 2.6.C (Suite)

Sample	Material	Site	Reflectance (in %)			
			MSS4	MSS5	MSS6	MSS7
09 E	beach sand with shells	Saint Enogat	63 1	65 1.03	79 1.25	81 1.29
10 eE	beach sand	Deauduc point	42 2	42 1	54 1.29	54 1.29
11 eE	beach sand	Soulac	64 1	70 1.09	88 1.38	88 1.38
12 eE·	damped beach sand	Soulac	38 1	38 1	50 1.32	50 1.32
13 eE	dune sand	Arcay spit	58 1	67 1.16	89 1.53	92 1.59
14 eE	beach sand	Arcay spit	49 1	56 1.14	76 1.55	77 1.57
15 eE	dry pasture	Dol marsh	14 .1	15 1.07	39 2.79	50 3.57
16 eE·	dune sand	Kersidan	69 1	76 1.10	93 1.35	93 1.35
17 eE	dune sand	Trevignon	49 1	61 1.24	90 1.84	93 1.90
18 eE	dune sand	Rospico	45 1	54 1.20	82 1.82	89 1.98
19 eE	dune sand	Kerboven	53 1	61 1.15	90 1.70	96 1.81

Tab. 2. 6.C (Suite)

Sample		Material	Site	reflectance (in %)			
				MSS4	MSS5	MSS6	MSS7
20	eE	beach sand	Guimorais	55	66	82	81
				1	1.20	1.49	1.47
21	eE	beach sand	Keloidan	66	66	81	81
				1	1	1.23	1.23
22	G	snow	Montrouge	70	78	68	62
				1	1.11	0.97	0.89
23	G	snow	Montrouge	58	66	64	60
				1	1.14	1.10	1.03
24	G	snow	Montrouge	60	70	68	65
				1	1.17	1.13	1.08
25	G	thawed lawn	Lille	22	23	68	90
				1	1.05	3.09	4.09
26	G	lawn	Lille	9	10	42	57
				1	1.11	4.67	6.33
27	G	beach pebbles	Collioure	14	17	25	21
				1	1.24	1.79	1.53
28	G	beach pebbles	Sete	18	15	32	36
				1	0.83	1.75	1.98
29	G	dry beach sand	Collioure	18	21	20	20
				1	1.19	1.14	1.13
30	G	dry beach sand	Port la Nouvelle	22	28	30	33
				1	1.30	1.37	1.52

Tab. 2. 6.C (Suite)

Sample		Material	Site	reflectance (in %)			
				MSS4	MSS5	MSS6	MSS7
31	G	dry beach sand	Fontignan	15 1	23 1.56	24 1.58	26 1.71
32	G	dry beach sand	Fontignan	10 1	13 1.32	14 1.41	16 1.58
33	G	rippled dry beach sand	Port la Nouvelle	24 1	31 1.32	29 1.21	36 1.50
34	G	beach sand under film of water	Port la Nouvelle	.8 1	11 1.40	11 1.44	17 2.13
35	G	beach sand under film of water	Sete	16 1	24 1.51	26 1.62	27 1.67
36	G	beach sand under film of water	Sete	17 1	25 1.46	28 1.61	31 1.79
37	G	rippled damp beach sand	Port la Nouvelle	11 1	12 1.05	16 1.39	26 2.29
38	G	damp beach sand	Port la Nouvelle	16 1	21 1.33	21 1.38	25 1.63
39	G	damp beach sand	Sete	25 1	34 1.32	37 1.46	38 1.50
40	G	damp beach sand	Frontignan	19 1	25 1.33	25 1.33	30 1.61
41	G	shell sand	Sete	27 1	37 1.39	42 1.57	50 1.87
42	G	shells and pebbles	Sete	36 1	45 1.26	47 1.32	66 1.86

Tab. 2. 6.C (Suite)

Sample		Material	Site	reflectance (in %)			
				MSS4	MSS5	MSS6	MSS7
43	G	shells	Sete	24	39	45	52
				1	1.64	1.89	2.19
44	G	shells	Frontignan	14	20	24	27
				1	1.40	1.67	1.89
45	G	muddy sand	Sete	10	14	17	21
				1	1.34	1.67	1.99
46	G.	muddy sand	Sete	12	18	19	21
				1	1.43	1.57	1.73
47	G	muddy sand	Sete	13	18	19	24
				1	1.39	1.48	1.63
48	G	muddy sand	Sete	15	21	21	24
				1	1.44	1.45	1.59
49	G	muddy sand with film of water	Sete	18	23	26	31
				1	1.27	1.47	1.72
50	G	red soil	Frontignan	10	30	43	47
				1	2.94	4.18	4.60
51	G	muddy sand with film of water	Sete	7	10	14	10
				1	1.33	1.94	1.45
52	G	muddy sand with film of water	Sete	7	10	14	10
				1	1.25	1.86	1.35
53	G	muddy sand with film of water	Sete	8	10	15	12
				1	1.36	2.01	1.54

Tab. 2. 6.C (Suite)

| Sample	Material	Site	reflectance (in %)			
			MSS4	MSS5	MSS6	MSS7
54 G	obione field	Sete	8	12	41	59
			1	1.50	5.31	7.53
55 G	obione field	Sete	7	12	42	60
			1	1.72	5.84	8.38
56 G	salicorne field	Sete	4	5	12	20
			1	1.16	2.86	4.93
57 G	ocean d = 3.0 m	Port Vendres	1.86	0.81	0.41	0.27
			1	0.44	0.22	0.15
58 G	ocean d = 3.0 m	Port Vendres	1.90	1.04	0.45	0.30
			1	0.55	0.24	0.16
59 G	ocean d = 3.5 m	Port Vendres	1.70	0.81	0.30	0.21
			1	0.48	0.18	0.12
60 G	ocean d = 3.5 m	Port Vendres	2.15	1.13	0.45	0.65
			1	0.53	0.21	0.30
61 G	ocean d = 4.0 m	Port Vendres	1.98	0.90	0.38	0.21
			1	0.45	0.19	0.11
62 G	ocean d = 4.5 m	Port Vendres	1.92	0.99	0.44	0.22
			1	0.52	0.23	0.11
63 G	ocean d = 4.5 m	Port Vendres	2.13	1.25	0.75	0.85
			1	0.59	0.35	0.40
64 G	ocean d = 3.5 m	Port Vendres	1.87	0.77	0.28	0.18
			1	0.41	0.15	0.10
65 G	ocean d = 4.5 m	Port Vendres	2.00	1.29	1.09	1.11
			1	0.65	0.55	0.56

2. 7 - DETERMINATION OF TIDAL CURRENTS AND TIDAL HEIGHTS

Since a large part of the works of the FRALIT team are related to the tidal coast of France, it was necessary to compute the tidal heights as well as the speed and heading of the tidal currents at satellite overpass. Those determinations were drawn from data collected by the Service Hydrographique and Oceanographique de la Marine and sometimes fr other data sources (E.D.F., direct observations, ...).

Figures 2.7.1 through 2.7.18 provide this type of information for 15 images of the French Atlantic littoral which were computer processed processed by the FRALIT team ; those images are ordered by geographical area and for each geographical area by chronological order.

Latitude axes	Orbit axes	Date	Tidal coefficient
26	217	September 27, 1972	92
"	"	March 8, 1973	100
"	218	June 6, 1975	55
"	"	July 30, 1975	56
"	"	October 28, 1975	47
27	217	September 27, 1972	92
"	"	March 8, 1973	100
"	"	July 29, 1975	65
"	"	March 28, 1976	70
"	"	June 8, 1976	65
"	"	June 26, 1976	68
"	218	October 28, 1975	47
28	216	July 11, 1973	44
"	"	June 4, 1975	45
"	"	December 19, 1975	84
"	217	March 8, 1973	100
"	"	July 29, 1975	65
29	216	June 4, 1975	64

Note : Tidal coefficients are locally determined for satellite overpass with high water in Brest.

ASA _ ERTS 1. FRALIT .
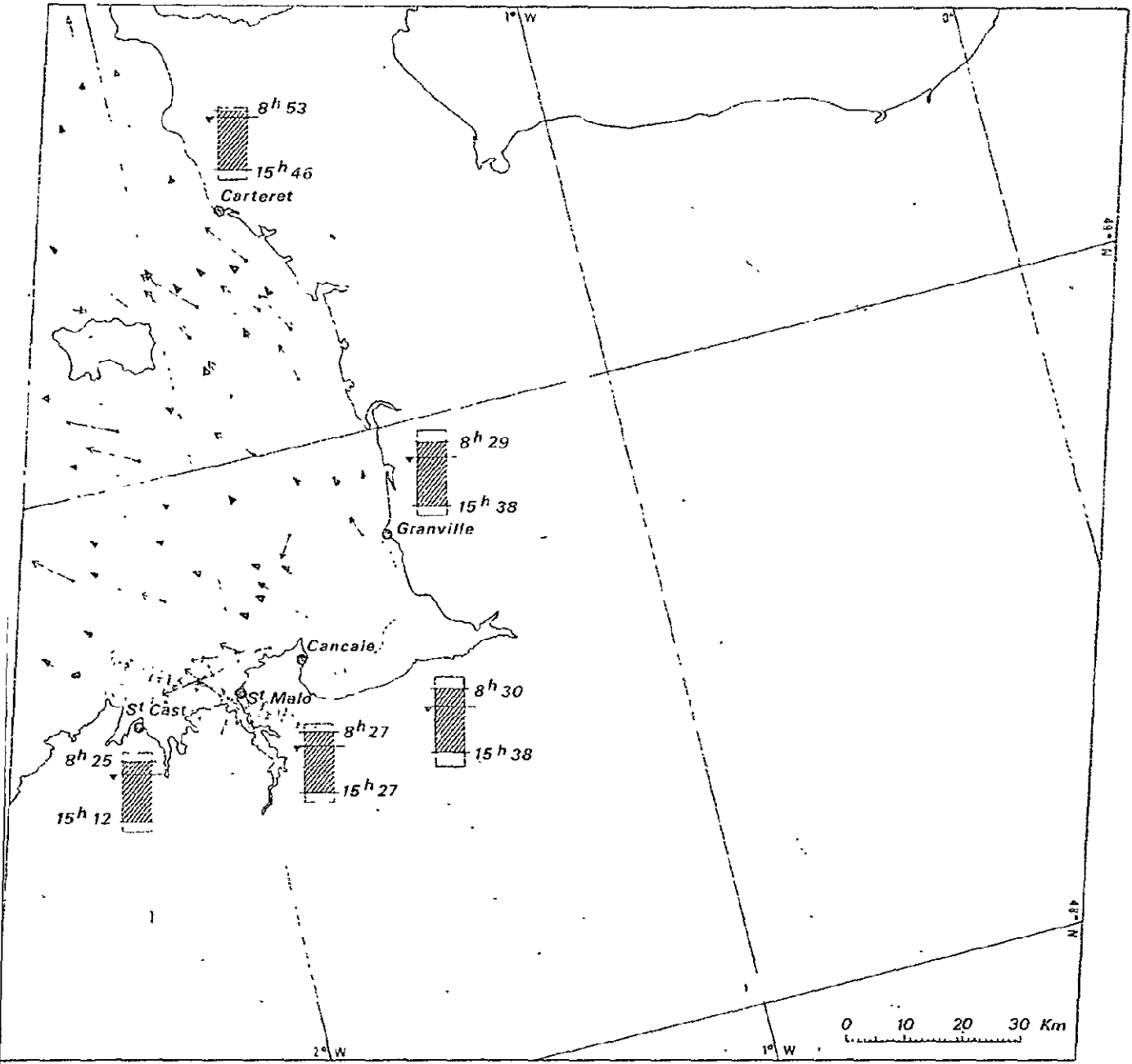
Tidal   currents   (1cm = 1 m / s)

Tidal   range   and water   level   (1 mm = 1 m)

Data issued from :

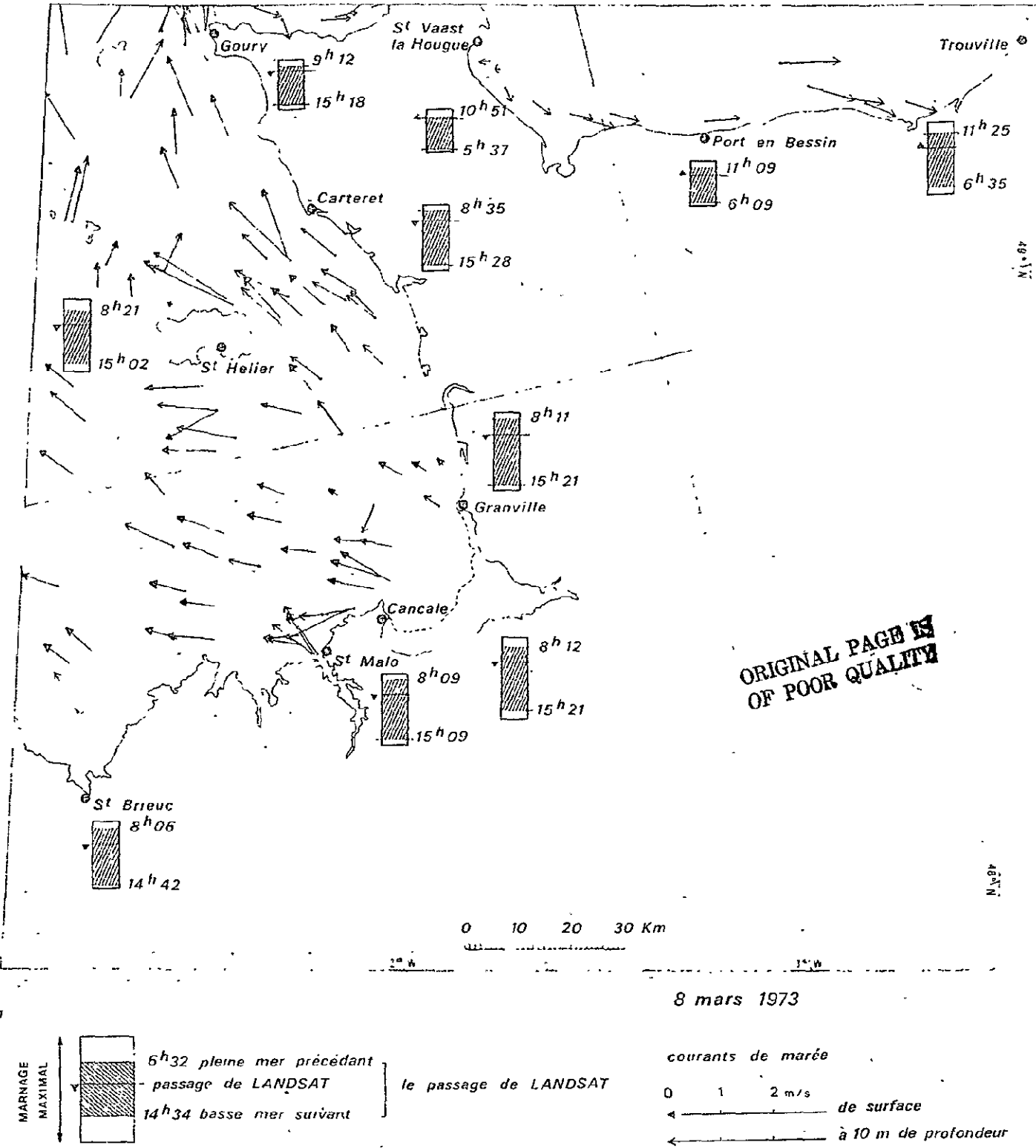Laboratoire National d' Hydraulique

S H O M

Maximum high water springs

falling tide
rising tide

September 27. 1972

High water

Tide level 10ʰ30 TU

Low water

Chart datum   0

Fig. 2.7.1 - Hydrological ground truth data

8 mars 1973

Fig. 2.7.2 - Hydrological ground truth data
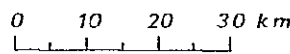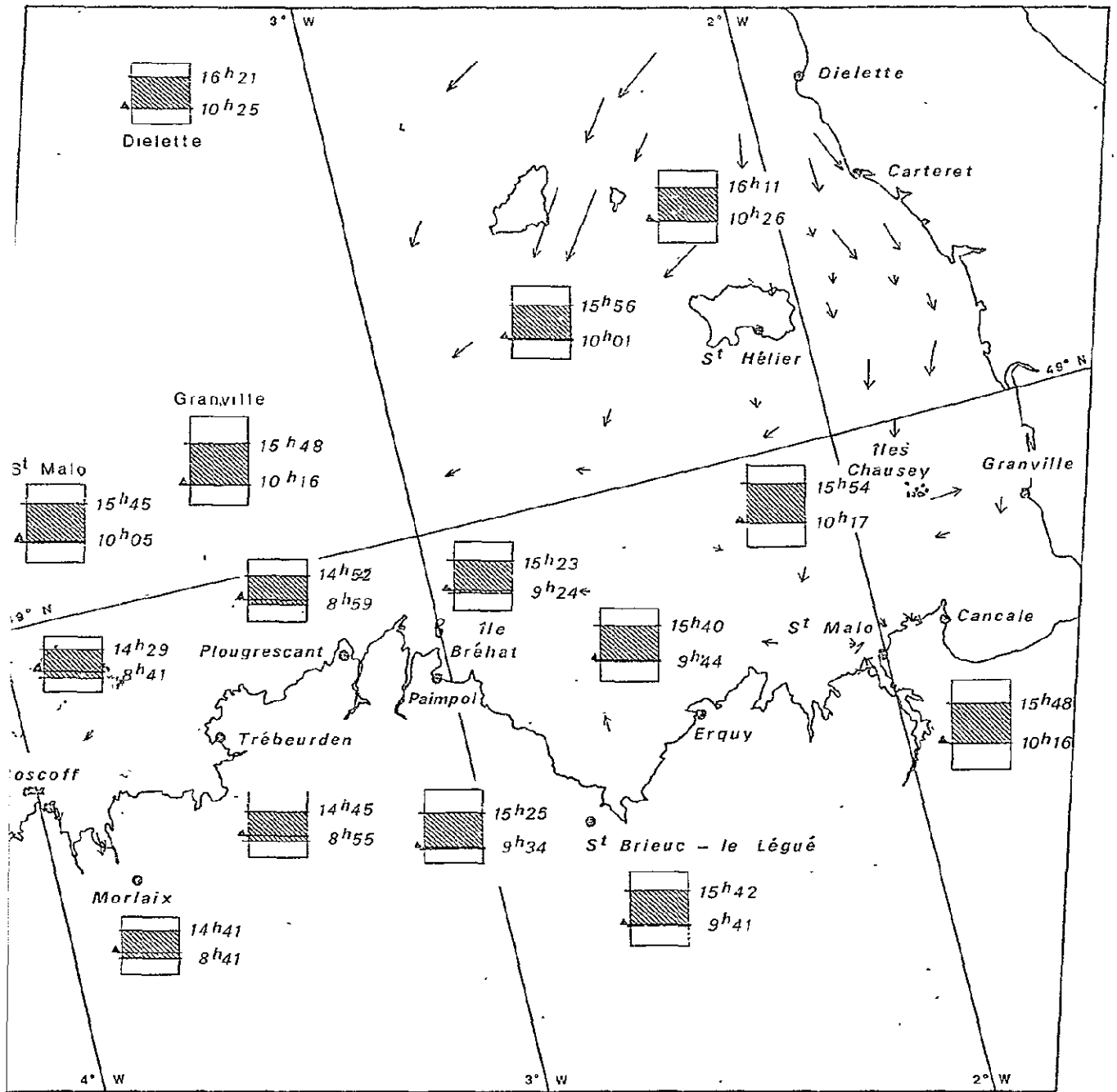
ASA - LANDSAT 2 - FRALIT   2135   10235
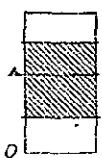
Fig. 2.7.3 - Hydrogological ground truth data

Fig. 2.7.4 - Hydrological ground - truth data.

Port St Pierre

Carteret

11^h26
6^h24

11^h30
6^h06

11^h11
6^h00

St Hélier

49·N

11^h03
6^h11

Granville

Les Minquiers

Granville

11^h36
6^h19

Iles Chausey

10^h28
4^h28

Plougrescant

Ile
de
Bréhat

Cancale

10^h22
4^h16

10^h56
4^h46

Ploumanach

Tréguier   L.   Paimpol

Erquy

St Malo

11^h02
6^h11

Trébeurden

Portrieux   Dahouet

10^h31
4^h24

10^h58
5^h00

10^h56
5^h47

11^h00
6^h00

Roscoff

Le Légué

10^h55
5^h51

Morlaix

10^h57
5^h41

10^h58
4^h54

10^h05
4^h14

Lézardrieux

10^h20
4^h05

10^h54
5^h38

11^h12
6^h10

10^h31
4^h31

Portrieux

Iles   Chausey

Tréguier

4·W   3·W   2·W

0   10   20   30km

tidal currents (1cm = 1m / s)   Tidal range and water level (1mm=1m)

October 28 1975

Maximum high water springs

S H O M   ORIGINAL PAGE IS
OF POOR QUALITY   High water

            falling tide
            rising tide   Tide level 10^h22
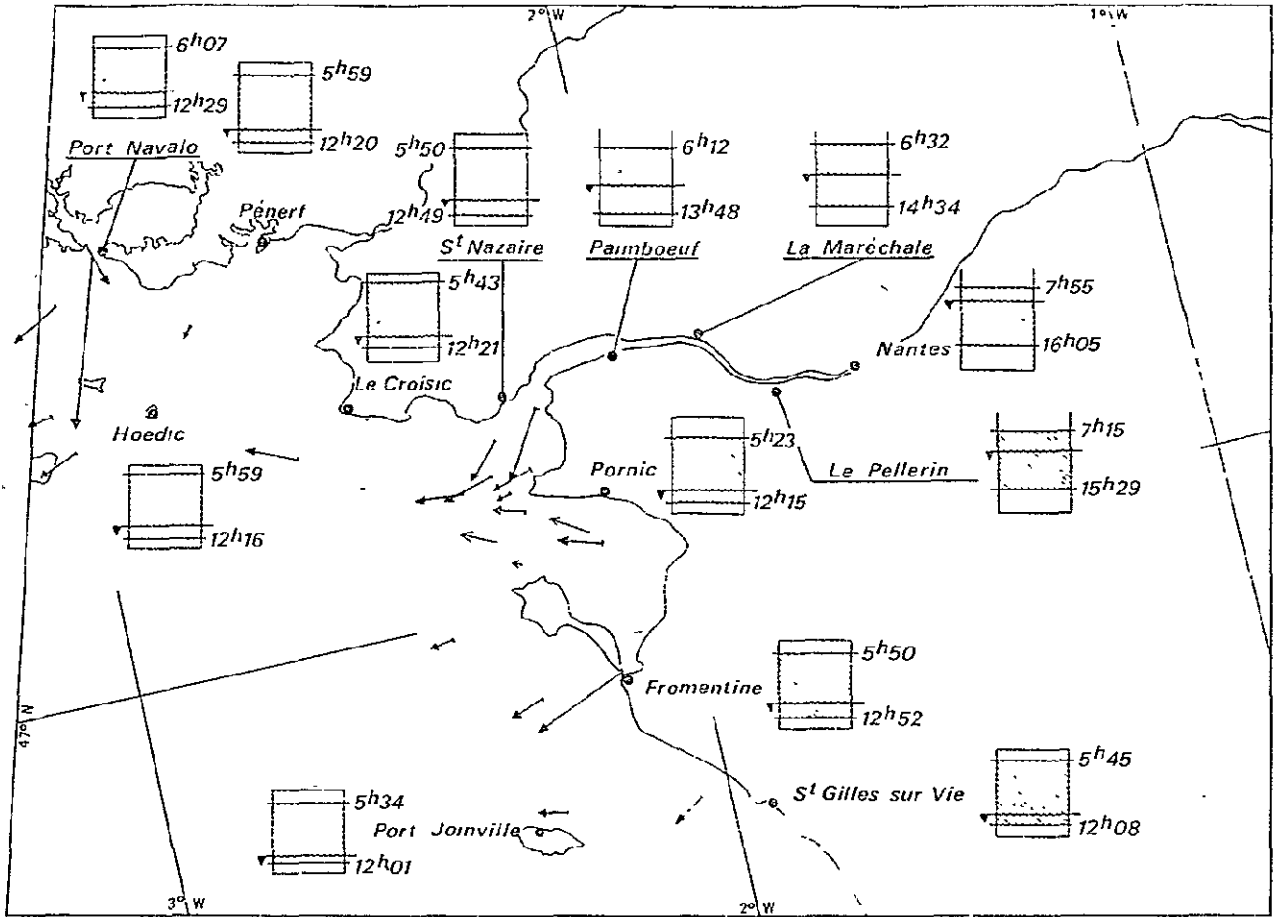   TU
                                        Low water

Laboratoire National d'Hydraulique   Chart datum   0
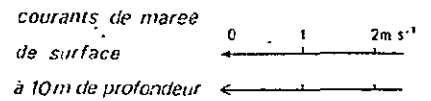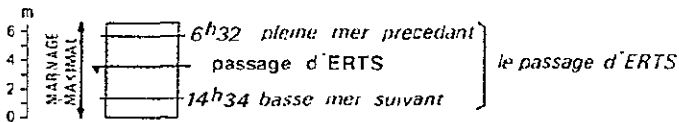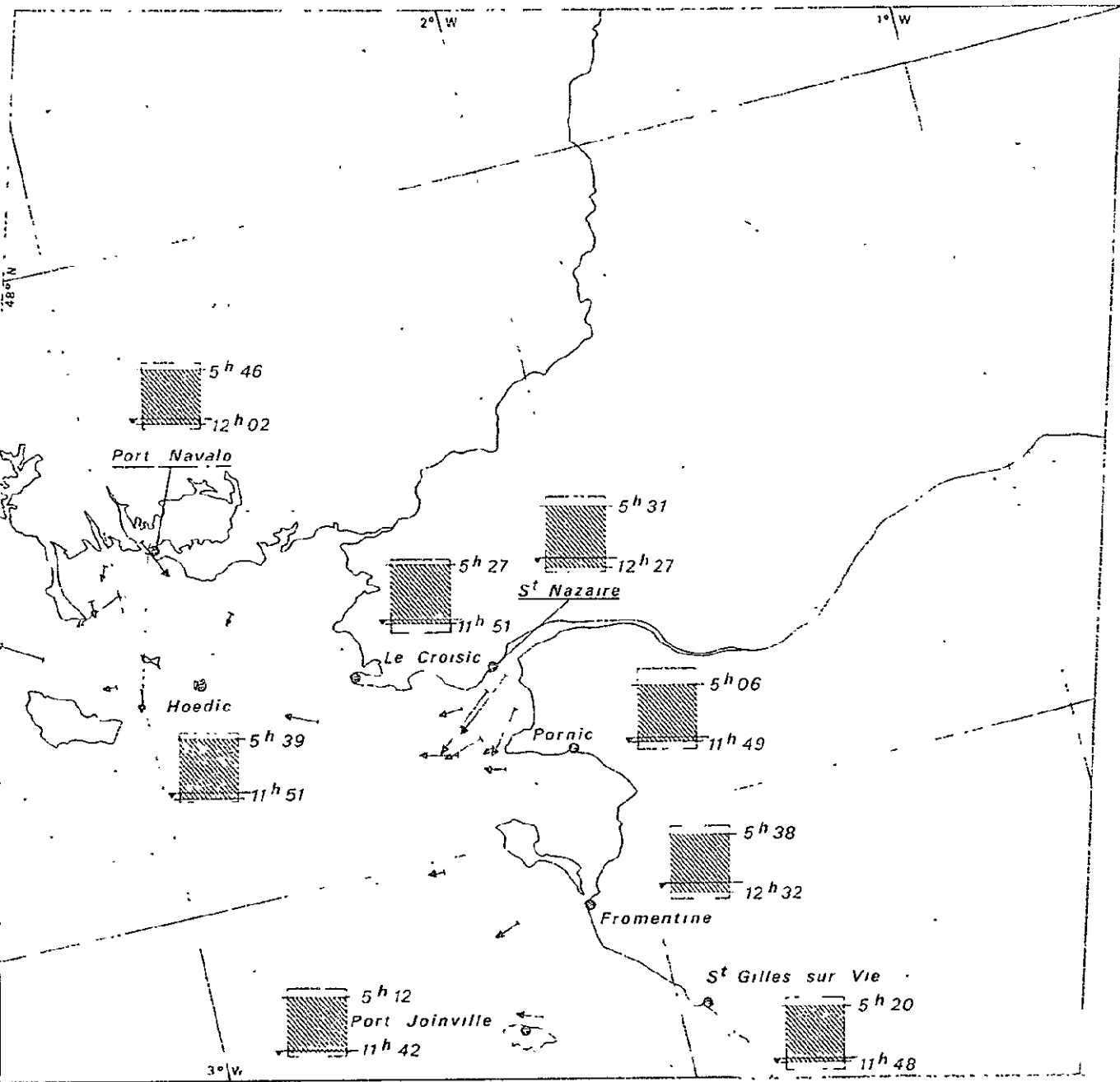
Fig. 2.7.5 - Hydrological ground truth data

Fig. 2.7.6 - Hydrological ground truth data

8 mars 1973
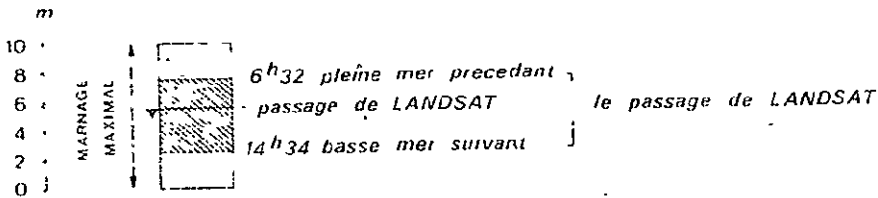
Fig. 2.7.7 - Hydrological ground truth data
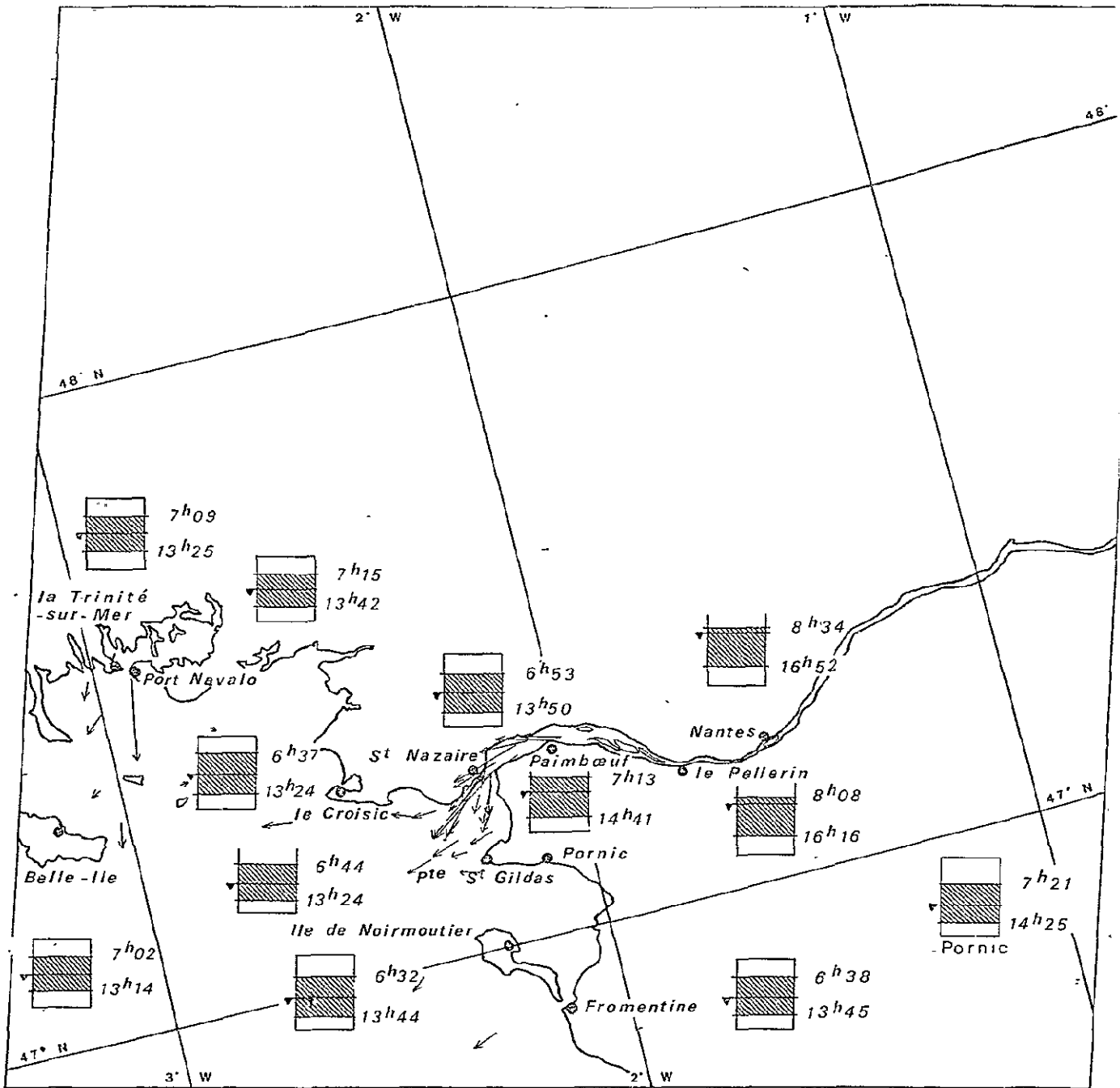
Tidal currents (1 cm = 1 m/s)

Tidal range and water level (2 mm   1 m

July 2 . 1

→   S H O M

ORIGINAL PAGE IS
OF POOR QUALITY

Maximum high water springs

▽── falling tide
▲── rising tide   ▽

High water
Tide level

Low   water

Chart datum 0

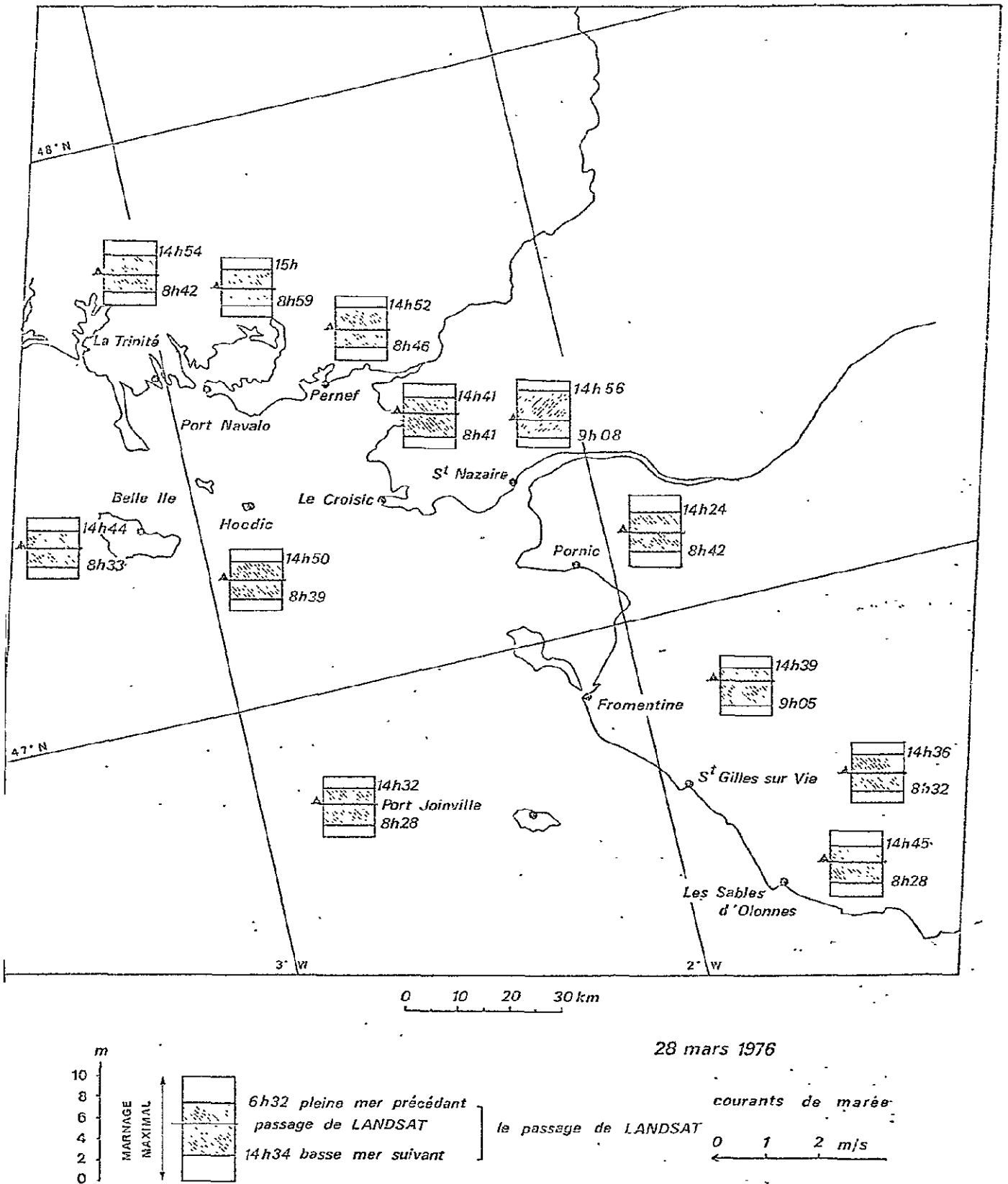Fig. 2.7.8 - Hydrological ground - truth data.

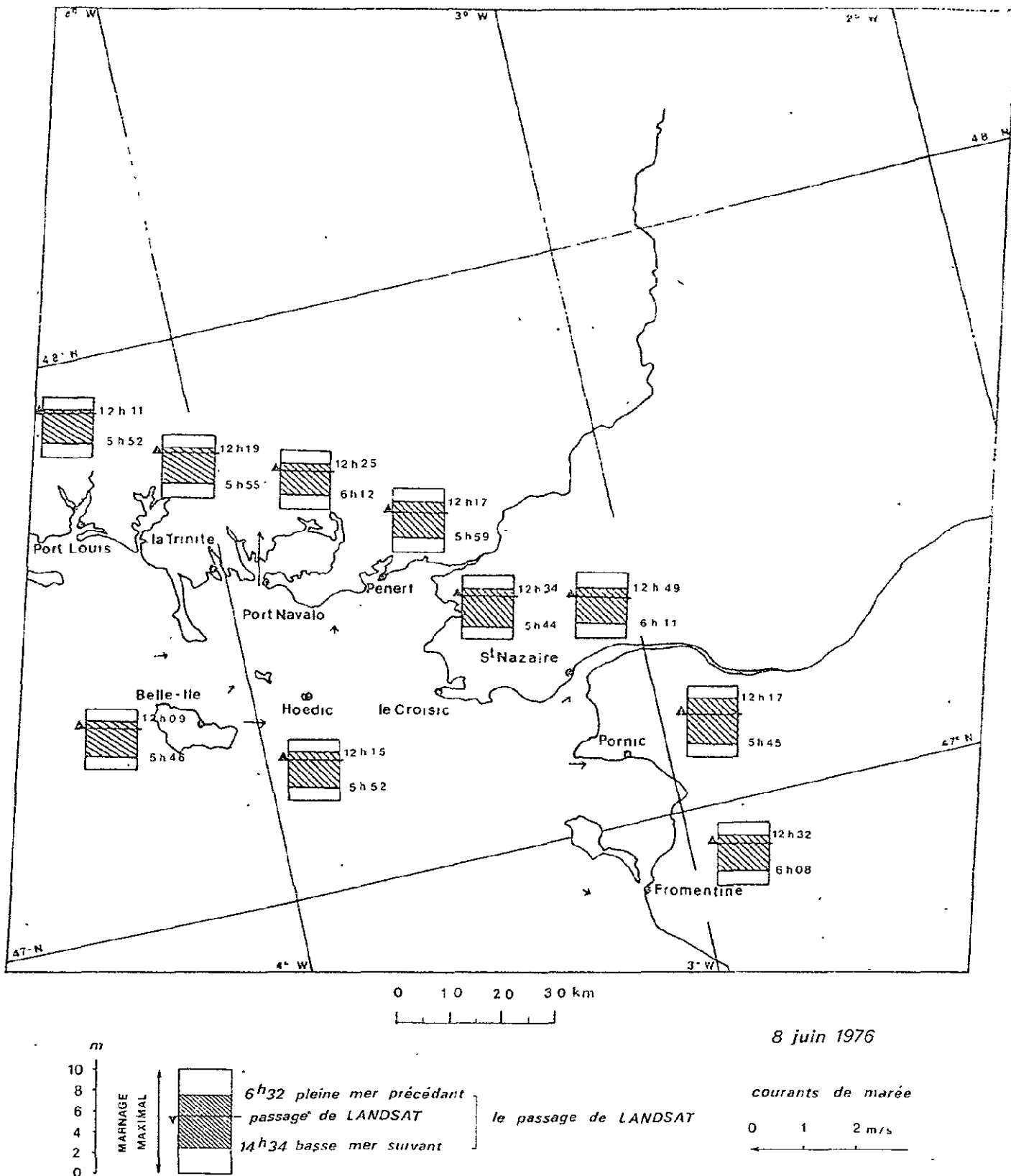Fig. 2.7.9 - Hydrological groung truth data

Fig. 2.7.10 - Hydrological ground truth data
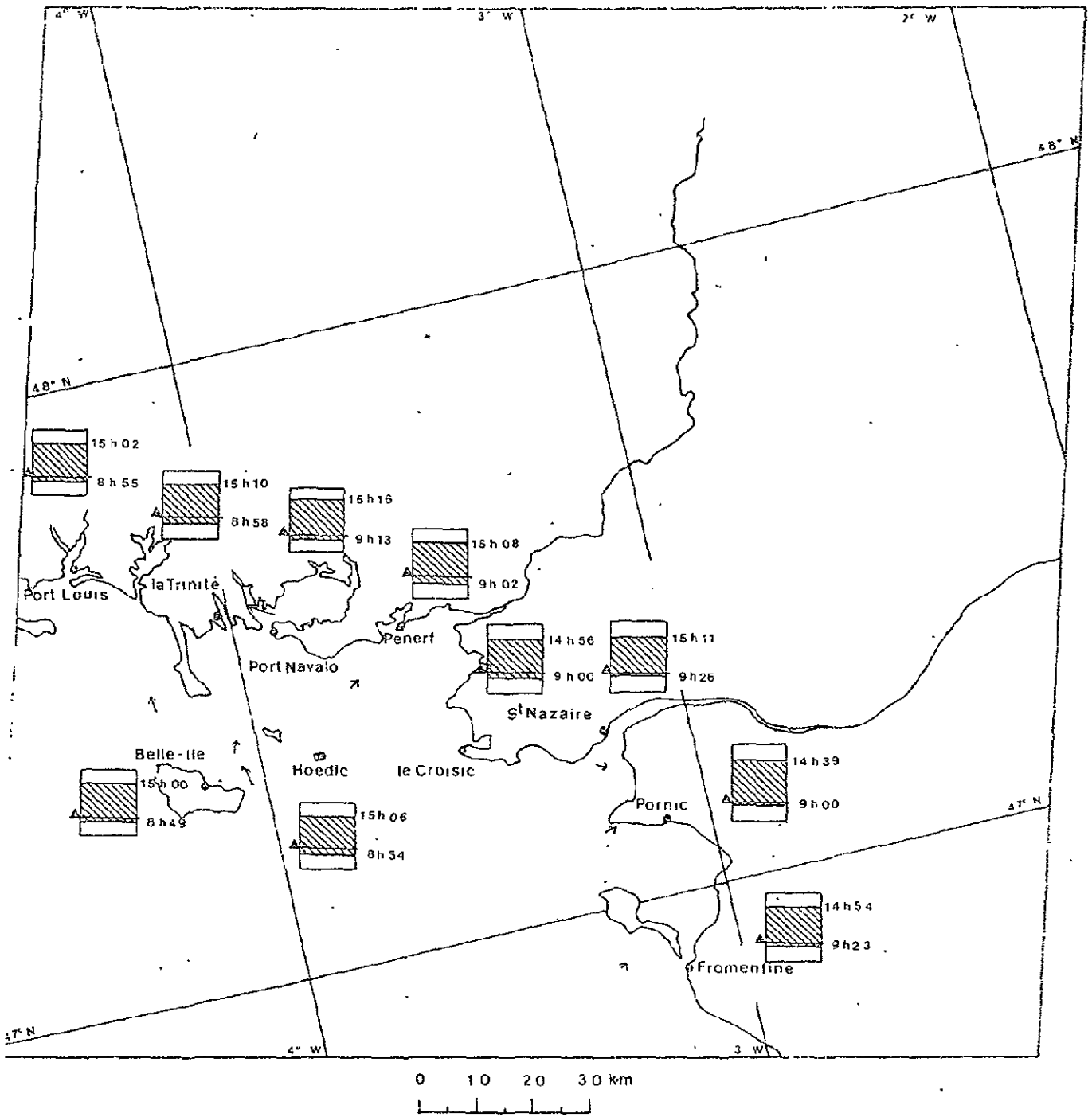
26 JUNE 1976

Tidal currents (1 cm = 1 m/s)   Tidal range and water level (2 mm = 1 m)

Maximum high water springs

falling tide
rising tide

High water
Tide level 10 h 30
Low water
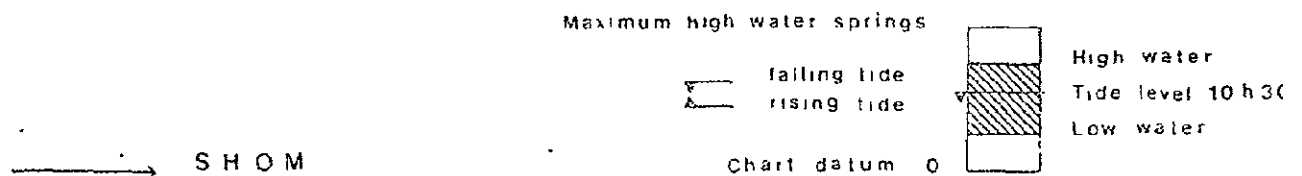
SHOM

Chart datum 0

Fig. 2.7.11 - Hydrological ground truth data
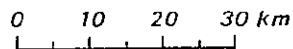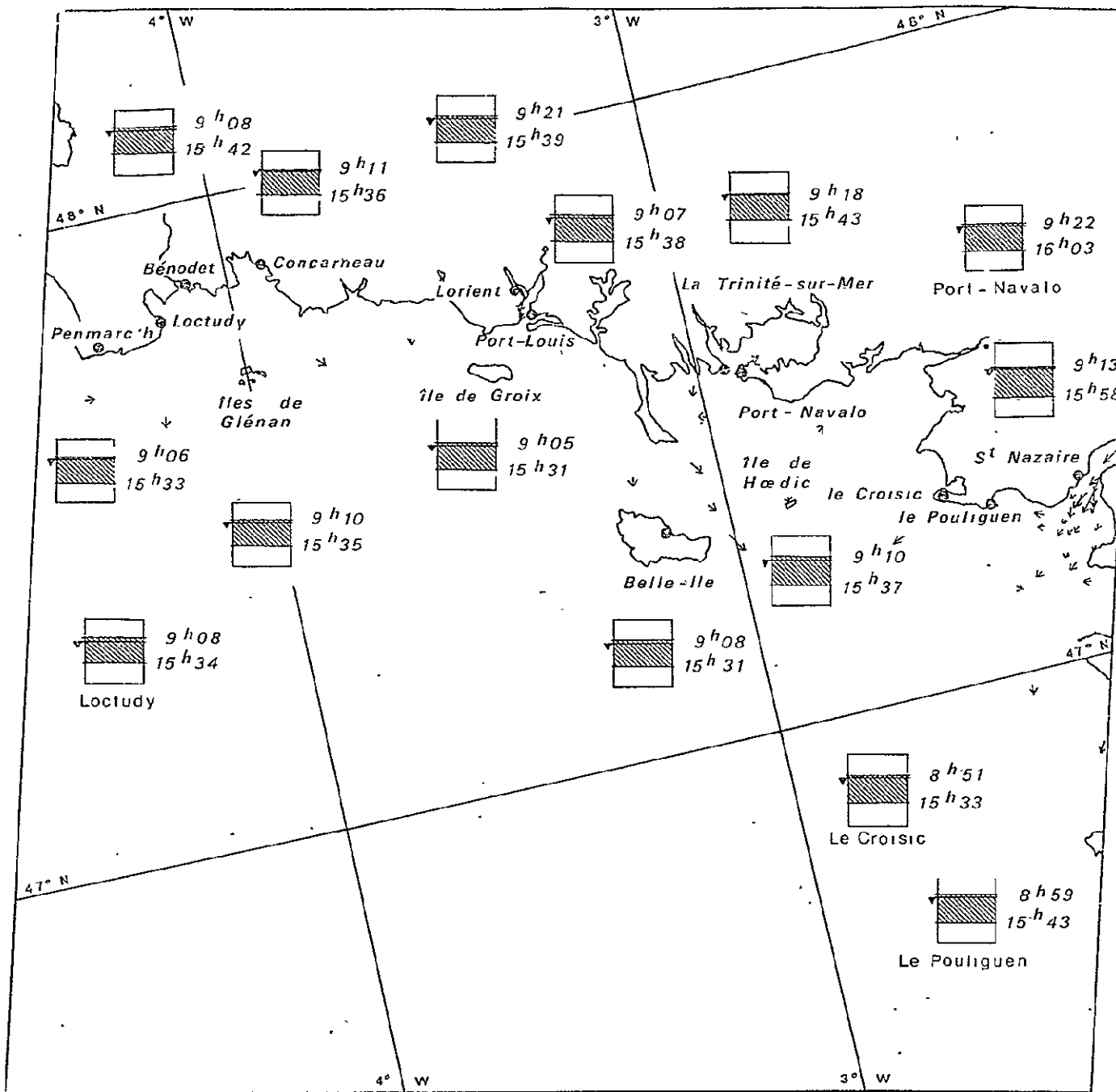
Fig. 2.7.12 - Hydrological groung truth data

ASA _ ERTS 1 . FRALIT   1353_10244

11 juillet 1973

Fig. 2.7.13 - Hydrological ground truth data

NASA – LANDSAT 2 – FRALIT

2133 1013

2° W

1° W

Les Sables d'Olonne

12ʰ11
5ʰ08

St Martin
de Ré

11ʰ41
5ʰ30

La Rochelle

11ʰ45
5ʰ22

46° N

11ʰ49
5ʰ23

Ile d'Aix

Rochefort

11ʰ59
6ʰ27

46° N

La Cayenne

11ʰ41
5ʰ15

Royan

12ʰ14
5ʰ23

C
P

12ʰ27
5ʰ57

Richard

Lamena

12ʰ37
6ʰ22

11ʰ52
5ʰ14

Cordouan

12ʰ15
5ʰ28

45° N

Pointe de Grave

14ʰ10
9ʰ28

Bordeaux

2° W

1° W

0   10   20   30 km

Tidal currents (1 cm = 1 m/s)

Tidal range and water level (2 mm = 1 m

June 4, 197

Maximum high water springs

falling tide

rising tide

High water

Tide water 10ʰ13

Low water

Chart datum 0

S H O M

Fig. 2.7.A4 - Hydrological ground truth data
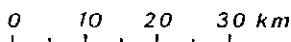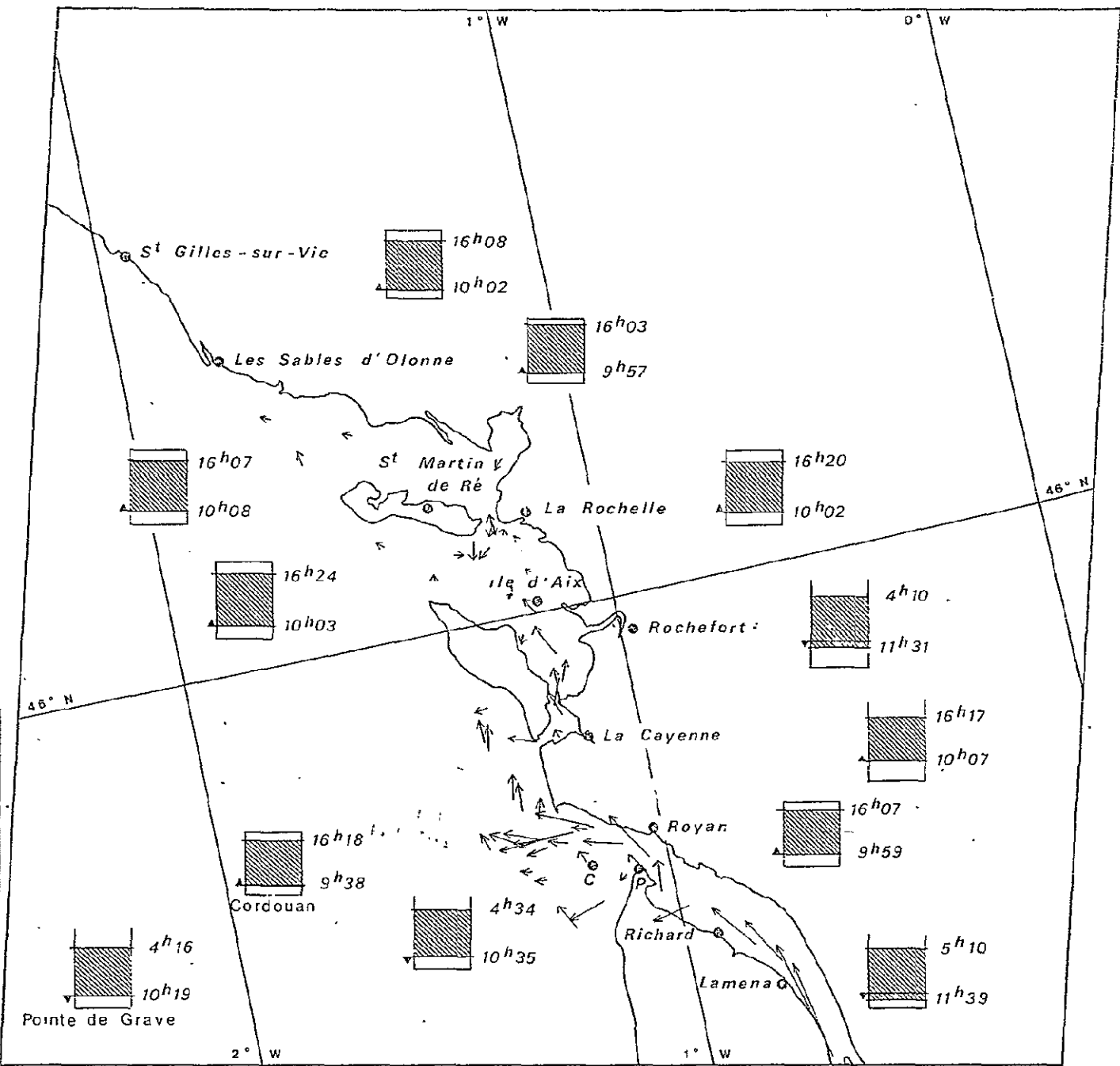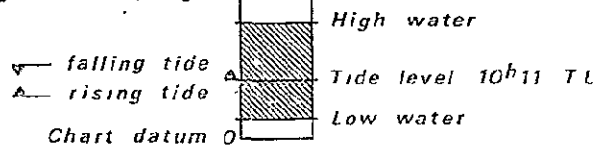
Fig. 2.7.15 - Hydrological ground truth data

3° W

St Gilles sur Vie

Port Joinville

$5^h 32$

$5^h 21$

$5^h 18$

$11^h 44$

$11^h 38$

$11^h 35$

Les Sables d'Olonne

St Martin de Ré

$5^h 12$

$12^h 01$

ORIGINAL PAGE IS
OF POOR QUALITY

N

46°

0   10   20   30 km

8 mars 1973

m

10
8
6
4
2
0

MARNAGE MAXIMAL

$6^h 32$ pleine mer précédant

passage de LANDSAT

$14^h 34$ basse mer suivant

le passage de LANDSAT
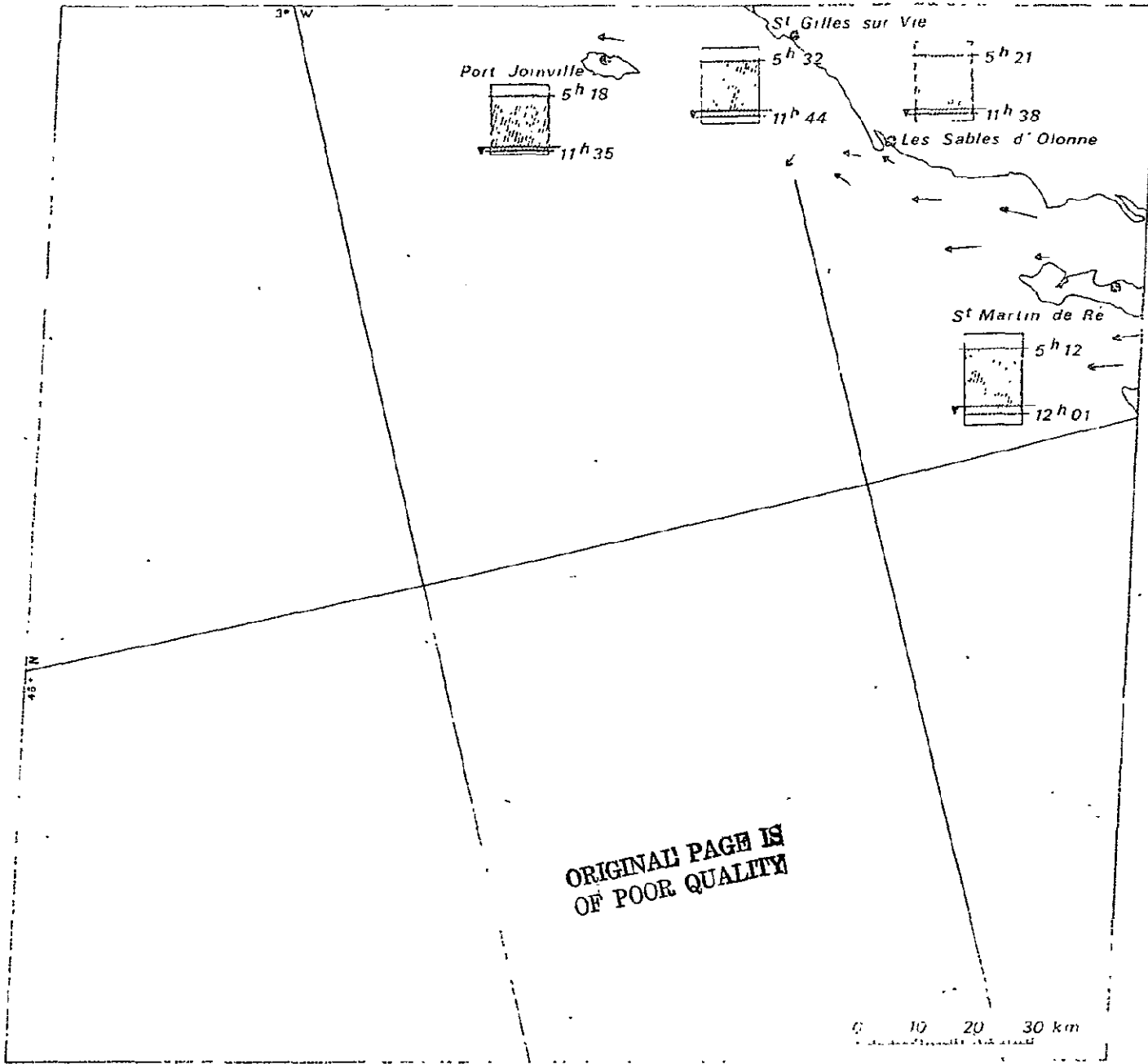
courants de maree

0   1   2 m/s

Fig. 2.7.16 - Hydrological ground truth data
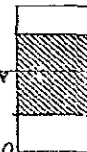
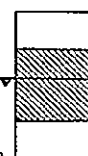Fig. 2.7.17 - Hydrological ground - truth data.
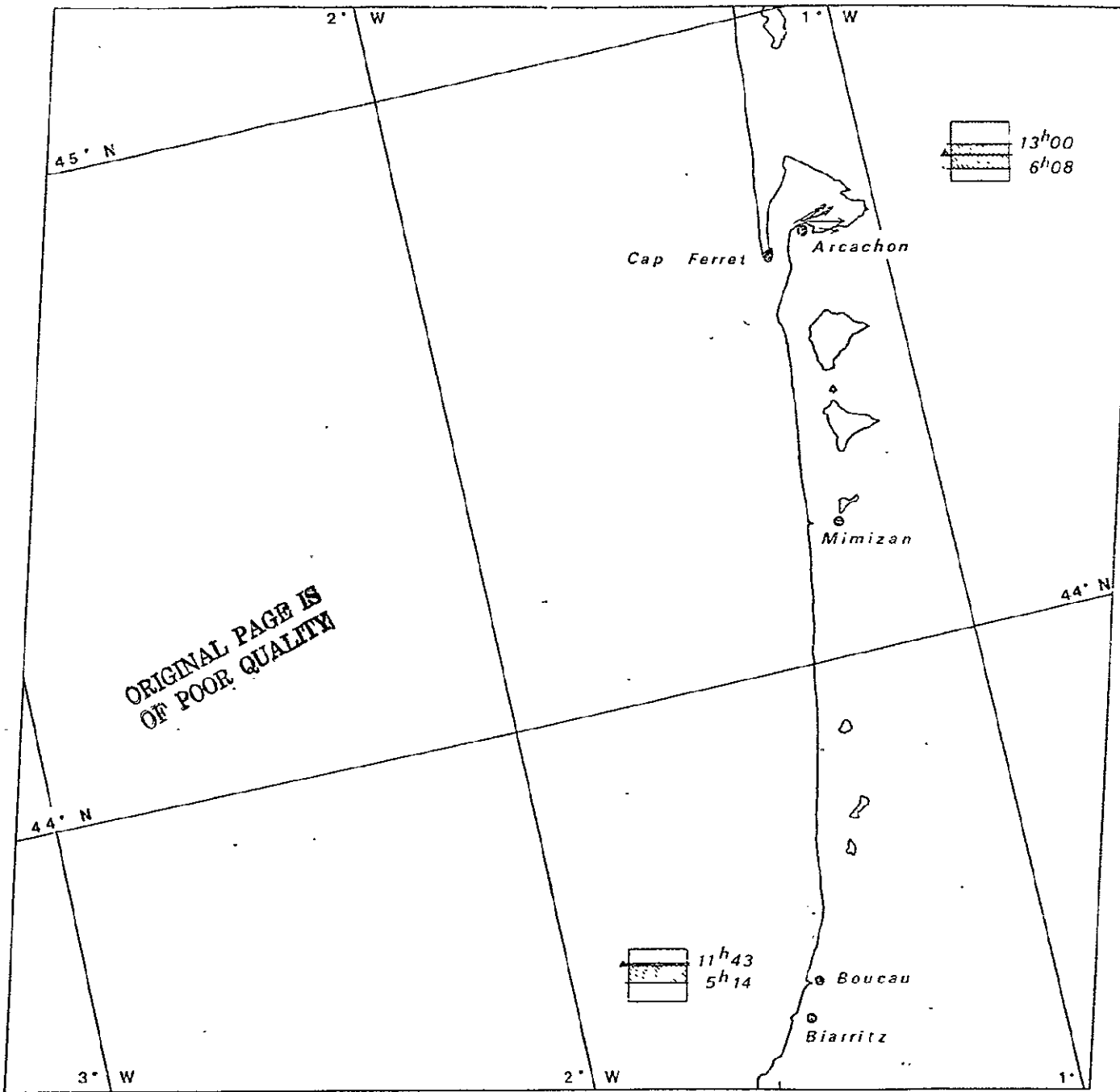
Tidal currents (1 cm = 1 m / s)   Tidal range and water level (2 mm = 1 m

June 4, 1975
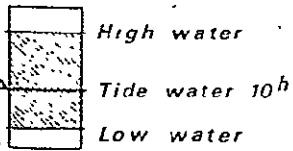
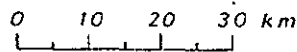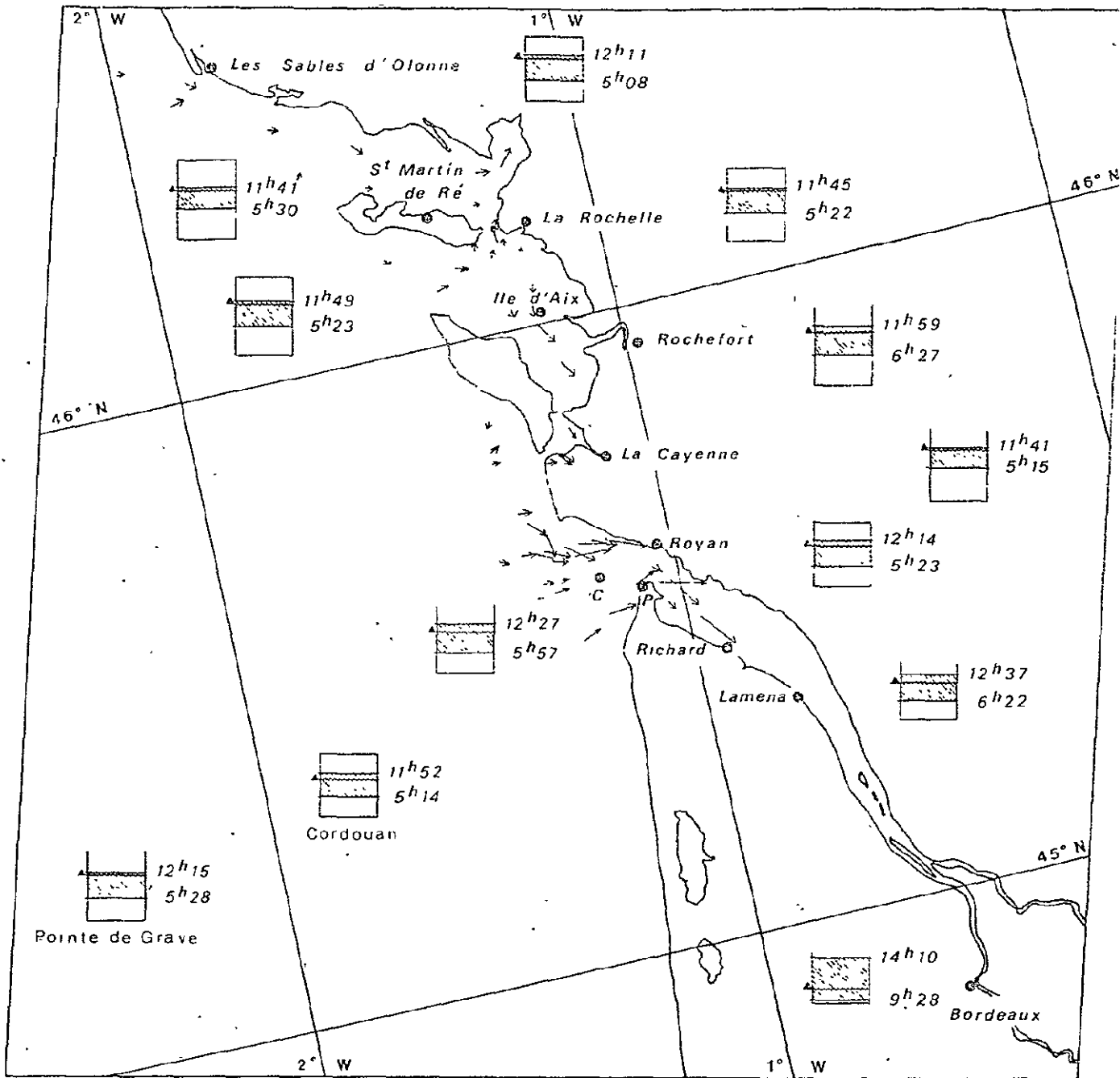Fig. 2.7.18 - Hydrological ground truth data

3 - SIGNIFICANT RESULTS AND ACCOMPLISHMENTS

3. 1 - AN AUTOMATIC CLASSIFICATION OF LANDSAT-2 DIACHRONIC DATA ON THE

FORESHORE OF THE ISLAND OF JERSEY

3. 1.1 - Data description

Landsat-2 data from June 6th 1975 and July 30th 1975 were used
to draw up a diachronic (multitemporal) map of the island of ·
Jersey. These two dates were chosen for the differences in tide
levels between them. In the first case, satellite overpass took
place 20 minutes after low water at St-Helier, and twenty
minutes after high water in the second case.

3. 1.2 - Data processing

Diachronic processing requires the overlayging of the two
digital images, using significant landmarks identified on
single channel imagery as tiepoints. At the end of this step,
a single date file is available, where each pixel is characteri-
zed by eight different spectral bands (4 bands for each date).

Preliminary to dat analysis, radiance histograms in each of
the 8 spectral bands are divided into radiance intervals. This
subdivision is used in order to generate a binary coding of the
original data. When the radiance histogram of a spectral band is
unimodal it is divided in isopopulation intervals. However if
this distribution in bi or multimodal, a rapid interpretation
of the main spectral contrasts allows to interactively adapt the
radiance intervals to this situation. This second situation was
the case for the MSS7 bands at the two differents dates analysed
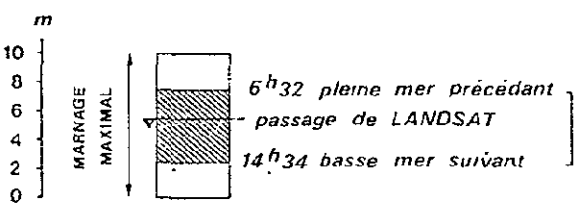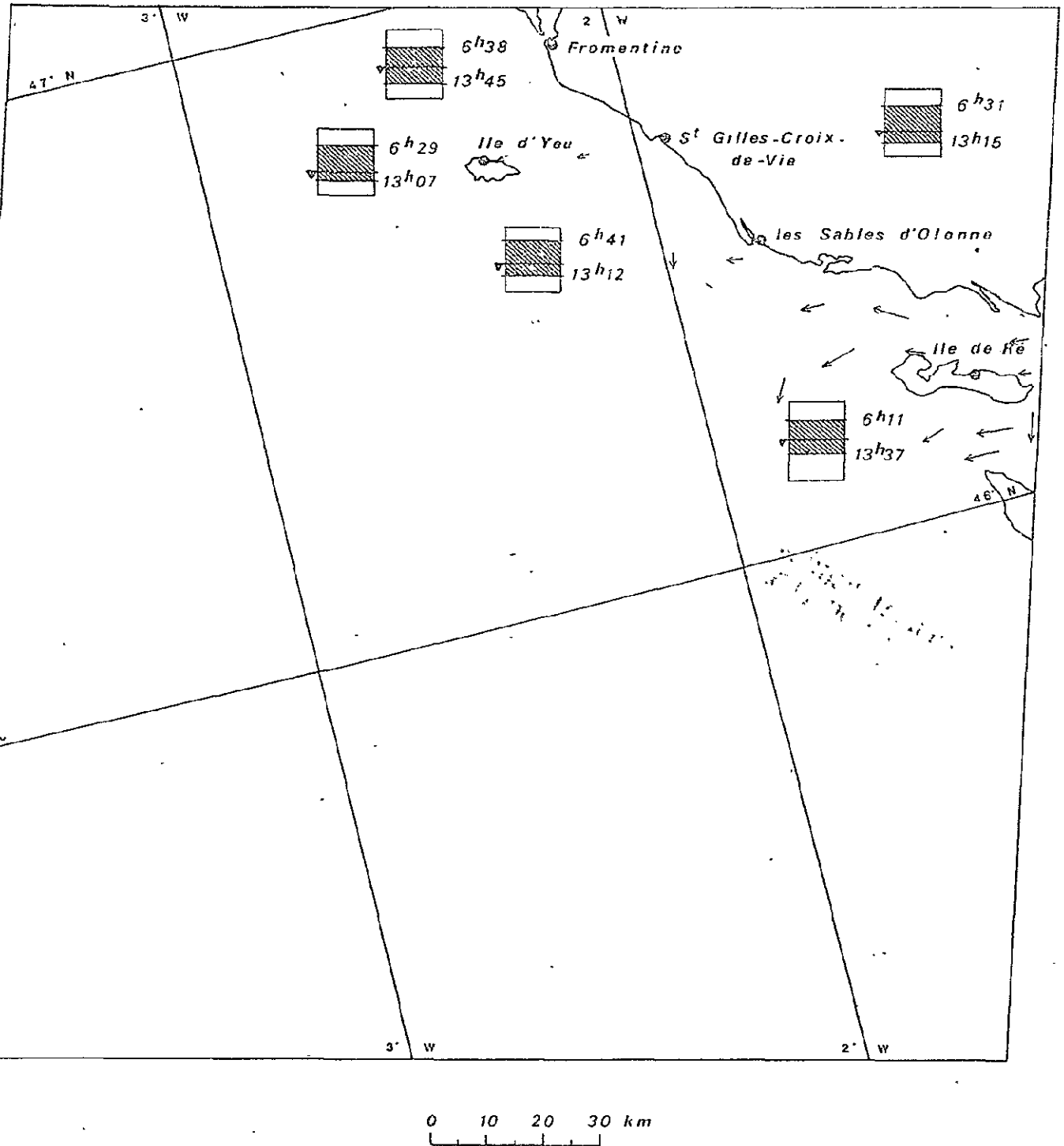here. The emphasis was put on the contrast existing between sea
and land signatures.

After correspondence analysis of coded data using the FRACAM
system, a hierarchical classification reveals the similarities
existing between spectral bands. The groups of spectral bands
thus determined are displayed as nodes of a hierarchical tree
structure (dendogram) in Fig. 3.1.A.

The lenght of each branch of this tree is proportional to the
distance between the groups it links. Operator interaction is
required for the determination of the maximum group diameter
as well as the number of desired groups. This step is followed
by an adaptative clustering of radiance spectra leading to a
spectral classification.

It is possible to control the results of this classification by
displaying the class spectral histograms and spectral statistics.
The analysis can then be refined in a layered fashion by reproces-
sing each class for further subdivision. The present study being
mainly related to the tidal flats dynamics, classes 3 and 7 were
subdivided in 3 subgroups each.
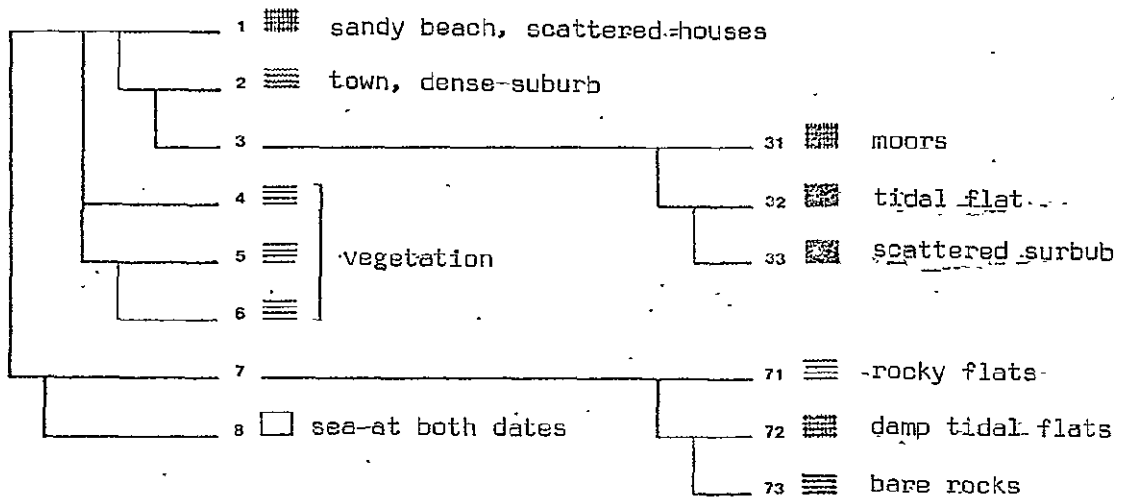
Fig. 3.1.A - Spectral similarity tree between mapped categories

3. 1.3 - Interpretation of classification results

The map legend (Fig. 3.1.B) shows each taxon in its relative position within the hierarchy defined by the classification.

For interpretation purposes, two types of taxons have been defined according to their variability in time. On the whole, taxons with a similar spectral signature at both dates can be opposed to those with strongly varying spectral signature.

a - Categories with low diachronic variation

. Class 1 shows the upper part of beaches (South and south-east coast) which was not covered by the neap tide of July 30 th. . It also borders class 2 and occurs inland, generally, where it shows low-density built-up areas.

. Class 2 covers the town of St-Helier and the discontinuous urban areas along the South and East coasts.

. Class 31 occurs along the North coast in moorland. This subset of the vegetation class was individualized during the second stage of classification.

. Class 33 shows low density built-up areas.

. Class 4, 5 and 6 are different types of vegetation. The same symbol has been used to map them because of the lack of approriate ground-truth data for accurate interpretation.

. Class 71 represents bare rock, in the cliffs to the North East of the island, and in the new harbour area under construction southward of St-Helier.

. Finally class 8 is an example of "false stability" in time since it shows areas which were covered by the sea at both dates.

b - Categories with strong diachronic variation

These are mostly foreshore areas, with a land-type spectral signature at low tide and a sea-type signature at high tide. At the first level of classification, the foreshore was defined by class 3 and 7, but some of their subclasses are in fact land area as mentioned above.

Class 31 and 72 show different moisture levels ideally illustrated in St-Aubin's bay where class 1, 31 and 72 occur in sequence between the high and low tide marks.

Class 71 covers the emerged parts of the rocky shoals south-east of the island.
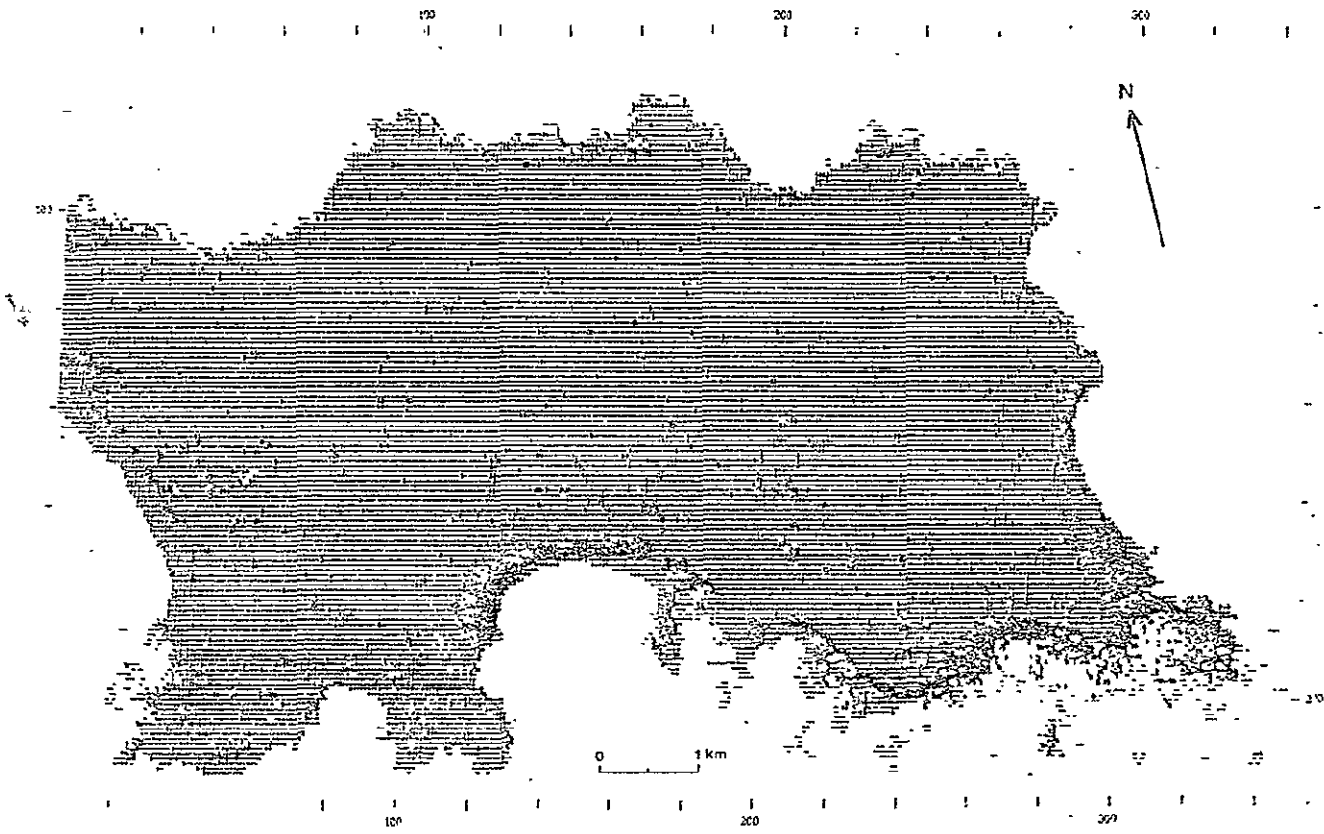
Fig. 3.1.B - Automatic diachronic classification of Jersey
island using LANDSAT-2

3. 1.4 - <u>Critics</u>

The diachronic classification used for this study has both the simplicity and rapidity of implementation of post assisted automatic classification, and the good identification obtained by diachronic techniques. For observation of rapidly changing terrain types such as the foreshore, diachronic techniques make the best possible use of the respetivity and fairly good geometric repeatibility of satellite remotely sensed data.

3. 2 - INTERPRETATION OF LANDSAT DATA ON THE LANDWARD PART OF THE FROMENTINE TEST AREA

3. 2.1 - Data description

Data analysed on the Fromentine test area are related to the following dates of overpass :

27 September 1972   -   LANDSAT 1 -

11 July   1973   -   LANDSAT 1 -

29 July   1975   -   LANDSAT 2 -

3. 2.2 - Data processing

The Fromentine test area has been analysed using various analysis techniques described in part 2 (Cf 2-2 to 2-5). The results presented were respectively related to the following dates : 27 September 1972 (cf. 2-3), 11 July 1973 (cf 2-4) and 29 July 1975 (cf 2-2 and 2-5).

3. 2.3 - Interpretation of results before classification smoothing

The interpretation is restricted to the landward part of the Fromentine area including the sand beaches which are often difficult to spectrally separate from the barren coastal dunes in the southern part of Noirmoutier island as well as along the Breton marsh.

Comparisons are made between results more than between processi methods because they usually depend upon the quality of operato assistance. This parameter has obviously improved in time with the knowledge acquired by the FRALIT team on the test area.

A certain number of conclusions can be drawn :

a - All methods of classification easily separate water from land categories

b - All methods of classification map relatively abondant sand formations which present high radiances for the whole set of MSS spectral bands. Their spectral separation is usually the best (cf. 2-3, AGREG). This category is associated to barren sands, sandy bars and various open spaces with varyi proportion of buildings and sands.

c - The various classification techniques are usually successfu in the separation of the maritime pine forest (Monts forest

. The FRACARTE classification (Fig. 2.2.C, 29 July 1975) maps in category 8 the well outlined forest area as well as polders which were taken over by the sea.

. The AGREG classification (Fig. 2.3.D, 27 September 1972) displays a restricted and homogeneous forested area (categor Certain parts of the forest under peculiar stress condition have been omitted but on the average the recognition of the Monts forest by this classification is excellent.

. The FRACAM classification (Fig. 2.4.N, 11 July 1975) splits
  the forest into two parts ;

    31   to which are associated the low parts of the old
           ·Grande Prise polder and a part of the Monts forest ;

and 33   where an other part of the Monts forest is displayed

A FRACAM classification of another date (29 July 1975) is
presented· in Fig. 3.2.A. It also points out a division of the
Monts forest into two parts·. The first symbol is related to
a dense stand of maritime pines which comprises numerous young
trees along the Monts coastline or older patches of wealthy trees
It is this denser part of the forest which is associated to
the old Grande Prise polder taken over by the sea. This confu-
sion is due to the fact that the spectral signatures of those
two types of objects are quasi identical (cf. 2.2.B).

Could it be that the use of a multitemporal approach would
eliminate this ambiguity which is present for the LANDSAT
scenes of 11 July 1973 and 29 July 1975 ? This similarity
between spectral signatures of otherwise distinct types of
objects makes their possible separation a difficult task, in
particular when this confusion can be repeated in the data of
distinct dates (11 July 1973 and 25 July 1975). The use of
diachronic data could save this problem if for instance one
of the survey dates would correspond to the flood of a very
high tide (which is impossible due to the time periodicity
of LANDSAT coverage) or the period following the uncovering
of old polder by the sea. In this second type of situation the
presence of water in one of the environments (old polder)
associated to its absence in the other one (forest) would
help in order to perform a successful separation.

d. - The other types of land use are mapped with a varying amount
of success by the various classifications. We will only compare
the results obtained for the 29 July 1975 by FRACARTE (cf 2.2.C)
and FRACAM (Fig 3.2.A).

One remark has to be done before any interpretation. The mapping
of agriculture areas was not undertaken in full detail during
preassistance of FRACARTE. Motivations of the operator were
biased by a coastal mapping approach so that more details were
sought in tidal flats or ocean waters than in the vegetated
marshes. On the contrary the operator while performing the
FRACAM coassistance phase is taking into account the spectral
statistics of the data more than the "a priori" nature of the
environments to be mapped.
For the FRACARTE classification two symbols only are associated
to the marsh land use type.

    - symbol 9 is related to psammophyte dune cover, most
       of the marsh pastures as well as some of the cultivated
       fields of Noirmoutier island and the Breton marsh ;

    - symbol 10 represents essentially cultivated areas as well
       as some grass pastures.

On the contrary, the FRACAM classification results propose
six different categories on the marsh :

- symbol 3 : cultivated areas (mostly on the rim of the
  Monts forest) ;

- symbol 4 : partially built open spaces (Fromentine, th
  Barre de Monts pier, La Fosse) ;

- symbol 6 : psammophyte covered dunes, marsh pastures ;

- symbol 7 : cultures with small plant canopy cover most
  on sandy soils ;

- symbol 8 : vegetation along drainage ditches and canal

- symbol 9 : lower parts of polders taken over by the se

3. 2.4 - Interpretation of results after classification smoothing

We will compare the mapping results of the raw and smoothed
FRACAM classification of the 29 July 1975 data set. Cartograph
improvements due to classification smoothing will be assessed
(Table - 3.2.B).

a - Common properties to the two types of smoothing

It is noticeable that conditional and majority vote smooth
algorithms have the common property to suppress artificial
categories generated by the classification processes at th
boundary between two types of well contrasted objects.
Symbol 5, for example, is mostly representative of muddy
tidal flats but it has been introduced as an artefact alon
the seaward part of the Monts forest sandy coast (Fig 3.2.
This misclassification can be eliminated by each of the
smoothing algorithms working on "clean" categories such as
the sandy beach (12) and the turbid part of the sea water

In the Noirmoutier island, the Trou de Sebastopol (lines
24 to 25, columns 5 to 6 in Fig 3.2.A) is partially stable
under a two iterations conditional smoothing. The pixels o
this water pool take very low values in MSS7 which are ver
different from those taken by the surrounding pixels. This
spectral discontinuity insures the stability of the Trou d
Sebastopol pixels through conditional smoothing because th
process is more influenced by spectral contrasts than by t
relative geographic position of the pixels (Fig 2.2.E). Th
pool can still be outlined after a simple majority vote
smoothing (Fig 2.2.C) but if this type of algorithm is
iterated, the Trou de Sebastopol can no longer be identifi
because it is merged with the nearby ocean surface (Fig 2.
This confusion is due to the suppression of the polder dit
. which separates the pool from the Bourgneuf Bay.Majority v
rule does in fact drastically alter linear shaped objects
like ditches, canals, piers, bridges ...

Cultivated plots represented by two symbol 3 (ligne 99 and columns 111 to 112, for example) are surrounded by symbol 4 pixels in Fig 3.2.A (unsmoothed classification).

Those plots are left untouched by a two iterations conditional smoothing due to the fact that their spectral individuality is good and their shape is not too similar to horizontal striping artefacts (Fig 2.2.E). On the contrary, the presence of category 6 on the lines 98 and 100 causes the removal of those isolated plots at the first iteration of the majority vote smoothing process (Fig 2.2.C).

b - <u>Differences between properties of the two smoothing algorithms</u>

Conditional smoothing results are usually different from those of the majority-vote algorithm, even if both of them succeed in suppressing most of the "artificial" category assignments.

The numerous isolated singularities which are present in our landscapes, often influenced by human activities, are usually unaltered by conditional smoothing. This is the case of small entities such as : the Trou de Sebastopol pool, the small clear cuts of the Monts forest, the cultivated plots scattered in the pastured marsh and associated to farm buildings, pastures intermixed with the fields along the rim of the Monts forest, small pools of the active or abandoned salt mills.

The majority vote smoothing, on the contrary, has a trend towards strong generalizations. It is more suited to the enhancement of global contrast such as the one which separate the forest into two parts. The specific land use pattern along the forest rim, mixing cultivated field ans houses, is also well outlined by majority vote (Fig 2.2.D).

Each of the two smoothing algorithms has particular advantages and drawbacks, they should be selected in relation to the type of geographical theme to be studied.

CLASSIFICATION AUTOMATIQUE A CO-ASSISTANCE SPECTRALE ET POST-ASSISTANCE TAXONOMIQUE
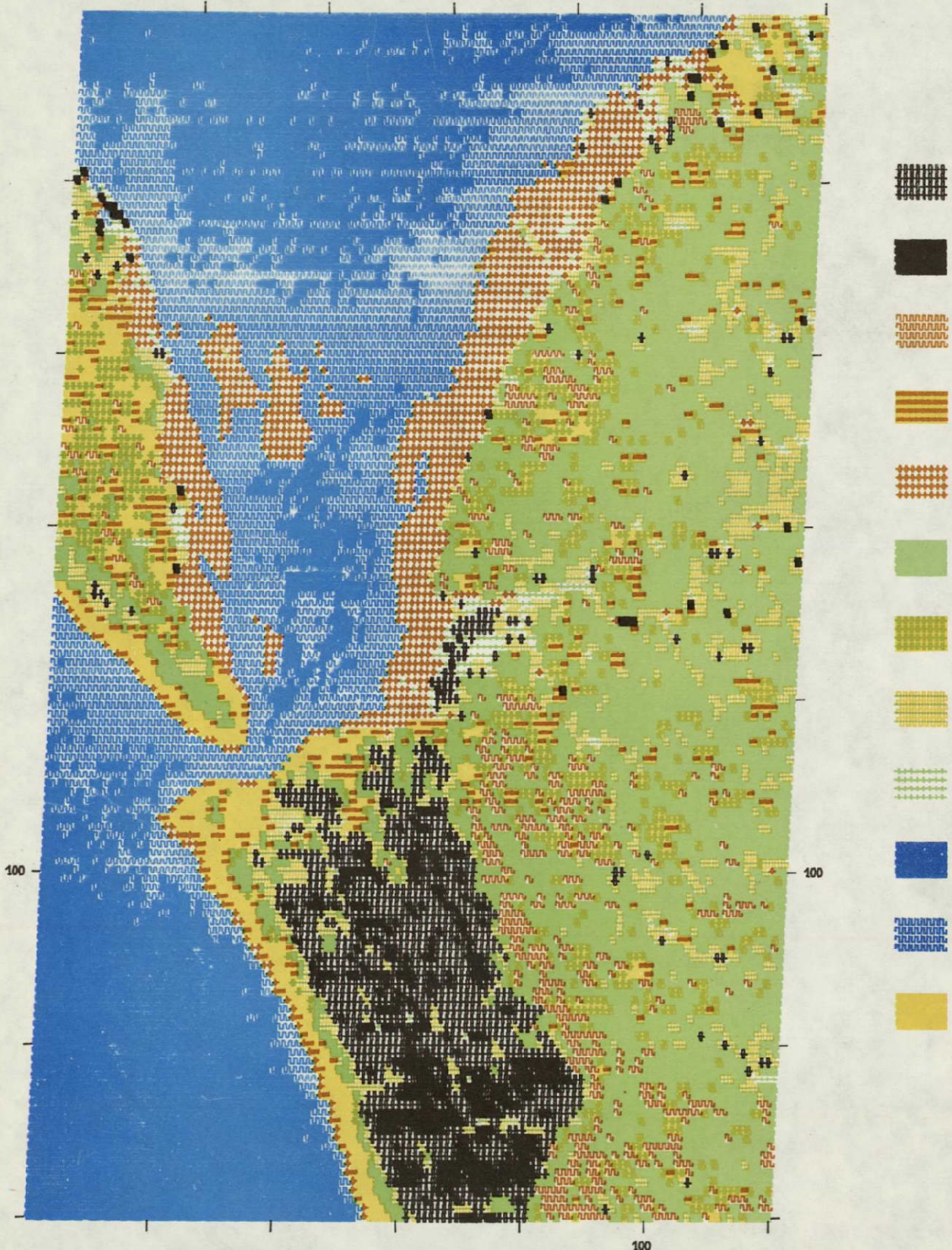
Fig. 3.2.A. - FRACAM Classification display of the Fromentine
area for the 29 July 1975

FRACAM classification (29 July 1975)

symbol n°	no Smoothing	With FRACARTO smoothing		
	FRACARTO mapping program	Majority vote		Conditional
		simple	itérated	
	Fig. 3.2.A	Fig. 2.2.C	Fig. 2.2.D	Fig. 2.2.E
1	1 095	1 236	1 303	1 124
2	433	298	258	390
3	614	472	446	541
4	472	205	146	330
5	1 251	1 260	1 264	1 247
6	3 928	4 612	4 864	4 068
7	967	733	665	879
8	1 038	651	501	875
9	236	163	145	165
10	3 330	3 180	3 200	3 170
11	2 939	2 920	2 923	2 941
12	497	554	569	554
Total	16 800	16 284	16 284	16 284

Table 3.2.B - Number of pixels pertaining to each category

When smoothing data, a rim of pixels is lost along each sides of the processed area

3..3 - INTERPRETATION OF LANDSAT DATA COVERING THE LOIRE ESTUARY

An accurate knowledge of the position of sandbanks in the Loire estuary
(Fig. 3.3.A) is essential for navigation up to the major harbour at
Nantes - St Nazaire and the new docks at Donges (10 km upriver). Navigable
channels are frequently dredged to maintain a constand depth. Outside thes
channels the shallows silt up continuously. This is most apparent off
Paimboeuf where low tides uncover numerous sandbanks, visible on charts
and survey maps. Extension and location of these banks varies considerabl\
according to map type and date. There are three main causes for these
variations :

- The banks have very weak slopes and a 10 cm error in soundings or
  levelling can lead to tens of meters in planimetric error.

- The nature of these banks (mud or sand) makes accurate bathymetri\
  or topographic measurement practically impossible.

- The combined action of currents, waves and estuaire sediment
  transport is constantly modifying the size and shape of each bank
  These actions can be very rapid, especially during a storm.

The long and costly depth-sounding missions are not very frequent. Survey\
were carried out by the Port of Nantes - St Nazaire harbour authority in
1969 (resulting in a 1/25 000 scale map) and in 1976-77.

Aerial surveys are also fairly infrequent, and are merely used for
updating terrestrial topographical maps.

Knowledge of sandbank movements is thus very inaccurate and is mostly
based on word-of-mouth reports from local fishermen who describe the
difficulties encountered in their navigation and the new channels they
occasionnaly find.

3. 3.1 - Landsat imagery used in this study

Technical conditions seemed. to be ideally suited for an
application of satellite imagery to see if this was adapted to
sandbank monitoring.

The following table shows the images used and the corresponding
tidal height.

Figure number	Date	Source	Tide height (meters)	Cycle
Fig. 3.3.D	Sept. 27 1972	NASA	2.37	EBB
E	March 8 1973	"	1.44	EBB
F	July 29 1975	"	3.18	EBB
G	March 28 1976	Telespazio	1.46	FLOW
H	June 26 1976	"	1.55	FLOW

Two other images were available covering this area but were not
used because of their high tide level (over 4 meters).
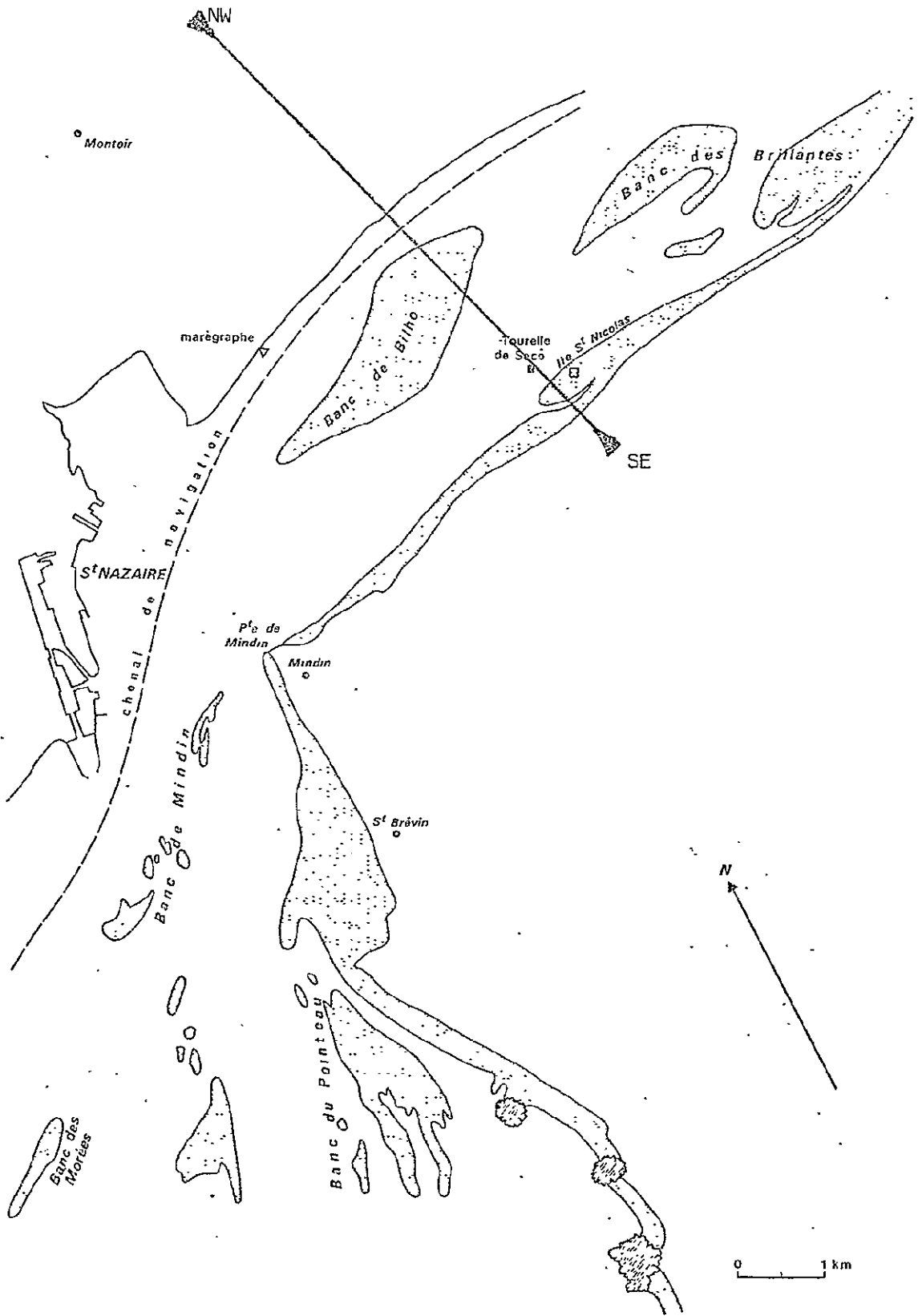
Fig. 3.3.A - The Loire estuary.
Location of transect cutting through
The Banc de Bilho is indicated

3. 3.2 - <u>Data processing in relation to local conditions of interpretatic</u>

Interpretation of the maps shown here is not straightforward

a - Three of the images show an <u>ebb tide</u>. This situation is characterized by powerful seaward currents with a heavy sediment load which is largely carried out to sea. These currents sweep the shallows and raise most of their fine sediment cover. It is therefore fairly difficult to distingui the actual sandbanks from turbid water.

The flow tide which predominates on the remaining two image: brings clear oceanic water into the estuary and the banks ar then clearly distinguishable.

Four transects (Fig. 3.3.B and 3.3.C) have been drawn up near the Banc de Bilho : two show ebb tides with Nasa-type digital values (5 to 8 in MSS7 for emerged banks) and two flow tides with Telespazio digital values (20 to 40 MSS7 fo: emerged banks). In both situations, the distinction between banks and water is easiest when the river outflow is lowest. During the low discharge periods, the estuarine turbidity area does not extend this far down channel whereas in flood periods this turbid area extends further seaward.

b - The part of the river between the port of St Nazaire and th new docks at Donges is heavily industrialised. <u>Aerial pollu:</u> is occasionally blown over the study area (cf <u>Fig. 3.3.F)</u> : has a similar spectral signature to sandbanks. This can lea to certain misclassification. Urban areas are also misclass: fied but their known position does not hinder interpretatio

c - Finally, the most difficult element of misclassification is the quasi-identical signature of <u>turbid water and sandbanks</u> Fig. 3.3.E shows a long turbidity plume near Mindin Point, developped in the same direction as the current. This is probably connected with the drilling operations in progress then for the construction of a bridge across the estuary at St Nazaire. There is a second, lighter, plume to the north, where drilling was less advanced. The muddy waters move alternately up and downstream with the tides.

3. 3.3 - <u>Significant results on the evolution of the sandbanks</u>

Observed variations cannot be accurately measured due to the differences in sea level between satellite overpass (1.74 to 0. meters) : pixel size is not compatible with this type of scene variation.

a - <u>Overall evolution from 1972 to 1976</u> : Throughout this perio at similar tide levels, the banks reduce in area. The two high river discharge images (3.3.E and 3.3.G) show over a two year period an identical outline for the Bilho bank to seaward whereas upstream the bank has receded in same tim to a line joining Paimboeuf to Montoir. The Brillantes bank has receded at both ends, partly because of dredging operations in the access channel to Donges harbour.
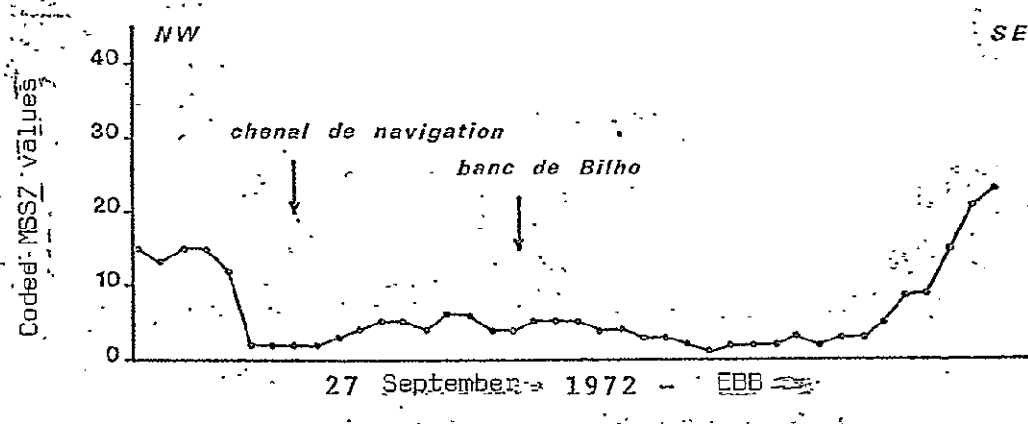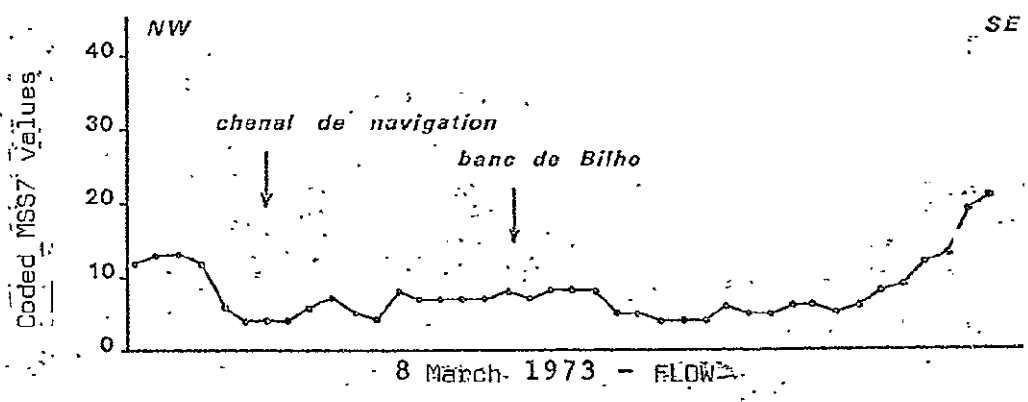
Fig. 3.3.B - Radiometric transects cutting through
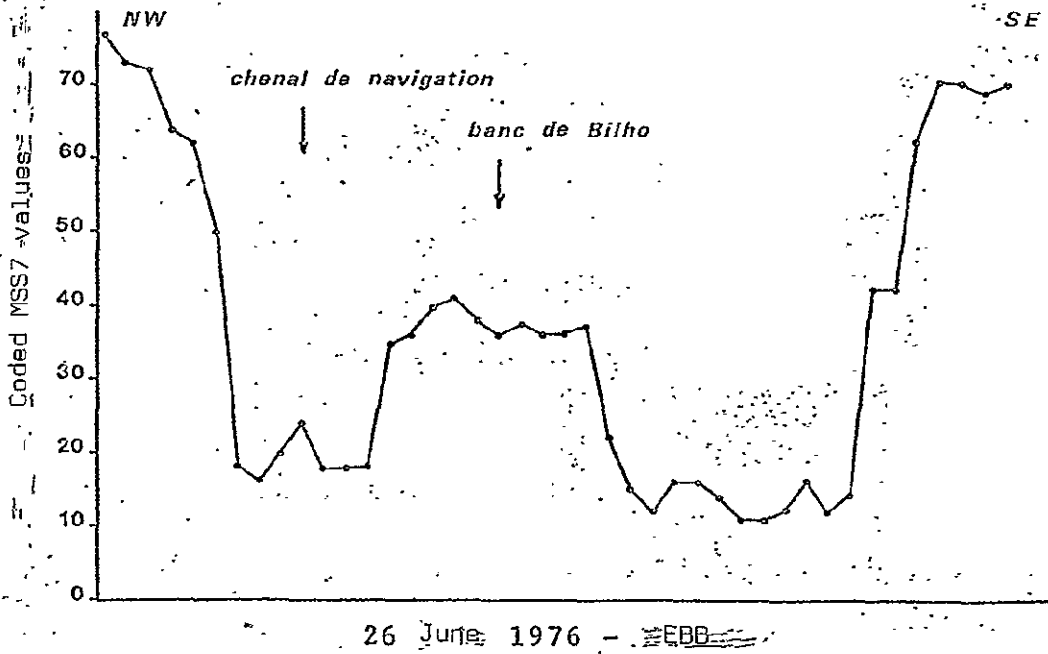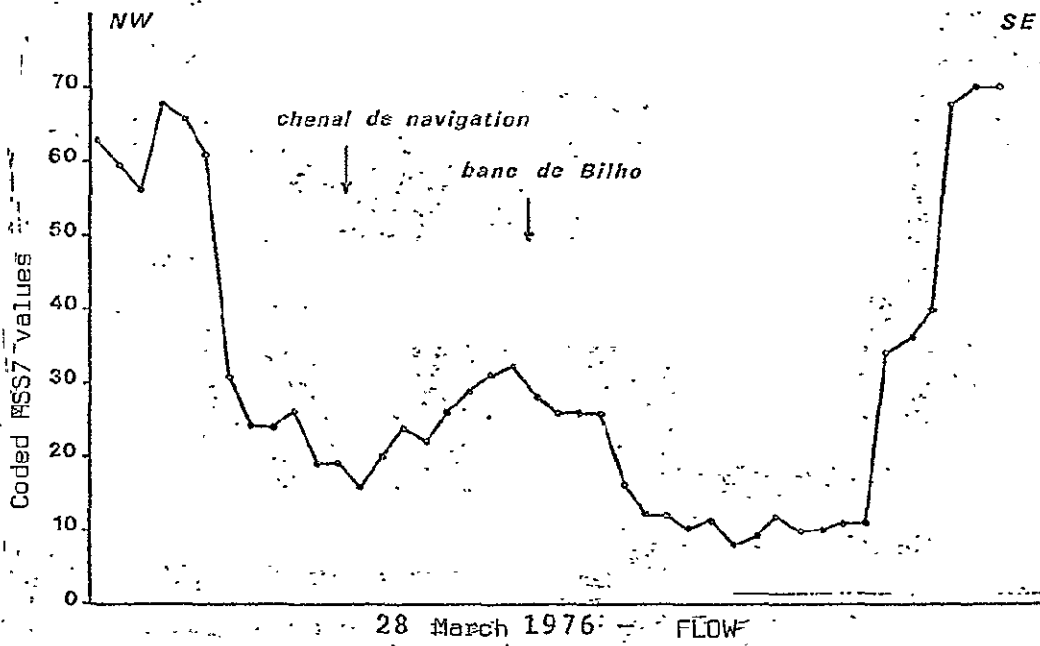the Banc de Bilho. LANDSAT-1 data received
from NASA

Fig. 3.3.C - Radiometric transects cutting through
the Banc de Bilho. LANDSAT-1 data received
from TELESPAZIO

The Mindin bank, clearly visible in 1973, has almost disppeared in 1976 where it is obscured by smoke from the St Nazaire area. The St Brevin bank, extensive and separate from the coast in 1973, is not apparent in 1976. Finally the Pointeau bank with its typical y-shape is considerably reduced in 1976. Thus the overall picture is an erosion of all the banks between 1973 and 1976.

The three low river discharge images confirm this interpretation especially since the water level is lowest at the time of the most recent image : Bilho and Brillantes banks are truncated to the north, Pointeau bank is thinned out and St Brevin bank has disappeared.

b - Seasonal variations

A seasonal cycle can be distinguished between the March images on one hand and the June and July ones on the other.

. The Bilho bank is seasonally stable, with little or no variation in its outline but the highest points of this bank (darkest tore on the maps) move fairly regularly upstrea from March to September. Remarkably, one of the culminating points in the March imagery (Fig 3.3.E and 3.3.G), located farthest downstream, disappears completely in the other image

The St Brevin bank is well separated from the coast in 1972 (Fig 3.3.D), and only linked to the coast at Mindin Point. During the winter, the whole bank moves nearer the shore and increases in height at both ends (Fig. 3.3.E). In March 1976 (Fig. 3.3.G) the remaining part of the bank is up against the coastline for most of its length. In June 1976 (Fig. 3.3.H) the bank is practically indistinguishable from the coastline. It appears, thus, that this bank is generally further offshore in the springtime than in the summer.

. The Pointeau bank forks into branches in the spring (3 in 1973 : Fig 3.3.E, 2 in 1976 : Fig 3.3.G) beginning at the Pointeau point and apparently modelled by currents. In June these branches are assembled into a triangular shape and in September a single curved ridge remains, probably reworke by the swells which strike it head-on.

c - Possible causes for these variations. For the three banks which show a seasonal evolution (Bilho, St Brevin, Pointeau) the spring state is conditionned by the geomorphological action of ebb-tide currents. The banks are stretched downstrea into divergent branches in the outer estuary. In the inner estuary, the banks move downstream where they are built up to a peak. Conversely in the summertime, when river discharge is reduced, wave influence is predominant and the banks are moved inshore and their outline is simplified, occasionally concave seaward. The banks of the inner estuary move back upstream and their situation is stabilised until the next spring floods

3. 3.4 - Conclusion

Long term evolution of the Loire river sandbanks has been evidence despite the scarcity of available imagery. Possible explanations have been proposed for the evolution but they can only be confirme by use of more frequent data covering other periods than spring or summertime.

TAXONS	MSS-4	MSS-5	MSS-6	MSS-7
	1-128	1-128	1-128	5-8
	1-128	1-128	1-128	4-4
	1-128	1-128	1-128	3-3

N

0   1   2 km
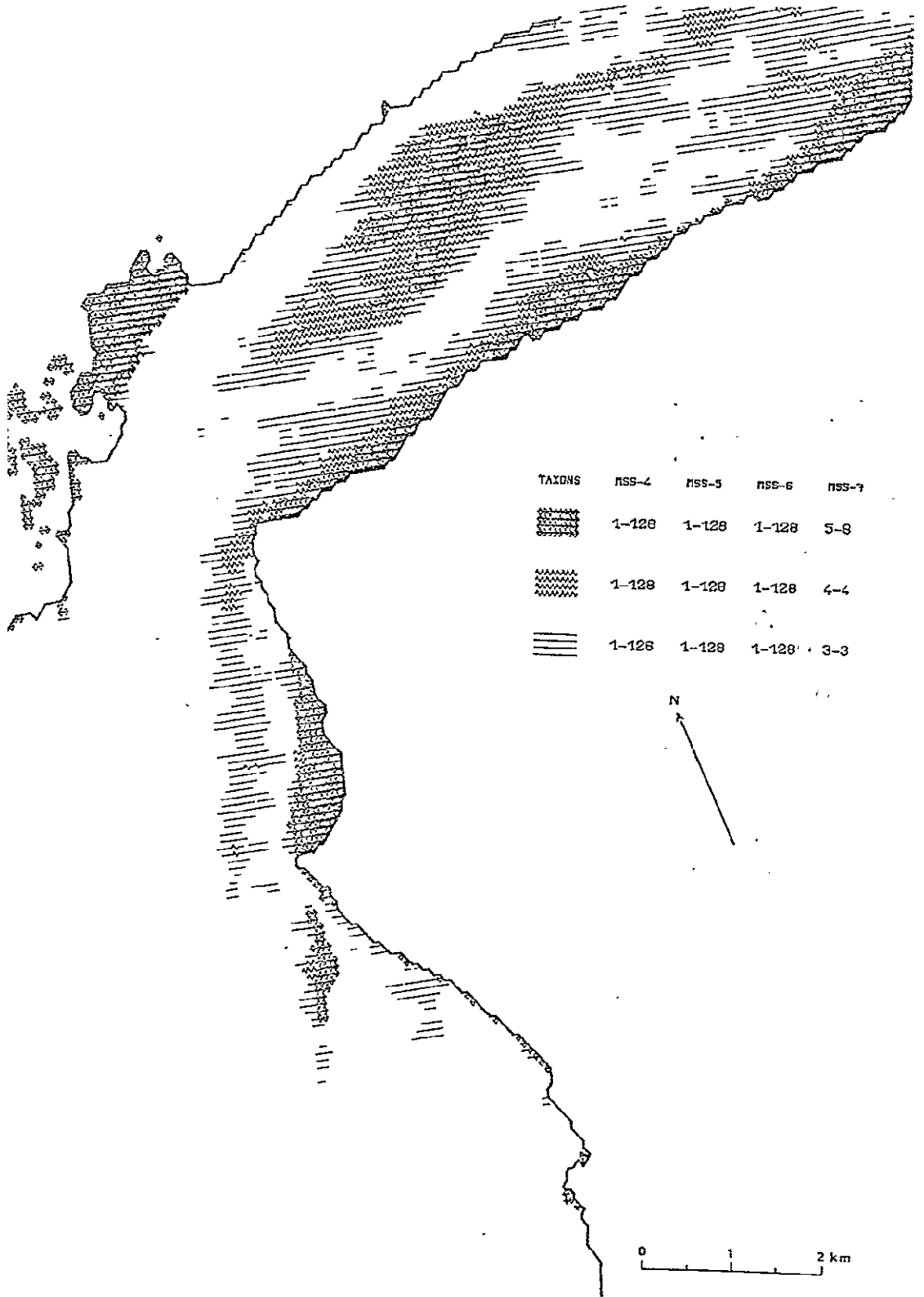
Fig. 3.3.D - Cartography of Sandbanks from LANDSAT
(Sept 27 1972)

TAIONS	MSS-4	MSS-5	MSS-6	MSS-7
	1-128	1-128	1-128	7-9
	1-128	1-128	1-128	6-6
	1-128	1-128	1-128	5-5

N

0   1   2 km
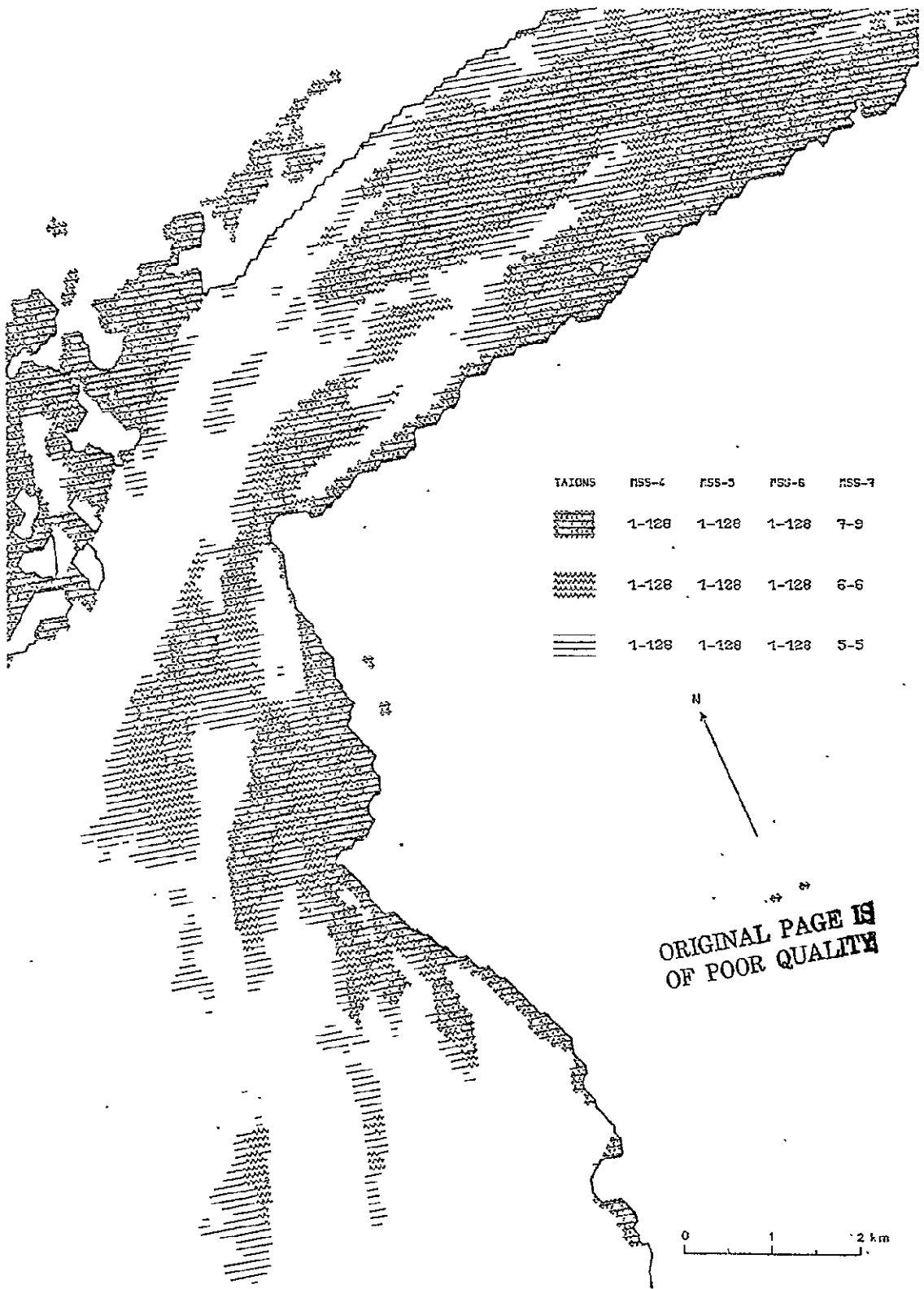
Fig. 3.3.E - Cartography of sandbanks from LANDSAT
(March 8 1973)

TAXONS   MSS-4   MSS-5   MSS-6   MSS-7

1-128   1-128   14-27   1-9

N

0   1   2 km
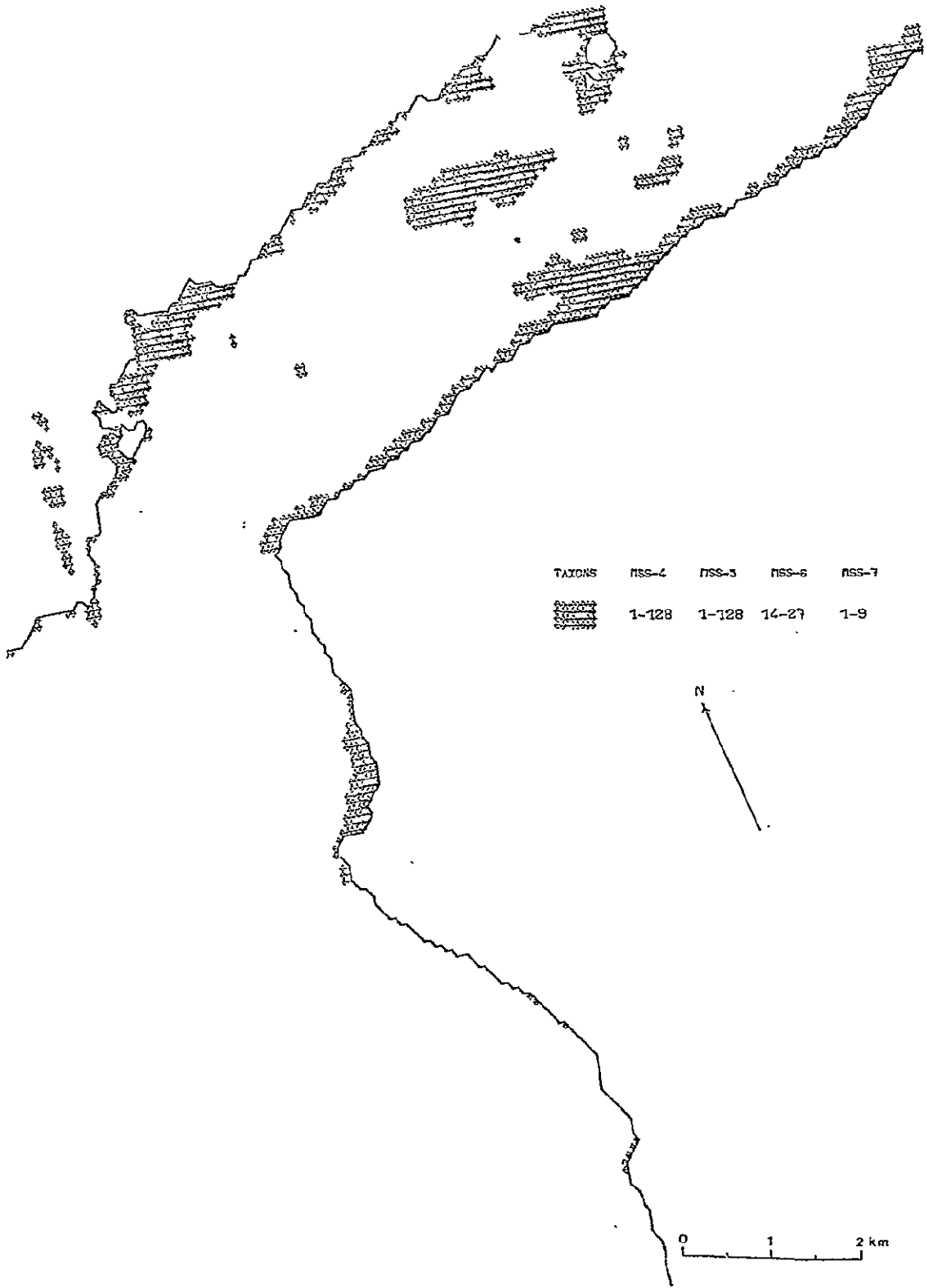
Fig. 3.3.F. - Cartography of sandbanks from LANDSAT
(July 29 1975)

	nss-4	nss-5	nss-6	nss-7
	1-128	1-128	1-128	32-37
	1-128	1-128	1-128	38-49

N

0   1 km
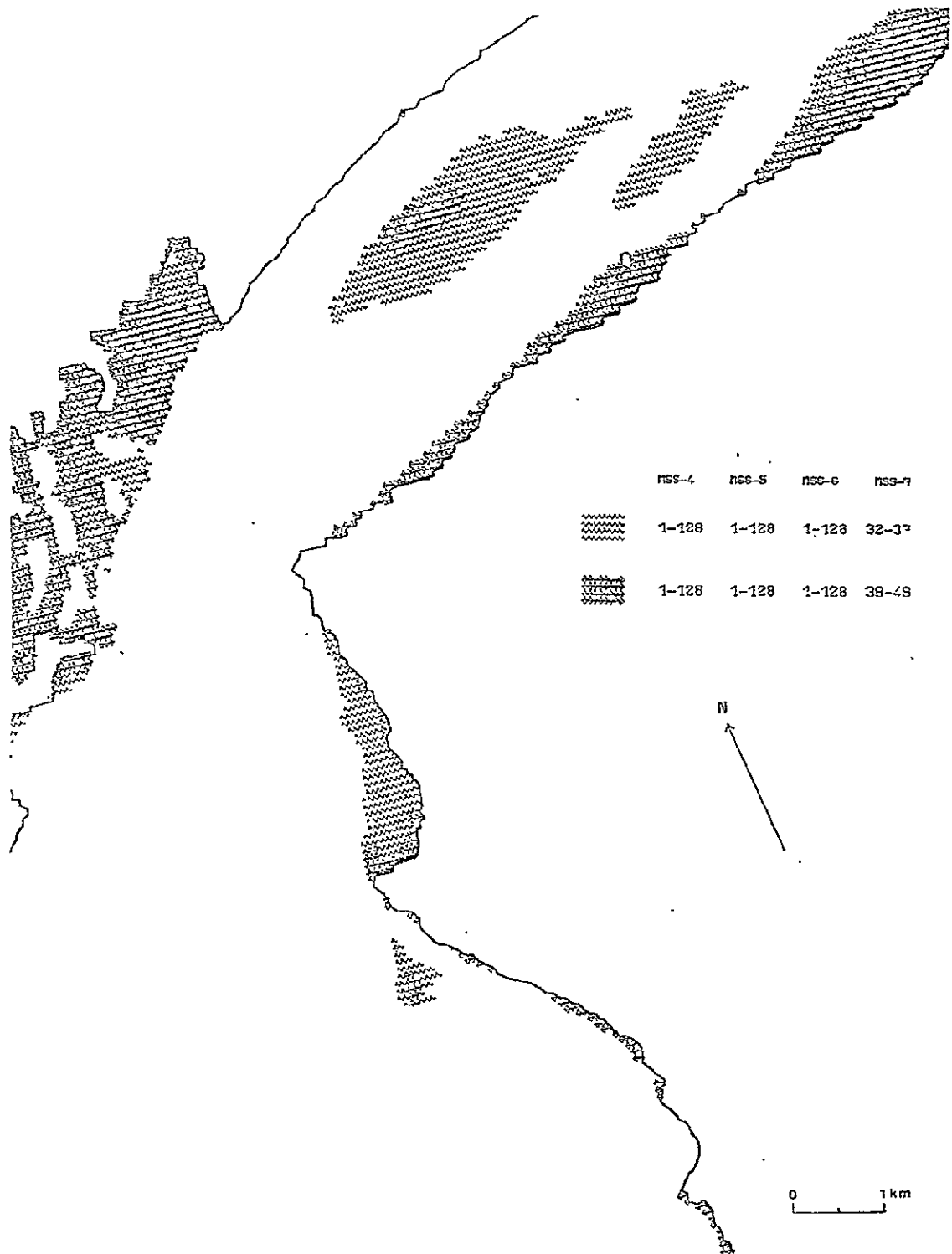
Fig. 3.3.G - Cartography of sandbanks from LANDSAT
(March 18 1976)

	MSS-4	MSS-5	MSS-6	MSS-7
	1-128	1-128	1-128	23-29
	1-128	1-128	1-128	30-40
	1-128	1-128	33-50	1-13
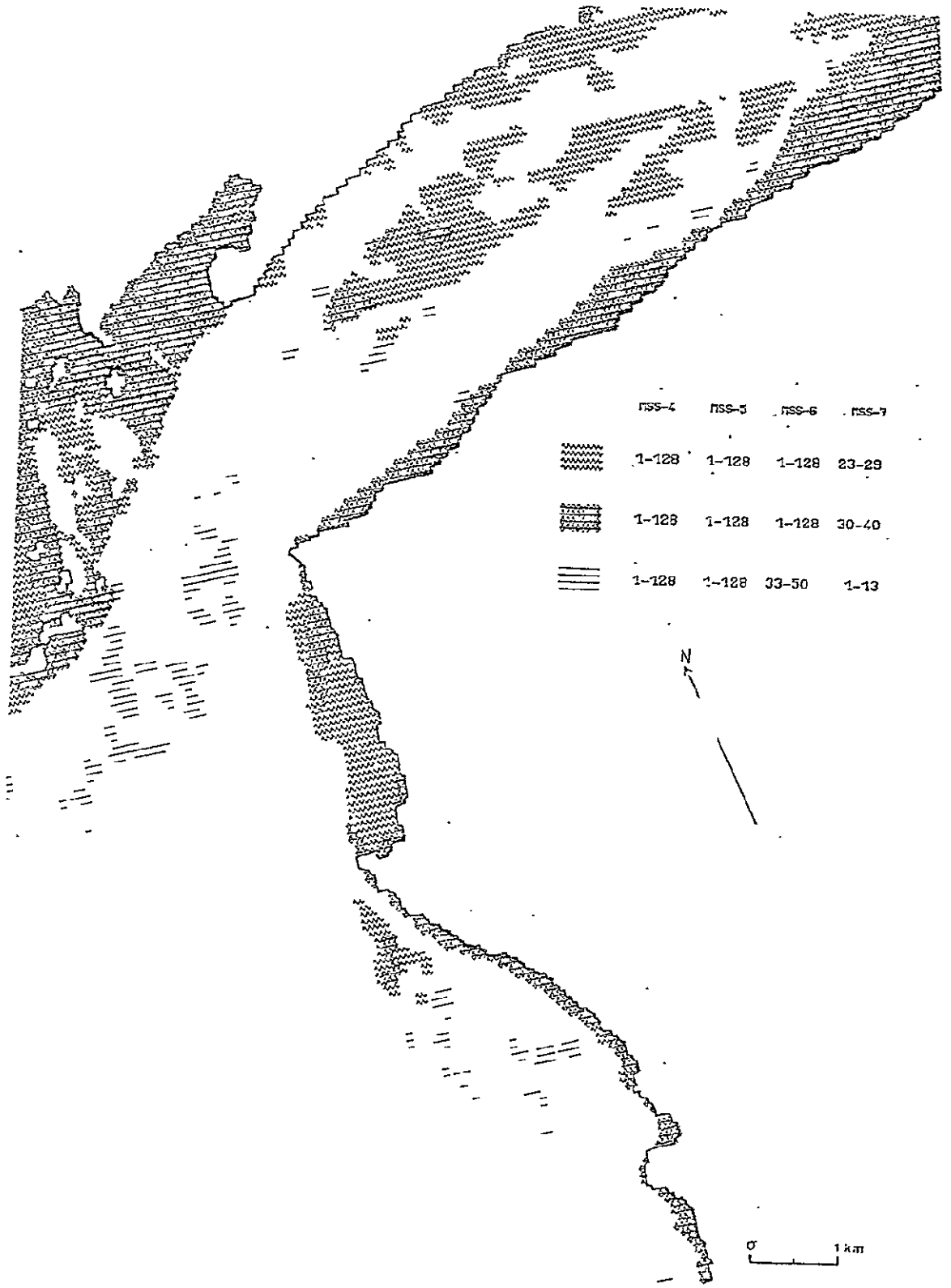
Fig. 3.3.H. - Cartography of sandbanks from LANDSAT
(June 26 1976)

3. 4 - INTERPRETATION OF GDTA SURVERYING OF MONT SAINT-MICHEL BAY

3. 4.1 - DATA SET SPECIFICATIONS

The aerial survey was carried out by the GDTA (Groupement pour le Développement de la Télédétection Aéorspatiale) on 26 June 1975 using a plane of Intitut Géograohique National.

a - Description of radiometers

Two DAEDALUS multispectral scanners were used in the visible and the thermal infra-red part of the electromagnetic spectrum.

These electro optical sensors are equiped with a mirror rotating at 80 r.q.s. and the entire optical system has an instantaneous field of view of 2.5 milliradians.

In the visible spectrum the DAEDALUS radiometer is equipped with a set of ten detectors whose wavelength characteristics are listed in. Tab. 3.4.A. In the thermal infra-red a second DAEDALUS radiometer was used with two spectral bands whose sensing windows are :

- 3 to 5 micrometers

- 8 to 14 micrometers

The analog output signals were recorded on a SANGAMO SABRE III 14-channel recorder along with a digital time base and continuous flight parameters such as : heading, roll and pitch.

b - Calibration schemes

The DAEDALUS radiometers are equipped with two internal calibration sources which are viewed at each mirror rotation before and after earth scan, they are called positive and negative reference values, respectively R^+ and R^-.

Transformation from output voltages to calibrated values is done on the basis of a running average of the R^+ and R^- time series with a time lag of 9 scans. Finally each of the 512 sample points of a scan line are transformed into calibrated values, using the following formula :

$$V_{ci} = (C_i \times V_{bi} - R^-_{ai}) / (R^+_{ai} - R^-_{ai})$$

where :

V_c = calibrated radiometric values of spectral band i

V_b = output voltage of spectral band i before transformation

C_i = amplitude coefficient of spectral band i used in order to generate an 8 bits (256 level) coding of V_c

R^-_{ai} = running average of negative reference values for spectral band i

R^+_{ai} = running average of positive reference values for spectral band i

Channel	Spectral band (in μm)	Ne De [I]
1	0,38 - 0,42	3,0 %
2	0,42 - 0,45	1,3 %
.3	0,45 - 0,50	0,4 %
4	0,50 - 0,55	0,3 %
5	0,55 - 0,60	0,2 %
6	0,60 - 0,65	0,2 %
7	0,65 - 0,70	0,2 %
8	0,70 - 0,80	0,2 %
9	0,80 - 0,89	0,2 %
10	0,92 - 1,10	0,3 %

Table 3.4.A – Spectral bands of the visible
DAEDALUS radiometer

(I) : Ne De is the minimum detectable
reflectance increment

The amplitude coefficient C_i is determined for each visible spectral band i as :

$$C_i = L_i \times K_i \quad \text{(visible and near infra-red)}$$

with

L_i = calibration coefficient equal to the equivalent radiance of the built-in reference source

K_i = conversion coefficient ensuring an 8 bit output code

It is worth noting that K_i is different from one spectral band to the next but is also dependent on the surveyed scene.

In the thermal infra-red, determination of C_i is slightly different :

$$C_i = (T_{i2} - T_{i1}) \times K_i \quad \text{(thermal infra-red)}$$

with :

T_{i1} = equivalent black body temperature of the negative reference source

T_{i2} = equivalent black body temperature of the positive reference source

c - <u>Survey planning</u>

The surveyed area (Fig.3.4.B) is organized as a meridian transect going from the Dol marsh in the south to the Chausey islands in the north. It displays transitions between various environments such as : a precambrian formation, a cultivated marsh, some semidentary and rocky tidal flats and various gradations of water turbidity.

Data gathered on 26 June 1975 are organized in five different overpasses labeled α to ε(Tab.3.4.C). Results presented here are related to overpass α because it was the only one for which photographic documents, DAEDALUS analog displays and corresponding digital data were available. Furthermore at time of survey (15h 20 mn) hydraulic conditions were good because tidal flats were uncovered by a low tide of coefficient 0.79.

During the days preceeding the survey no rain precipitation was noticed and winds were measured at the Pointe du Grouin semaphore as N.W with a 3 to 4 m/s speed.

3 .4.2 - <u>Data processing</u>

Computer compatible tapes were generated by GDTA for overpass 1 and 3 which are labeled α and ε in our nomenclature. Data analysis was limited to a subset of overpass α which regrouped a representative sample of objects to be mapped.

Different data processing methods have been used regarding the thermal infra red temperature imagery and the measured radiances in the visible and near infra-red.
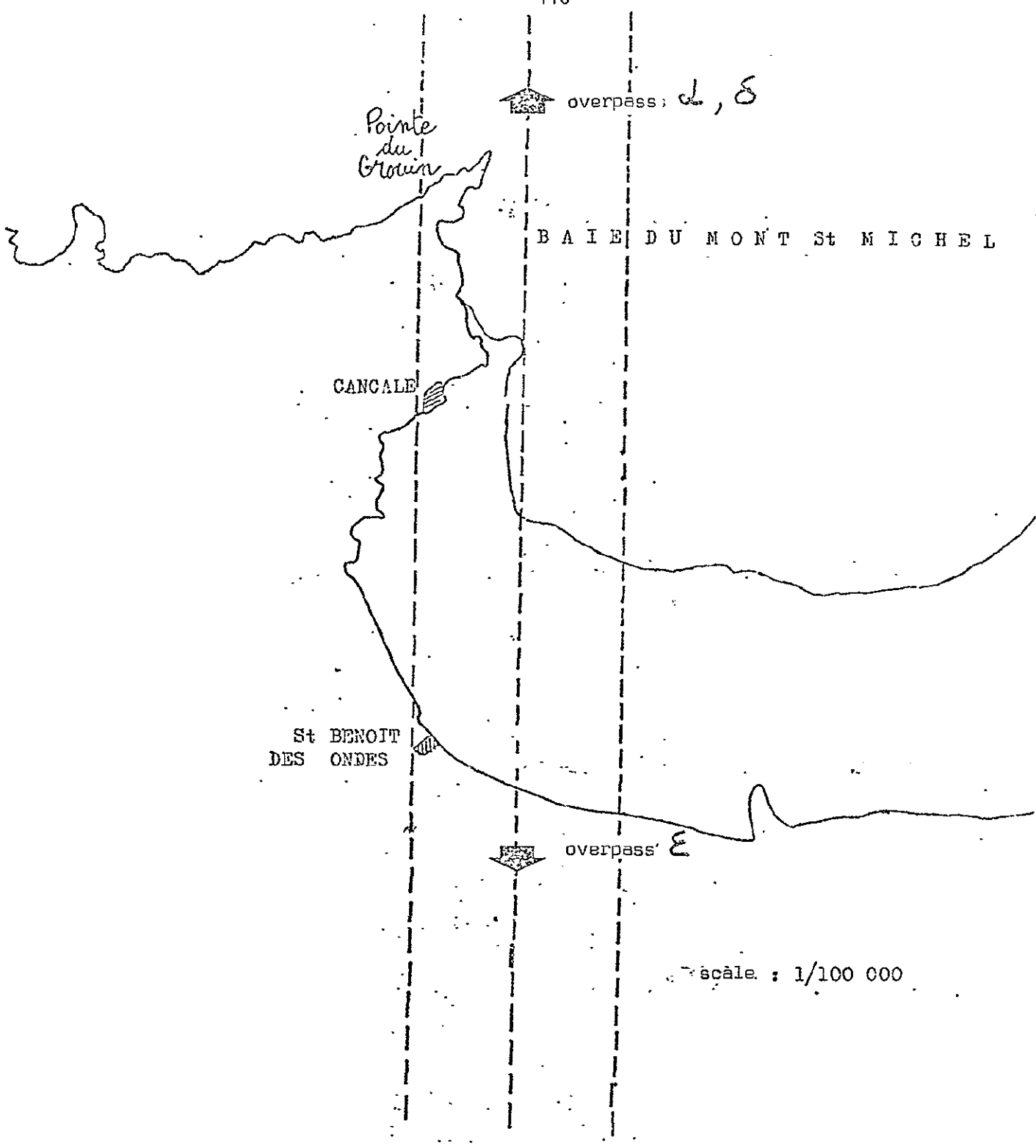
Fig. 3.4⸱B - Survey plan of the GDTA mission on 26 June 1975
This transect is related to overpass α,δ and ε

Overpass	Site	Heading	Altitude	Photography (1)	DEADALUS analog imagery	DAEDALUS digital data
α	Cancale	10°	2510 m	Yes	Yes	Yes
β (4)	Cancale	210°	4875 m	——	——	——
γ (5)	Mont St-Michel	35°	5060 m	——	——	——
δ	Cancale	10°	2510 m	Yes	Yes	No
ε	Cancale	190°	2510 m	No	Yes	Yes

Table 3.4.C - Missions characteristics of
Mont Saint-Michel GDTA survey

(1) : Infra-red photography taken with a WILD RC8 camera
of 152 mm focal length and 74° aperture

(2) : channels 3, 4, 5, 10 and thermal I.R.

(3) : channels 1 to 5,7, 9, 10 and thermal I.R.

(4) : documents not available

(5) : documents available at I.G.N.

a – Thermal infra-red processing

Data recorded for the 8-14 μm band are transformed into surface tempera
tures using calibration parameters stored in the first records of the
magnetic tape. Output of this preprocessing phase in a file of pixel
values in Celsius degrees uncorrected from atmospheric absorption.
Format of this file has been made compatible with the input format
of the NOAA VHRR thermography processing program (TSS system).

Following treatment done by TSS is in two phases :

- removing of striping effect noise by resetting the sequence of
  line histograms

- smoothing using a 7 x 7 boxcar filter conditioned to contrast
  enhance significant boundaries.

Results can be displayed on various peripheral equipments : line printe
electrostatic printer-plotter (VERSATEC) for intermediate maps and
incremental color pen plotter (BENSON) for final edition.

b – Visible and near infra-red processing

Measurements recorded in the eight channels (C1 to C5, C7, C9 and C10)
are preprocessed in order to estimate and subsequently correct for
along scanlines systematic bias trend. This trend is due to the variati
along the scan of the relative geometry of viewing angle versus solar
angle.

After bias correction, the different typesof ground objects are cate-
gorized using the FRACAM interactive classification system (cf 2.4.)
Some groups can be subdivided after the initial classification phase
using the adaptative descending classification approach.

Final results are displayed as color maps using the FRACARTO program
(cf   2.5).

·3. 4.3 – Significant results

a –. Test area presentation

The. test area presented here includes most of the infra-tidal and
continental categories which can be characterizedôin the west part of
Mont Saint-Michel bay.

Category and terrain description are drawn from observations which
were made at airplane overpass time or a few hours after it.

a – 1 – Infra-tidal zone

The infra-tidal zone is characterized by flat expanses always
carbonaté rich with a N.W oriented slope ranging from 2.5 o/oo
to 3 o/oo along tidal channels.

a – 2 – Infra-tidal zone

In front of Vildé – la – Marine village where ground- truth was
collected, the tidal flats are wide (of the order of 3 km in
width) and dip to the sea with a gentle slope (of the order of
3 o/oo). Sediments are made of "tangue" which is granulometry
and minerally defined as follows :
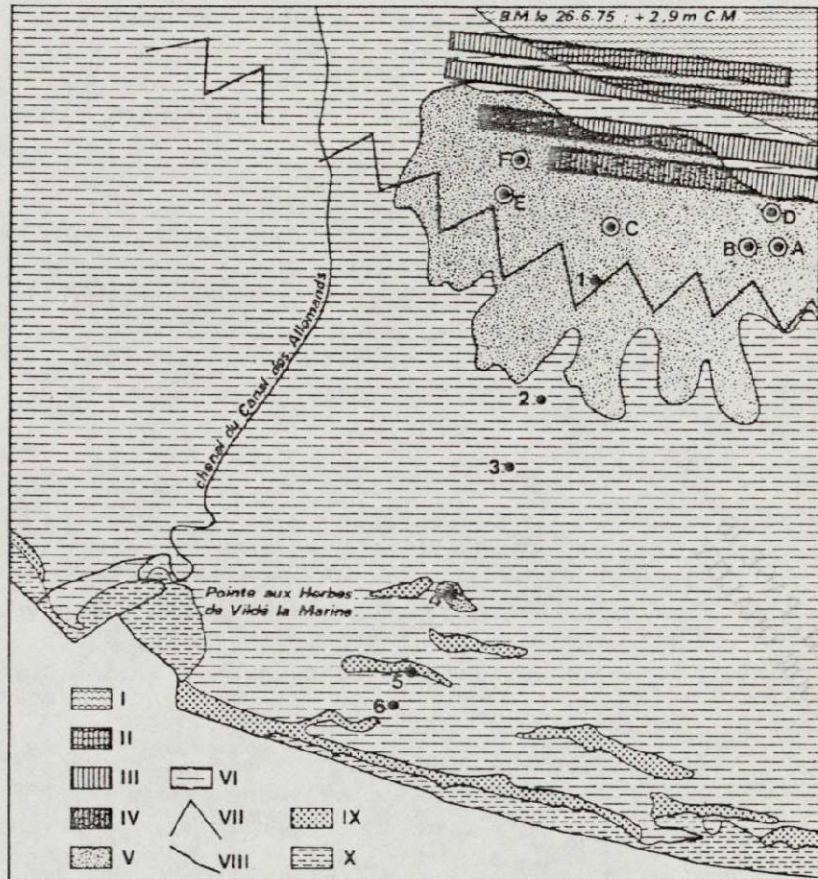
Fig 3.4.D - Localisation of categories (taxons)
present on the infra and inter-tidal zones
A to F : diatomee samples ; 1 to 6 : sediment
samples :
I   : turbid to non turbid water ;
II   : flooded mussel nurseries
III : dry mussel nurseries ;
IV   : mussel nurseries on diatomee covered "tangue" ;
V   : diatomee covered "tangue" ;
VI   : bare "tangue" ;
VII : fish traps ;
VIII : channel ;
IX   : calcareous sand bar ;
X   : tidal flat (schorre)

- particle size median between 6 and 103μm ;

- percentage of the 2 to 200μm fraction ranging between 51 % and 84 %

- percentage in carbonates ranging from 28 % to 65 %

Thee is a trend to larger particle sizes and coarser sediments near the coast line (Fig. 3.4.D and Tab3.4.E, samples 1 and 3).

During the survey, concentration in organic matter was found to constant over the whole tidal flat surface with values ranging from 5 % to 7 %. On the contrary sediment water content was decreasing landward from the low tide line (36.5 %) to the salt marshes (18.5 %).

Finally, large expanses of the low flats were covered with a fir layer of diatomees (Tab 3.4.F).

In the upper part of the inter-tidal zone the monotony of "tangu flats is disrupted by sandy levees. The shell-rich material of these levees is quite different from "tangue" granulometry as well as their concentrations in water, carbonates and organic matter (Tab3.4.E, samples 4 and 5).

The only main tidal channel is the Canal des Allemands. It is deeply cut into the upper part of the flat resolving to a modest opening near the sea line.

It is also noticeable that the "tangue" flat bears a large numbe of human artefacts ; fish traps which are one to two meter high wooden constructions, mussel shells poles scattered seaward of the traps.

Near the upper part of the flat, the salt marsh (schorre) is gradually taking over the "tangue". The salt marsh is limited in the test area to a narrow triangular surface on the east bank of the Canal des Allemands. Its gramelometry and mineralogy are sin to those of the "tangue" (Tab3.4.E, sample 6). It is, however, different from the barren flat in its morphology and bears salt tolerant plant grouth mostly composed of Puccinella maritima, Aster tripolium and a thin strip of Obione portulacoides along channel banks.

a - 3 Continental zone

Behind the Duchesse Anne Lyke, the test area extends over the Dol marsh. This cultivated area has soil properties which are very close from "tangue".

b - Results interpretation

b - 1 Thermal infra-red

Interpretation of results obtained in the 8-14 μm wavelengths has helped in outlining several interesting phenomena (Fig. 3.4. Going landward from coastal waters to the Dol marsh :

Samples	20-2 mm in %	2-0,2 mm in %	200-20 m in %	20-2 m in %	inf. 2 m in %	Organic matter in %	Carbonate in %	Water content in %
1	-	0,2	27,6	29,6	42,6	7,0	27,9	36,5
2	-	0,6	42,5	25,4	31,5	6,0	38,2	31,0
3	8,4	31,4	45,6	5,7	8,9	5,5	59,8	18,5
4	9,5	39,0	51,5	-	-	1,5	64,8	12,0
5	10,7	85,6	3,7	-	-	0,5	83,9	1,0
6	-	1,2	60,5	23,2	15,1	5,5	42,5	26,0

Table 3.4.E - Granulometry, organic matter content, carbonate and water contents for
the various ground truth stations (cf. Fig. 3.4.D)

Samples	Stations					
	(A)	(B)	(C)	(D)	(E)	(F)
Coscinodiscus lineatus	+	+	+	+	+	+
Navicula cancellata	+	+	+	+	+	+
Gyrosigma fasciola	+	+	+	-	+	+
Amphiprora sp.	+	+	+	+	+	-
Coscinodiscus nitidus	+	+	+	-	+	-
Pleurosigma angulatum	+	+	+	-	+	-
Biddulphia regia	-	-	+	-	-	-
Melosira dubia	-	-	-	+	+	-

Table 3.4.F - Distribution of most abundant (+) diatomee species at
various stations [1] (cf. Fig 3.4.D)

---

(1) Measurements were made by Mr RICARD at the Laboratoire de
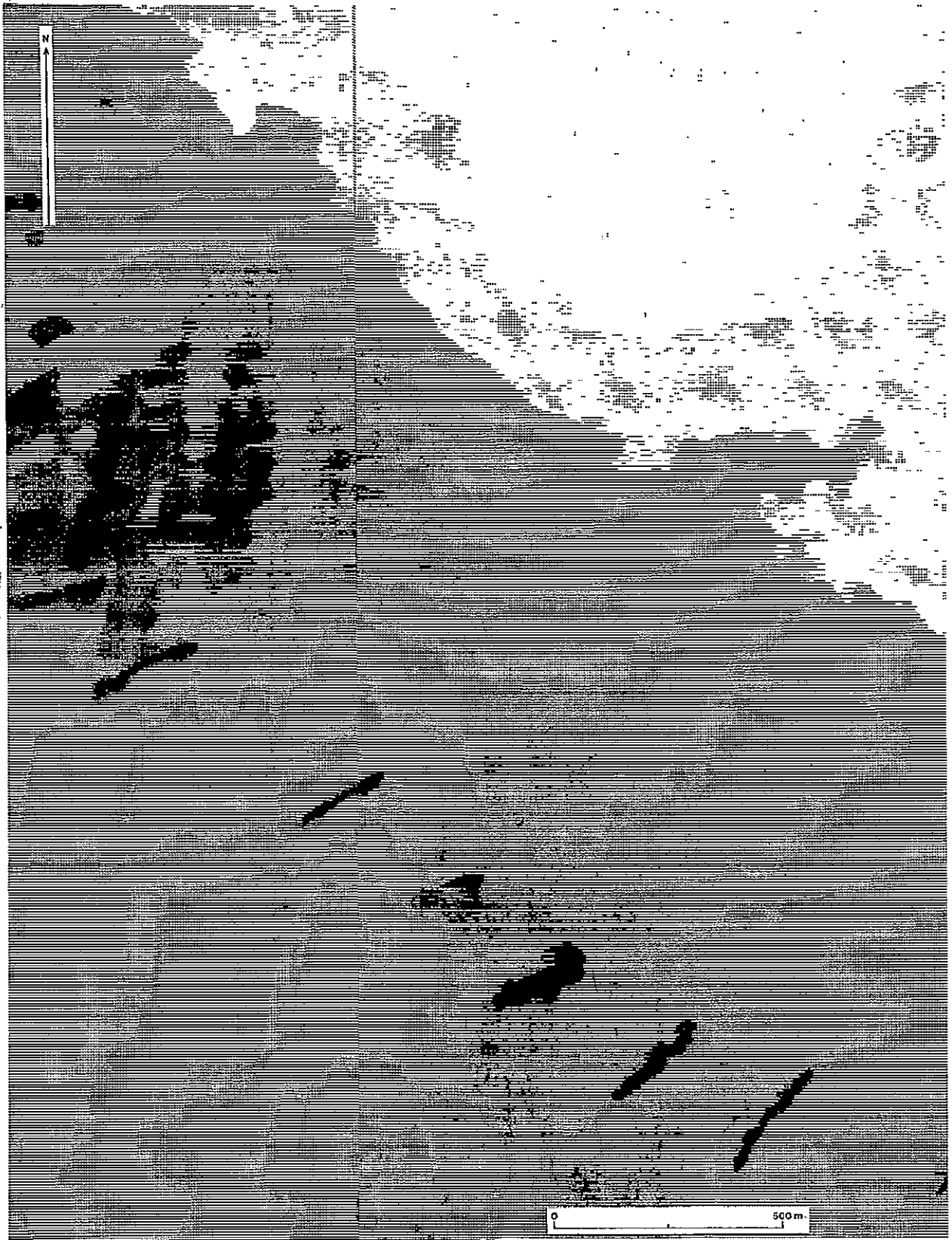Cryptogamie of Museum National d'Histoire Naturelle.

Fig. 3.4.G. - Thermal infra-red mapping of the inter-tidal
zone off the Dol marsh (Fig. 3.4.D.)

- arrival at the beginning of flow tide of cold and clear
  waters in turbulent mixing with warmer bay waters which are
  heavily loaded with sediments. This contact takes place
  around the Chatelier and Rimains islands.

- digitations of warm water coming from the tidal flat are
  abundant at the limit between infra and inter-tidal zones.
  This flow takes its origin in the fish trap which is near
  the east bank of the Canal des Allemands channel. Orientation
  of this flow is easily explained by the fact that tidal
  currents were running N.W during the experience.

- a temperature difference between warm diatomee covered
  "tangue" and colder barren flat.

- a specific thermal signature for the mussel shells nurseries
  (bouchots) which are higher in temperature than the diatomee
  covered "tangue" on which they are settled

- a thermal assymmetry between each side of the "V" shaped
  fish traps : the westward side being warmer than the east ward

- finally sand levees and barren fields of the Dol marsh are
  similar in surface temperature which is much higher than
  for the other targets.

b - 2 Visible and near infra-red

The analysis of spectral signatures present in a test area of
350 scan lines of 180 sample points has led to the study of a
complete disjunctive coded data set K_{IJ} (cf. 2.4) with $I = 63000$
sample points and $J = 64$ spectral coded equivalents. This matrix
was analysed by the FRACAM automatic classification system.

Interpretation of a classification in nine categories lead us to
the following conclusions :

- category limits are correct but some misclassifications
  subsist in detailed category assignments

- "tangue" is well discriminated by classification and
  subdivided in several classes depending on its water content

- sandy levees as well as locally sand rich "tangue" masses
  are correctly outlined

- diatomee covered areas are separated from barren ones but
  some misclassification occurs with cultivated fields of the
  Dol marsh

- finally salt marshes and other parts of cultivated fields
  fall into the some category.

4 - Criticism

In conclusion, two points must be emphasized :

- correction for systematic bias in the visible and near infra-red was estimated on the tidal flat zone. Unfortunately it appeared that forward scattering of solar light was function of target albedo and surface texture so that trend correction was not complete for sea water and continental zones. It is this phenomenon which is responsible for most of the misclassifications

- however results were sufficiently good to assess the feasibility of mapping tidal coasts by automatic classification of remotely sensed data. In the present study thermal infra-red was found to be best for knowledge of water movement and mixing in the west part of the Mont Saint-Michel bay while visible and near infra-red was better used for mapping tidal flats and associated organic films.

3. 5 - INVESTIGATION OF A COASTAL UPWELLING USING NOAA DATA

3. 5.1 - Data description

Since 1972 NASA has regularly launched on a yearly basis a series of meteorological satellites which are run under the supervision of the National Oceanic and Atmospheric Administrati The NOAA satellites (currently NOAA5) are equipped with various electro optical systems. Among them the two Very High Resolution Radiometers (VHRR) are of interest for oceanographic application

Satellite orbit is sun synchronous with an inclination of 101° over the equator ; this allows any point on earth to be surveyed twice a day. Time of overpass is approximately 9 AM and 9 P M Universal Time for the coast of France. The geometry of this quasi-polar orbit tends to simplify the problem of geometric correction.

The two radiometers operate in different spectral bands :

- in the infra-red (IR) domain, from 10.5μ to 12μ for the VH

- in the visible domain, from 0.6μ to 0.7μ for the VHRR2 thei identical systems consists of a 12.7 cm aperture elliptical mirror with a surface of 100.4 cm^2. Rotation speed of the mirror is stabilized at 1 revolution per 150 milliseconds.

The relative flux is reflected by the mirror and focused on a detector thus leading to a 0.6 str instantaneous field of view (IFOV). With the satellite cruising at an altitude of about 1460 kms, the ground resolution is 0.88 km. Rotation speed of the mirror and trajectory velocity are synchronised so that no overlapping occurs in the relative geometry of consecutive scan lines.

The horizon to horizon scanning is done through a 70° rotation angle, and during the remaining part of the 360° complete revolution, the mirrors scan various internal calibration equipement such as two black bodies maintained at a fixed temperature and a point in space opposite the sun. About twenty different calibration signals are acquired during one revolutior this information is used to convert the voltage output of the system into black body radiance.

The signals transmitted by the satellite are acquired at the Meteorologie Nationale station (CEMS) in Lannion (Bretagne). It is then digitized and preprocessed for data cleaning and compression of the calibration information. The data is availab) in 8 bit coded digital form on magnetic tapes which are sent upon request to various users outside the meteorological communit

At Ecole des Mines the main point of interest is deriving sea-surface temperatures maps at scales ranging from 1/100 000 to 1/250 000 for various areas along the Atlantic and Mediteranean coasts of France.

A data file corresponding to an acquired image of the Earth
includes one record for each scan line. Each record in physically
built as follows ;

- 20 calibration values (16 bits)
- 2068 pixel values (8 bits) for the IR channel
- 2068 pixel values (8 bits) for the visible channel

Processing is currently done on 800 to 2400 scan lines files.
The number of lines for a complete coverage of France is
approximately 1200.

3. 5.2 - Data processing

In the production of surface temperature maps, the first step
is to convert the 8 bit digital counts into black body radiances.
This is done using a locally linear approximation of the Boltzann
formula based on the calibration information. From this step
onwards, the data of interest, usually a subset of the entire
scene, is handled in degree Clesius stored in binary floating
points form.

The maps are produced as false-color displays or contour plots.
The direct interpretation of these results has been very difficul
due to the presence of spurious disturbances in the data. These
problems were not experienced in other oceanographic applications
such as the mapping and tracking of Gulf Stream meanders done by
various NOAA experiment teams.

This is due to the fact that in Europe our scientific interests
are more localized geographycally and that we are looking at
temperature gradients of a few degrees using the VHRR scanner
which has a nominal performance between 1° C and 0.5° C.

Due to these differences in scientific approach, the oceanographi
community in France is much more demanding on the refinement of
the data processing necessary to bring out useful details in the
sea-surface temperature structure.

Two types of disturbances have been identifield

- a background noise caused by transmission or analog to
digital conversion
- a striping effect due to sensor gain losses affecting the
calibration signals.

The striping effect is similar in nature to the one currently
experienced in LANDSAT imagery. However, in this case, one does
not observe the six band repetitivity which is particular to the
LANDSAT scanner technology. The jitter in average value from one
line to the next displays on the contrary a random structure with
characteristics varying in time during data acquisition. The
variability can be as wide as it can be a purely random noise or
a rather smooth modulation expanding over 10 to 20 scan lines.
The lack of a typical frequency in this jitter led us to discard
frequency domain filtering as used in various oceanographic
applications of LANDSAT imagery.

Other methods were used such as smoothing averages or modes of the scan line histogram time-series. These approaches did not prove sufficient to eliminate the scan line noise in NOAA data. This is why a new method was developed which takes into account the complete structure of the marginal distribution of each scan line instead of only using a condensed information extracted fro this distribution such as an average or a mode value.

The so called background noise is essentially isotropic in natur and evenly·distributed in the image plane. It is responsible for the "salt and pepper" aspect of the display. Its elimination involves a straightforward two-dimensional weighted smoothing · algorithm.

The cleaning effect is satisfactory especially when the algorith is iterated several times, leading to a contouring effect in the display which is rather useful for oceanographic applications. The drawback of this approach is that the contrast at the bounda between the earth and the sea is smeared at each iteration with a consequent degradation of the geographic location of the coastline.

This annoying effect is of particular importance for coastal applications where one would like to retain the original spatial definition of the coastline·as produced by the ground resolutior of the NOAA scanner data (approximately 1 km). In order to meet this goal the smoothing was conditionned to the local gradient i relation with average RMS of the background noise.

The unstriping and the iterative conditionned smoothing are sequentially applied to the data set of sea-surface temperatures the final product is a smooth isocontour temperature field whicl can be easily interpreted by the oceanographers and have been found of great value when stored and compared for different . satellite overpass dates.

3. 5.3 - Significant results

A - Interpretaion of imagery

The data we have used for our interpretation is NOAA4 image acquired on 30 July 1975 at 9h 17 mn TU. The generated maps (Fig. 3.5.A and B) cover the oceanic waters surrounding the Finistère shoreline. In the visible band the gray scales ar related to various radiance levels expressed in FT.L. In th thermal infra-red band the gray scales are associated to radiometric temperatures measured in Celsius degrees (°C).

The land features are characterized by radiances greater than 10 FT.L and temperatures greater than 21°C, they appea respectively in white (VIS) and black (IR) on the imagery. In the visible band, some confusion is possible between lan and clouds and the coastline is rather fuzzy around the Crozon Cape.
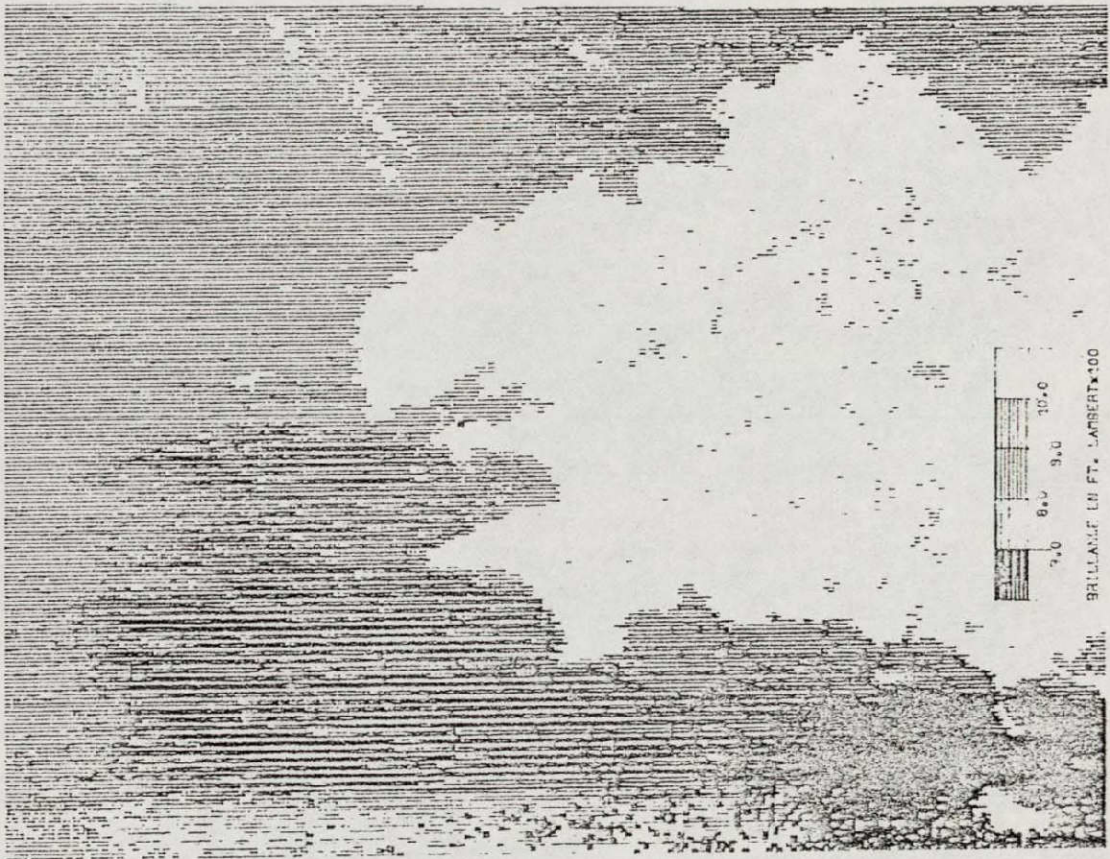
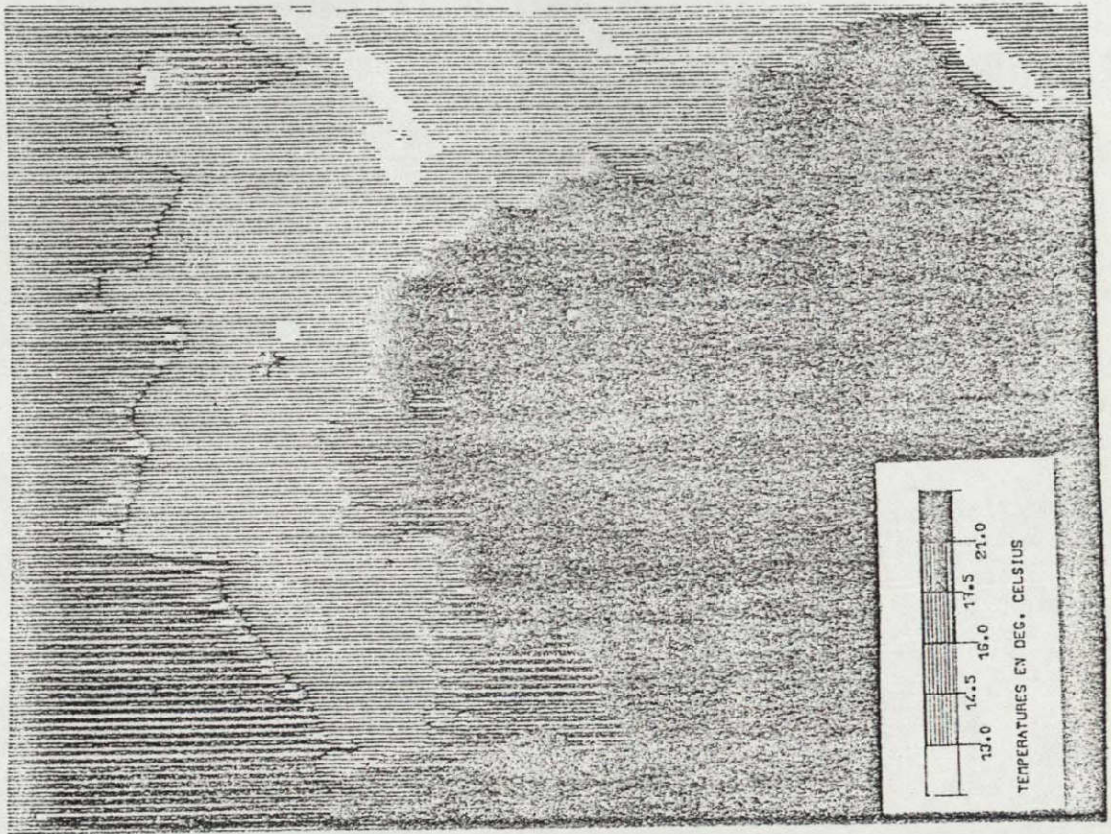Fig. 3.5.1 - Display of the NOAA-VHRR visible band
Finistère coastal area.

Fig. 3.5.B - Display of NOAA-VHRR infra-red band
Finistère coastal area.

The clouds with high radiance are easily outlined in the visible band North of Finistère, organized in North-West strips. The corresponding features in the infra-red have temperatures under 13°C. However they are generally broader masses than in the visible, this is due to the inertia of the infra-red sensor whis is less capable of following instant contrasts. The resulting contamination has lead us to eliminate from our oceanographic interpretation most of the English channel, North of Finistère.

Coastal fog is frequent along these coasts in summer, and their detection is more complex than that of the preceeding features. For example, in the Saint-Brieuc bay they could be interpreted in the visible as patches of turbid water whith rather high radiances. This confusion is easily avoided when using the I.R because their apparent temperature is much lower than the average seasonal temperature of the coastal waters of Brittany (typically 16°C). Probable presence of a small cloud of fog can be suspected North-West of Ouessant.

A cold surface front expands in the ocean waters West of Finistère. Organized in a crescent like shape from the Raz point to the North of Ouessant it is characterized by surface temperatures between 13°C and 16°C. They are easily separated from the waters of the mouth of the English channel (> 16°C) and also from the coastal waters of South Brittany which are even warmer (above 17.5°C). Warm water pools are also locally trapped along the Finistère coast, South of the Raz point, in the Douarnenez bay and in the Brest sound.

b - Ground truth checking

Simultaneously with satellite overpass, a team of English oceanographers [1] was performing a detailed study of this cold front using classical surveying methods. The situation of the thermal gradients drawn from their maps is in excellent agreement with the NOAA4 observations. As far as the numerical values are concerned, the difference between in-situ measurements and satellite observations are no greater than 1°C. The radiometric temperatures are always lower than sea-truth which could be due to atmospheric losses.

Absolute temperature errors in the mapping of oceans thermal gradients using VHRR data are mainly due to the water content of the lower levels of the atmosphere and they can be corrected by the use of atmospheric models based for example on radio-sounding results. Large clouds are seldom an interpretation problem due to their straightforward separation in the visible

(1) R.D. Pingree, P.R. Pugh, P.M. Holligan and G.R. Forster

Summer phytoplancton blooms and red tides along tidal fronts in the approaches to the English Channel.

Nature - Vol 258 - PP 672-677

and in the infra-red but this is not the case for coastal
fogs and scatters of small low clouds. The detection of
these features is done by low clouds. The detection of these
features is done by careful comparison between measured
radiometric temperatures and seasonal average surface
temperatures available for the surveyed area through
classical physical oceanography observations.

In the strong thermal gradient area of the coast of Finistère,
measurements had also detected a fair increase in chlorophyll
A concentration due to phytoplancton activity. These concen-
trations should have modified the colour of the ocean by it
is disappointing that the visible VHRR display does not show
such a feacture.

Several reasons can be conjectured :

- the visible VHRR band, identical to the LANDSAT MSS5,
  is not suited to chlorophyll mapping in water ;

- light penetration ($\simeq$ 2 m) could blurr the precise
  definition of the colour gradients ;

- the resolution (1 km) is too coarse regarding the
  detection of phytoplancton patches which follow the
  edge of the thermal front and are therefore of a width
  comparable in size with the VHRR resolution.

The results presented here show the utility of infra-red
thermal imagery for oceanographic applications but they also
suggest caution in the interpretation of rather coarse
resolution future satellites such as NIMBUS-G.

3. 5.4 Conclusion

Although the processing techniques outlined in this work appear
satisfactory for the available data some remarks can be made
regarding the suitability of the resulting output for the user
community's needs.

The accuracy of sea surface temperatures obtained from NOAA data,
although useful, is not up to the standards currently applied by
oceanographers who are able to measure sea temperature to $1/100^{th}$
of a degree Celsius, using thermistors. The $1/10^{th}$ of a degrees
Celsius forecasted for future satellites will be closer to
oceanographyc needs.

Nonetheless thermal infra-red applications in general are more
adaptated to oceanographic applications than, for instance, Landsa
data which provide ocean colour measurement at the surface or at a
depth which is not always easily identified.

On the other hand, the spatial (1 km square) resolution of the NOA
VHRR is adequate for oceanographic applications, whilst Landsat da
has the minimal resolution for coastal geomorphology applications.

The density of observations is almost excessive in oceanography
and provides a great deal of redundant information.

Finally, repetivity of coverage (twice daily for NOAA) provides
time series wich can be used for pratical monitoring of fast-
changing situations. At the present time we have mostly processed
day-time coverage (9 a.m.) but we are planning to use both day-time
and evening (9 p.m.) data in conjunction with HCMM data (12 a.m. -
12 p.m.) for an evaluation of high frequency coverage which should
enable us to monitor most of the tidal cycle over a short period.
In this last case, the low frequency of Landsat coverage makes it
practically impossible to obtain a complete series since some tidal
situations have not occured concurrenty with a Landsat overpass
since we began to receive Landsat data.

4 - BIBLIOGRAPHY

4. 1 - Expositions

- Novembre 1974. Nantes. Exposition organisée par l'Institut
  Géographique National à la Bibliothèque Univer-
  sitaire de la Faculté des Lettres de Nantes :
  Présentation du programme FRALIT de télédétection.

- 26 Avril-9 Mai 1975. Rennes. Exposition des travaux de l'équipe
  FRALIT au stand du Centre National de la Recherche
  Scientifique de la Foire de Rennes :
  La Télédétection du Littoral.

- 23 Mai-6 Juin 1975. Amiens. Exposition de Télédétection au
  Centre d'Etudes Géographiques de l'Université
  de Picardie :
  Traitement photographique, traitement informa-
  tique et cartographie automatique.

- 29 Mai-8 Juin 1975. Le Bourget. Exposition des travaux de
  l'équipe FRALIT au stand du Centre National
  d'Etudes Spatiales du XXXIe Salon de l'Aéronau-
  tique et de l'espace au Bourget.

- Juillet-Août 1975. St Valery. Station d'Etude en Baie de Somme :
  Télédétection du littoral français et, en parti-
  culier, du littoral picard par l'équipe FRALIT.

- Novembre-Décembre 1975. Budapest. Exposition internationale
  des cartes hydrographiques organisée par l'Office
  foncier et cartographique national du Ministère
  de l'Agriculture et de l'Alimentation de la
  République Populaire Hongroise :
  Présentation de cartes des turbidités littorales
  établies par l'équipe FRALIT (estuaire de la
  Loire).

- 3-10 Août 1976. Moscou. Exposition de la huitième conférence
  internationale de cartographie-section C :
  Cartes obtenues à partir des données de
  Télédétection.

- 2-5 Octobre 1976. St Quentin. Exposition organisée par l'Union
  St Quentinoise de Philatélie :
  Philatélie et satellites.

- 2-18 Décembre 1976. Amiens. Exposition réalisée pour la semaine
  "Recherches Universitaires et Région Picardie" :
  Télédétection par satellites.

:Short course

- 1-15 septembre 1974. Dinard. Stage de techniques d'études
  littorales au laboratoire de l'Ecole Pratique
  des Hautes Etudes.

- 21-24 octobre 1974. Paris. Semaine de formation permanente
  sur la télédétection pour le Centre National
  de la Recherche Scientifique.

- 21-25 Avril 1975. Fontainebleau. Semaine d'étude sur les
  divers aspects de la télédétection au labora-
  toire de Ressources Terrestres (K. Albuisson,
  J-M. Monget, P. Roux).

- septembre 1975. Dinard. Stage de techniques d'études litto-
  rales au laboratoire de l'Ecole Pratique des
  Hautes Etudes (J. Dambricourt, D.J. David,
  J. Dupuis, J-M. Monget, J-P. Pinot, R. Regrain,
  F. Verger).

- 21-24 octobre 1975. Paris. Semaine de formation permanente
  sur la télédétection pour le Centre National
  de la Recherche Scientifique.

- Août 1976. Alpach (Autriche). Ecole d'été de l'Austrian Space
  Agency (J-M. Monget) :
  Présentation des résultats de l'équipe FRALIT,
  méthodes de traitements numériques.

- Septembre 1976. Dinard. Stage de techniques d'études litto-
  rales au laboratoire de l'Ecole Pratique des
  Hautes Etudes (Ch. Cazabat, D.J. David, J. Dupuis,
  J-M. Monget, J-P. Pinot, R. Regrain, F. Verger).

- 1976. Toulouse. Cours de technologie spatiale du CNES (F. Verger):
  Observation de la Terre, cartographie des
  phénomènes littoraux à partir des données LANDSAT.

- 26-28 Octobre 1976. Toulouse. Journées du GDTA :
  Télédétection de la région de Cancale : cartes de
  classification des données multispectrales et cartes
  thermographiques.

4.3 - <u>Seminars and Symposiums</u>

- 1er Décembre 1973. Paris. Colloque sur les méthodes de la
        télédétection appliquée au littoral français
        (F. Verger).

- Janvier 1974. Frascati (Italie). Symposium sur les résultats
        obtenus par les investigateurs ERTS-1 (R. Brossier

- Mars 1974. Aussois. Colloque sur les applications des techniques
        spatiales organisé par le Centre National d'
        Etudes Spatiales (P. Demathieu).

- Avril 1974. Ann Arbor (USA). Symposium international de télé-
        détection (R. Brossier).

- 29 Avril 1974. Toulouse. Table Ronde des Investigateurs ERTS
        organisée par le Centre National d'Etudes Spatiale.
        (F. Verger).

- 30 Avril 1974. Toulouse. Journée d'information des utilisateurs
        français de la télédétection (F. Verger) :
        Présentation du programme d'étude du littoral
        français de l'Atlantique.

- 17 Mai 1974. Montrouge. Animation du séminaire INFORMATIQUE
        ET TELEDETECTION à l'Ecole Normale Supérieure
        (D.J. David, F. Verger).

- 20 Novembre 1974. Paris. Comité français de cartographie
        (F. Verger) :
        Présentation du programme FRALIT de télédétection.

- 28 Février-3 Mars 1975. Nice. Journées Géographiques (J. Deries
        F. Verger) :
        Communications sur la cartographie automatique
        à partir des données de ERTS-1.

- 9 Avril 1975. Londres. Symposium sur "European participation
        in Earth Resources (Space) Projects" organisé au
        Collège Universitaire de Londres par la British
        Interplanetary Society (D.J. David).

- 18-19 Avril 1975. Bordeaux. Journées d'information sur l'utili-
        sation des clichés ERTS-1 pour l'étude de
        l'environnement tropical (F. Verger).

- 23-24 Mai 1975. Amiens. Colloque "Télédétection, Informatique,
Ressources Naturelles" au Centre d'Etudes
Géographiques de l'Université de Picardie
(D.J. David, J. Deries, J-M. Monget, P. Pirazzoli,
R. Regrain, F. Verger).

- 5-6 Juin 1975. Bruxelles. Table Ronde de la Commission des
Communautés Européennes sur la télédétection
(F. Verger).

- 18-27 Juin 1975. Bucarest. VI° colloque roumano-français de
Géographie (F. Verger) :
Communication sur l'intérêt des cartes automatiques
des régions littorales à partir des données de
la télédétection.

- 6 Décembre 1975. Paris. Réunion de la Commission d'Océanographie
du Comité National de Géographie (O. Guérin,
P. Pirazzoli, M. Poisson, R. Regrain, F. Verger) :
La Télédétection.

- 22 Avril 1976. Paris. Cycle d'études sur "La télédétection
et la photointerprétation" au Centre d'Etudes,
d'Information et de Formation pour les ingénieurs
de la Construction et de l'Industrie (F. Verger) :
Exposé sur l'océanographie : problèmes du littoral.

- 20 Mai 1976. Amiens. Cours public à l'Université de Picardie
(R. Regrain) :
Télédétection par satellites.

- 17-18 Juin 1976. Philadelphia (USA). Assemblée du COSPAR
(Committee on Space Research) (J-M. Monget).

- 19 Octobre 1976. Greenbelt (USA)."Landsat coastal applications
review panel"au NASA Goddard Space Center
(J-M. Monget) :
Présentation des résultats de l'équipe FRALIT.

- 26-28 Octobre 1976. Toulouse. Journées du GDTA (M. Albuisson,
Y.F. Thomas, F. Verger) :
La télédétection dans la région de Cancale
(exploitation des données du GDTA).

- 9 Novembre 1976. Paris. Conférence de presse sur "La télédé-
tection des ressources terrestres" (F. Verger).

- 10 Décembre 1976. Nantes. Colloque de la Commission d'océano-
graphie du Comité National de Géographie (J-M. Monge
R. Regrain, F. Verger) :
Télédétection et aménagement des marais maritimes
de l'Ouest.

- 15 Décembre 1976. Amiens. Semaine de la Recherche à l'Université de Picardie (R. Regrain) :
  La télédétection par satellites en Picardie.

- 15 Décembre 1976. Amiens. Emission Radio sur FR 3 Nord-Picardi
  (R. Regrain).

- 17 Décembre 1976. Reading (G.B.). Assemblée générale de la
  Remote Sensing Society (M. Poisson) :
  Présentation de thermographies NOAA.

4.4 - Publications

Albuisson M., Guérin O., Pinot J-P. - L'expansion en mer des
eaux de la Loire en mars 1975.
Bulletin de l'Union des Océanographes de France, 1975- 3-4,
p. 4.

Albuisson M., Monget J-M.- Températures de surface de la
mer d'après les données de NOAA 4.
Photo-Interprétation, 1976- 5.

Albuisson M., Dambricourt J., Millou A., Monget J-M., Thomas
Y.F., Verger F. - Télédétection multispectrale du littoral
de la baie du Mont Saint-Michel.
Journées de télédétection du GDTA, Toulouse, 1976.

Albuisson M., Monget J-M., Poisson M. - Investigation of
coastal and marine environments using NOAA digital data.
Remote Sensing Society proceedings.

Cazabat C., Demathieu P., Dupuis J., Verger F. - Le programme
FRALIT. Télédétection, par le satellite ERTS-A, du littoral
océanique de la France.
Bulletin d'information de l'Institut Géographique National,
1972- 19, p. 17-24.

Callame B. - Notes sur l'interprétation de la carte info-
graphique "Le pertuis breton et ses rivages" établie à
partir des données du satellite ERTS 1.
Bulletin Société Française Photogrammétrie, 1976- 62, p. 33-35.

Couderc J-M., Desire E., Flament E., Regrain R. - Images
ERTS (LANDSAT) de la Touraine à la frontière belge.
Bulletin Société Photogrammétrie, 1976- p. 3-13.

Coudoux J., Flament E., Regrain R. - Images LANDSAT du Nord
de la Picardie.
Communication 101ème Congrès National des Sociétés Savantes,
Lille. Pré-print Université de Picardie, 1976, 32p.

David D.J., Deries J., Verger F. - Cartographie automatique
des marais et wadden à partir des données multispectrales
d'ERTS 1.
Mémoires du laboratoire de Géomorphologie de l'Ecole Pratique
des Hautes Etudes, 1974- 26, 80 p.

David D.J., Deries J., Verger F. — Automatic cartography
of ERTS remote sensing data.
Journal of British Interplanetary Society, 1975— 28,
p. 624-628.

David D.J., Deries J., Verger F., Joly G. — Cartographie
automatique des données des satellites LANDSAT.
Bulletin Société Française Photogrammétrie, 1976— 62,
p. 25-31.

David D.J., Joly G., Verger F. — Visualisations et traitements
d'images de télédétection par satellites.
Congrès AFCET, panorama de la nouveauté informatique en
France, Paris/Gif-sur-Yvette, 1976— p. 655-664.

David D.J., Joly G., Verger F. — Computer elaboration and
visualization of remote sensing data.
Journal of British Interplanetary Society.

Delacroix F., Thomas Y.F., Verger F. — Classification des
paysages à partir des données multispectrales de télédétection.
La Documentation Française.

Delanoe Y., Pinot J-P. — Sédimentologie sous-marine et télé-
détection : les traînées graveleuses de l'avant-côte de
l'Ile-Tudy (Bretagne méridionale).
Bulletin Société Sciences Naturelles Ouest de la France,
1975— LXXIII, p. 130-139.

Démathieu P., Verger F. — Etude d'une image composite couleur.
Photo-Interprétation, 1973— 5, p. 17-22.

Demathieu P., Verger F. — The utilization of ERTS 1 data
for the study of the french atlantic littoral.
Third Earth Resources Technology Satellite-1 Symposium
NASA, 1974— 1 p. 1447-1450.

Deries J. — La photographie composite couleur. Colloque sur
les méthodes de la télédétection appliquée au littoral
français.
Bulletin de l'Association de Géographes Français, 1973—
p. 703-710.

Guérin O., Monget J-M. — L'intérêt de la télédétection pour
la connaissance du milieu estuarien : exemple de l'estuaire
de la Loire.
Bulletin de l'Union des Océanographes de France, 1975— 1-2,
p. 47-54.

Joly G., Verger F. - Télédétection du littoral. Programme
FRALIT. Représentation graphique.
dans : saisie et structuration de l'information. Journées
d'études du 12 mai 1975.
Publication laboratoire tectono-physique, Université Pierre
et Marie Curie, 1975- p. VIII à VIII-4.

Monget J-M. - An unsupervised classification of multispectral
scanner data using correspondence analysis (CLAMS).
Proceedings of the NASA Earth Resources Survey Symposium,
Houston, 1975.

Monget J-M., Sarrat D., Verger F. - Environmental mapping of
the french coastal zone by remote sensing.
COSPAR, 1976.

Monget J-M., Verger F. - Un exemple d'assistance au traitement
automatique des données de télédétection.
Photo-Interprétation, 1976- 5.

Monget J-M. - Classification automatique des données multi-
spectrales utilisant l'analyse des correspondances. Le
système CLAMS.
Bulletin Société Française de Photogrammétrie, 1976- 62,
p. 15-23.

Poisson M. - Une classification automatique des données
LANDSAT diachroniques, les estrans de l'île de Jersey.
Photo-Interprétation, 1976- 5.

Regrain R. - Télédétection du littoral charentais par le
satellite ERTS 1.
Annales de la Société des Sciences Naturelles de Charente-
Maritime, 1973, p. 10-19.

Regrain R. - L'intérêt des images multispectrales, l'exemple
du littoral de la Manche orientale.
Bulletin de l'Association de Géographes Français, 1973,
p. 703-707.

Regrain R. - Télédétection et taxonomie géographique. La
région de Marennes (Charente-Maritime).
Bulletin Société Française Photogrammétrie, 1976- 62,
p. 37-42.

Regrain R. - La Picardie vue par LANDSAT.
Atlas de Picardie, Amiens, PL. B1, 1976.

Regrain R., Verger F. – Le programme FRALIT de télédétection
en Picardie (satellite ERTS 1 de la NASA).
Annales du Centre Régional de Documentation Pédagogique
d'Amiens, 1976– 45 p. + 11 planches.

Thomas Y.F. – Télédétection par satellite et analyse des
données. L'étude des turbidités des eaux littorales.
dans : Colloque sur les méthodes mathématiques appliquées à
la géographie.
Cahiers de géographie de Besançon, 1976.

Verger F., Demathieu P. – Les techniques d'exploitation des
données d'ERTS 1 utilisées dans le programme FRALIT.
La Recherche Spatiale, 1973– XII, p. 24–27.

Verger F., Demathieu P. – Etude diachronique des surfaces
d'eau et des surfaces mouillées sur deux images ERTS 1.
Photo–Interprétation, 1973– 5, p. 1–7.

Verger F., Demathieu P. – La télédétection littorale. Programme
FRALIT. ERTS 1.
Mémoires du laboratoire de Géomorphologie de l'Ecole Pratique
des Hautes Etudes, 1973– 23, 22 p.

Verger F. – L'utilisation des données par des techniques
quantitatives.
dans : Colloque sur les méthodes de la télédétection appliquée
au littoral français.
Bulletin de l'Association de Géographes Français, 1973–
p. 723–729.

Verger F., Demathieu P. – The utilization of ERTS 1 data
for the study of the french atlantic littoral.
NASA, January 1974– 91 p.

Verger F. – Une cartographie automatique des données de
LANDSAT 1.
Photo–Interpretation, 1974– 6, p. 1–6.

Verger F., Joly G. – Cartographie diachronique à partir des
données numériques de LANDSAT 1.
Photo–Interprétation, 1974– 6, p. 7–13.

Verger F., Monget J–M. – The french atlantic littoral and
the Massif armoricain.
NASA, December 1975– 5 p.

Verger F. - Le programme FRALIT de télédétection (ERTS 1).
Bulletin du Comité Français de Cartographie, 1975- 64,
p. 196-199.

Verger F. - Un programme de télédétection sur le littoral
français (satellite ERTS-A de la NASA).
Actes du 97ème Congrès des Sociétés Savantes, Imprimerie
Nationale, Paris, 1976, p. 33-37.

Verger F., Monget J-M., Scanvic J.Y. - The french atlantic
littoral and the Massif armoricain.
NASA, 1976- 26 p.

Verger F. - Les données LANDSAT et un exemple de leur utili-
sation.
Travaux et documents de géographie tropicale, 1976- 25,
p. 11-24.

Verger F. - L'apport des satellites LANDSAT à la connaissance
du littoral français.
L'ingénieur-Constructeur, Septembre-Octobre 1976, p. 51-55.

Verger F. - Cartographie des phénomènes littoraux à partir
des données LANDSAT.
Cours de technologie spatiale (observation de la Terre),
Toulouse, 1976- 18 p.

Verger F. - L'apport des satellites LANDSAT à la connaissance
du littoral français.
Géomètre, Février 1977, p. 44-50.

4 . 5 - <u>Film et émission de télévision</u>

" La galaxie des ordinateurs ", film produit par la
Télévision Suisse Romande (réalisation Pierre Barde)
avec la collaboration du CNRS. 1975.
Participation de F. Verger.

-